University of Wisconsin Milwaukee

UWM Digital Commons

August 2022

Enhancement of Energy Efficiency for Thermal Energy and Biomass Driven Applications

OSAMA Mansour Selim ELSAYED
University of Wisconsin-Milwaukee

Follow this and additional works at: https://dc.uwm.edu/etd

Part of the Chemistry Commons, and the Mechanical Engineering Commons

Recommended Citation

ENHANCEMENT OF ENERGY EFFICIENCY FOR THERMAL ENERGY

AND BIOMASS DRIVEN APPLICATIONS

by

Osama M. Selim

A Dissertation Submitted in

Partial Fulfillment of the

Requirements for the Degree of

Doctor of Philosophy

in Engineering

at

The University of Wisconsin-Milwaukee

August 2022

ABSTRACT

ENHANCEMENT OF ENERGY EFFICIENCY FOR THERMAL ENERGY AND BIOMASS DRIVEN APPLICATIONS

by

Osama M. Selim

The University of Wisconsin-Milwaukee, 2022
Under the Supervision of Professor Ryoichi S. Amano

The importance of gas turbine blades is to convert the thermal energy into shaft work output, which makes the turbine blades are one of the critical components of the gas turbines. Besides the mechanical stresses caused by the centrifugal force and the fluid forces, the thermal stresses arise because of the temperature gradient within the blade materials. This paper aims to have a uniform circumferential temperature field at the combustor exit, consequently reducing the thermal stresses caused by the non-uniform temperature distribution along the turbine blade. The validation of the simulation results with the experiments showed an acceptable agreement with available experimental data. The agreement includes the uniformity factor and the normalized mixture fraction at two different flowrates.

Furthermore, sixteen cases studies have been implemented to study the effect of changing Internal Guide Vanes location, concerning the test section holes and the primary stream. The results show that the best location of the Internal Guide vanes is to be placed on the large holes of the dilution section with a 30o angle to the primary stream direction. This method gives 25% higher in thermal uniformity compared to attach them to the small holes. Compared to different orientations, it provides 14% higher regarding the thermal uniformity. Another location of the guide vanes, External Guide Vanes, was experimentally and numerically tested. The results show

that the external guide vanes with a 30º orientation gave the most uniform temperature flow for the two different flow rates. Compared to the internal guide vanes with the same orientation, the external guide vanes gave a 7.5% higher uniformity factor and 2% lower pressure drop. The main reason for this result is that the external guide vanes direct the cold stream to penetrate the dilution zone with an angel enhance the swirling effect which are the main factors for excellent mixing, while the pressure drop is lower as the external guide vanes are facing the lower flowrate which is the secondary stream. Another advantage of the external guide vanes over the internal ones is that they are subjected to less thermal stresses as they are facing the cold flow. Furthermore, the external guide vanes are reachable and easy to maintain compared to the internal guide vanes. Finally, the combustor outer surface design has been investigated. Four different angles have been tested numerically and experimentally with a maximum error of 5% at two different Reynolds numbers. Designing the outer combustor surface with a 45-angle bend can give a more uniform temperature distribution of 37% higher than the basic design with only a 0.5% higher pressure drop.

Moving to biomass, different thermochemical conversion processes on different biomass species were presented. The results show it is recommended to use the lowest heating rate to allow a quasi-equilibrium state through slow heating, hence avoiding measurement errors. Chicken manure, thermal degradation of the three main components of the chicken manure was obtained. The initial results show that for the slow heating rates, 5oC/min, the thermal degradation of the cow manure is different compared to that one obtained from chicken manure. The Hemicellulose decomposition took place at 250ºC and 300ºC for the chicken manure and cow manure, respectively. The Cellulose decomposition was started at 300ºC for chicken manure and 470ºC for cow manure. Gasification, all reactions were endothermic when CO_2 used as a gasifying agent.

Consequently, the energy must be supplied in terms of heating to sustain the reaction while air gasification was exothermic, which means that the reaction can be sustained without external heating where the self-ignition was observed between 450°C - 600°C. In addition, it was observed that carbon dioxide had the most complicated mechanism with four stages. The cow manure as well has been tested for gasification using the air and CO2 as gasifying agents. At the same temperatures of pyrolysis process the breakup of the hemicellulose and cellulose has occurred 302 °C and 500 °C while the lignin thermal degradation occurred at 745 °C. The 5 °C/min heat rate shows the best results in terms of keeping a very stable exothermic reaction compared to the other heating rates. The CO2 gasification for the cow manure shows poor results (endothermic reactions). This means that the carbon dioxide cannot be used with the cow manure as a gasifying agent since it needs a lot of energy to generate syngas. CO-Pyrolysis, results show the 40%RH-60%CH decreasing the energy of activation by 12% compared to Chicken manure. In addition, an increase in the conversion greater than 3% was achieved. The 40% CM-60%CH shows a positive result in terms of keeping an exothermic reaction over the Co-Pyrolysis process. Finally, CO-gasification, air is used as a gasifying agent, of the cow manure with the sheep manure has been investigated to show that the blend mixture of 20% sheep manure and 80% cow manure give the highest exothermic reaction among all other cases.

Dedicated To My Parents, My Brother and My Sister for Their Unconditional Love, Support,

and Motivation

TABLE OF CONTENTS

LIST OF FIGURES

LIST OF TABLES

LIST OF NOMENCLATURE

A   Pre-exponential constant in Arrhenius equation

Cp   Specific heat at constant pressure

D   Diameter

dr   Radius spacing

DTA   Differential Thermal Analysis

DTG   Derivative Thermo-gravimetric

E   Energy

f Mixture fraction

HP   Horsepower

K   Thermocouple material type

K(T)   Temperature-dependent rate of reaction

LES   Large eddy simulation

m   mass

n   Order of reaction

P&G   Pyrolysis and Gasification

R   Exit duct radius

Re   Reynolds number

r   Arbitrary radius

t	Time
T	Temperature
TGA	Thermo-gravimetric analysis
v	Mass of volatile at any time
V	Velocity
w	Mass of biomass
χ	Uniformity number
y^+	Wall distance function

GREEK SYMBOLS

α	Extent of reaction
β	Linear heating rate
Δ	Change
ρ	Density

SUBSCRIPTS AND SUPERSCRIPTS

*	Superscript of normalized values
a	Activation
f	Final
o	Initial
t	At time t

*	Superscript of normalized values
a	Subscript of the axial component
eq	Subscript of the Ideal state
m	Subscript of mixture flow
P	Subscript of primary flow
S	Subscript of secondary flow
P	Subscript of primary flow
S	Subscript of secondary flow
·	Superscript of the Rates

LIST OF ABBREVIATIONS

EXGV   External Guide Vanes

INGV   Internal Guide Vanes

SH   Staggered Holes

ACKNOWLEGMENTS

CHAPTER 1- INTRODUCTION

1.1 Gas Turbines

A turbine is a component included in the thermal turbomachinery category. It converts enthalpy of the working medium, also call the working fluid (exhaust stream, gaseous decomposition products or compressed gas), into mechanical work, which results in the rotation of the rotor. The advantages of gas turbines such as the ability to develop high power in a compact and low weight structure, relatively high energy conversion efficiency of the process, simple structure, ease of use under different climatic conditions (particularly, at low ambient temperatures), and a fairly high reliability have made it were widely used in, e.g., power engineering, traction, marine and aircraft engines, and aerospace technology.

The basic principle of the airplane turbine engine is identical to all engines that extract energy from chemical fuel. The basic 4 steps for any internal combustion engine are:

1. Intake of Air (and possibly fuel)

2. Compression of the Air (and possibly fuel)

3. Combustion, where fuel is injected (if it was not drawn in with the intake air) and burned to convert the stored energy

4. Expansion and exhaust, where the converted energy is used

However, these same four steps occur at the same time but in different places. As a result of this fundamental difference, the turbine has engine sections called; inlet section, compressor section, combustion section (the combustor) and turbine section. The turbine section of the gas turbine engine has the task of producing usable output shaft power to drive the propeller. In addition, it must also provide power to drive the compressor and all engine accessories. It does

this by expanding the high temperature, pressure, and velocity gas and converting the gaseous energy to mechanical energy in the form of shaft power.

1.1.1 Engine Sections

- **Inlet**

The air inlet duct must provide clean and unrestricted airflow to the engine. Clean and undisturbed inlet airflow extends engine life by preventing erosion, corrosion, and foreign object damage (FOD). Consideration of atmospheric conditions such as dust, salt, industrial pollution, foreign objects (birds, nuts and bolts), and temperature (icing conditions) must be made when designing the inlet system. Fairings should be installed between the engine air inlet housing and the inlet duct to ensure minimum airflow losses to the engine at all airflow conditions. The inlet duct assembly is usually designed and produced as a separate system rather than as part of the design and production of the engine.

- **Compressor**

The compressor is responsible for providing the turbine with all the air it needs in an efficient manner. In addition, it must supply this air at high static pressures. Compressors are usually made up of several rows of alternating rotor vanes and stator blades, known as stages. To achieve highest pressure rations, the compressor is split into two or even three separate in-line compressors. Each is connected to its own shaft and driven by individual turbines.

- **Diffuser**

Air leaves the compressor through exit guide vanes, which convert the radial component of the air flow out of the compressor to straight-line flow. The air then enters the diffuser section of the engine, which is a very divergent duct. The primary function of the diffuser structure is aerodynamic. The divergent duct shape converts most of the air's velocity (P_i) into static pressure

(P$_S$). As a result, the highest static pressure and lowest velocity in the entire engine is at the point of diffuser discharge and combustor inlet. Other aerodynamic design considerations that are important in the diffuser section arises from the need for a short flow path, uniform flow distribution, and low drag loss. In addition to critical aerodynamic functions, the diffuser also provides:

- o   Engine structural support, including engine mounting to the nacelle

- o   Support for the rear compressor bearings and seals

- o   Bleed air ports, which provide pressurized air for:

    - ✓ airframe "customer" requirements (air conditioning, etc.)

    - ✓ engine inlet anti-icing

    - ✓ control of acceleration bleed air valves

- o   Pressure and scavenge oil passages for the rear compressor and front turbine bearings.

- o   Mounting for the fuel nozzles

- **Combustor**

Once the air flows through the diffuser, it enters the combustion section, also called the combustor. The combustion section has the difficult task of controlling the burning of large amounts of fuel and air. It must release the heat in a manner that the air is expanded and accelerated to give a smooth and stable stream of uniformly heated gas at all starting and operating conditions. This task must be accomplished with minimum pressure loss and maximum heat release.   In addition, the combustion liners must position and control the fire to prevent flame contact with any metal parts.

As shown in Figure 1-1, the exhaust gases are being provided to the turbine blades after passing three different combustion zones. Each zone has its function which can be summarized as follow;

primary zone, where only 20% of the pressurized air from the compressor is mixed with the fuel to start the combustion process. The secondary region, where an additional amount of pressurized air (20%) is being added to the flow to make complete combustion. The remaining 60% is being added through the third zone, dilution zone, to cool the exhaust gases and hence provide the turbine blades with a reasonable temperature that can be sustained by the turbine blades/vanes.
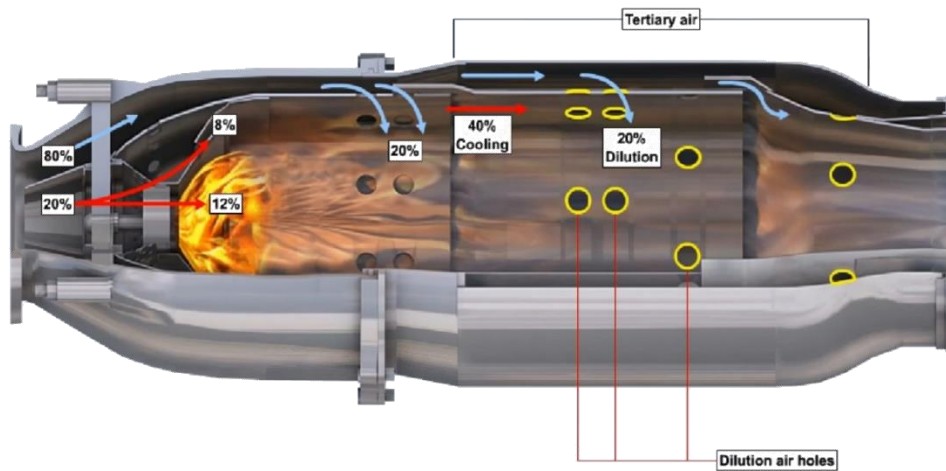
Figure 1-1: Diagram of air flow paths in a gas turbine combustor

- **Turbine**

The turbine converts the gaseous energy of the air/burned fuel mixture out of the combustor into mechanical energy to drive the compressor, driven accessories, and, through a reduction gear, the propeller. The turbine converts gaseous energy into mechanical energy by expanding the hot, high-pressure gases to a lower temperature and pressure. Each stage of the turbine consists of a row of stationary vanes followed by a row of rotating blades. This is the reverse of the order in the compressor. In the compressor, energy is added to the gas by the rotor blades, then converted to static pressure by the stator vanes. In the turbine, the stator vanes increase gas velocity, and then the rotor blades extract energy. The vanes and blades are airfoils that provide for a smooth flow of the gases. As the airstream enters the turbine section from the combustion section, it is accelerated

through the first stage stator vanes. The stator vanes (also called nozzles) form convergent ducts that convert the gaseous heat and pressure energy into higher velocity gas flow (P_i). In addition to accelerating the gas, the vanes "turn" the flow to direct it into the rotor blades at the optimum angle. As the mass of the high velocity gas flows across the turbine blades, the gaseous energy is converted to mechanical energy. Velocity, temperature, and pressure of the gas are sacrificed in order to rotate the turbine to generate shaft power.

- **Exhaust**

After the gas has passed through the turbine, it is discharged through the exhaust. Though most of the gaseous energy is converted to mechanical energy by the turbine, a significant amount of power remains in the exhaust gas. This gas energy is accelerated through the convergent duct shape of the exhaust to make it more useful as jet thrust - the principle of equal and opposite reaction means that the force of the exhausted air drives the airplane forward.

1.2 Problem Statement

Unfortunately, gas turbines have also their drawbacks, the most essential being high operating temperature of some of their parts such as blades, and large rotor speeds. Compromises are made in turbine design to achieve the optimum balance of power, efficiency, cost, engine life, and other factors. Several studies have shown that the flow field exiting a combustor is highly non-uniform in pressure, velocity and, most importantly, temperature. Apparent nonuniform temperature profile (hot streak) exists at the outlet of the combustor and the inlet of the gas turbine due to more complex combustion mechanism and cooling scheme, Figure 1-2 [87]. Such heat load exposes the rotor blade of the gas turbine to high heat transfer and hotspots. In recent years, many researchers implemented much experimental work to study the hot streak migration in turbine flow passage,

especially in the rotor blade tip region with the purpose of understanding the nonuniform temperature profile at the outlet of the combustor.
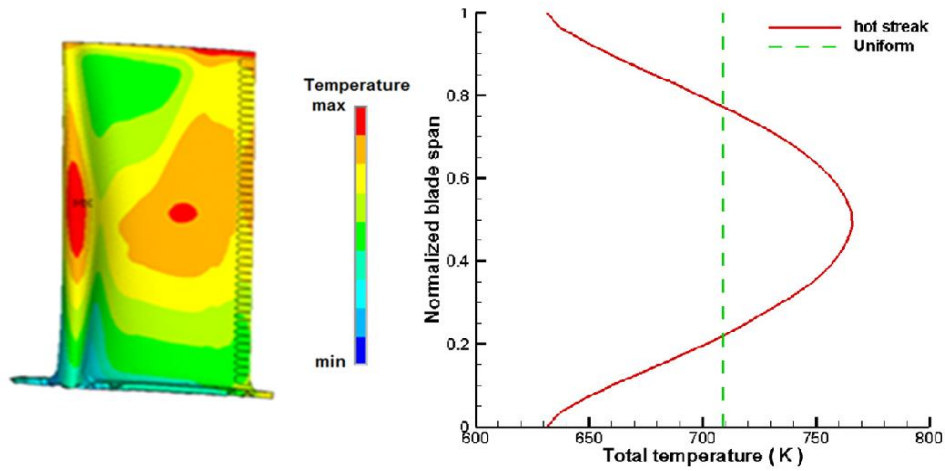
Figure 1-2: Nonuniform Temperature Distribution Along Turbine Blade [87]

Various methods have been developed and proposed to counter the challenges posed by the non-uniformities present in the exit flow from the combustor, which include both passive and active control techniques. Any geometrical modifications such as change in the combustor design or the way the cold air is introduced in the dilution zone, constitute the passive control techniques whereas modification other than just the geometry like the use of pulsed air jet, synthetic jet actuators, etc. to improve mixing in the dilution zone come under the active control techniques. The present work is another attempt to develop techniques to enhance mixing in a facility, simulating the dilution zone in a typical gas turbine combustor. Here, only the passive control techniques are analyzed to achieve the objective of producing a more uniform temperature.

1.3 Biomass Energy Resources

1.3.1 Motivation

Access to energy is a key pillar for human wellbeing, economic development and poverty alleviation. Ensuring everyone has sufficient access is an ongoing and pressing challenge for global development. However, our energy systems also have important environmental impacts. Historical and current energy systems are dominated by fossil fuels (coal, oil and gas) which produce carbon dioxide (CO_2) and other greenhouse gases– the fundamental driver of global climate change. If we are to meet our global climate targets and avoid dangerous climate change, the world needs a significant and concerted transition in its energy sources. Balancing the challenge between development and environment therefore provides us with an ultimate goal of ensuring everyone has access to enough sustainable energy to maintain a high standard of living.

a) **World Demand for Energy**. Global energy demand has been growing exponentially. Traditional energy resources (e.g., coal, oil, and gas) have contributed significantly to global electricity generation. However, they have also contributed to an increase in pollution in the world and a deterioration of human health. Energy Information Administration (EIA) in U.S. projects that world energy consumption will grow by nearly 50% between 2018 and 2050. Most of this growth comes from countries that are not in the Organization for Economic Cooperation and Development (OECD), and this growth is focused on regions where strong economic growth is driving demand, particularly in Asia.

b) **Depletion of Fossil Fuels**. The critical question is "will the current energy resources be enough until 2050?". According to British Petroleum statistical review, Figure 1-3, with the current production rate the current oil deposits could run out in just over 45.7 years,

47.8 for natural gas and 109 years for the coal. These energy resources represent 60% of the net electricity generation in U.S as shown in Figure 1-4

c) **Oil Crisis**. In addition, sometimes shortage in the fuel is because of some political issues. Oil embargo in 1970s is a good example where the oil prices jumped to the double from in just one year from 1973 to 1974, Figure 1-5, and the gas was limited to 10 gals per customer. Or even with the current situation because of the Corona Virus where the oil price is the lowest, $20 per barrel. Lower oil prices mean less drilling and exploration activity because most of the new oil driving the economic activity is unconventional and has a higher cost per barrel than a conventional source of oil
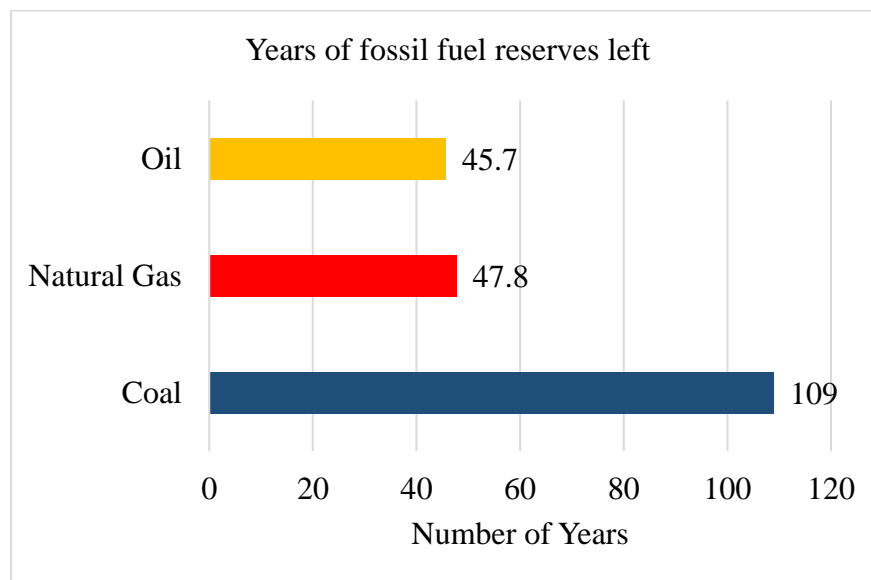
Figure 1-3: British Petroleum Statistical Review of World Energy 2019
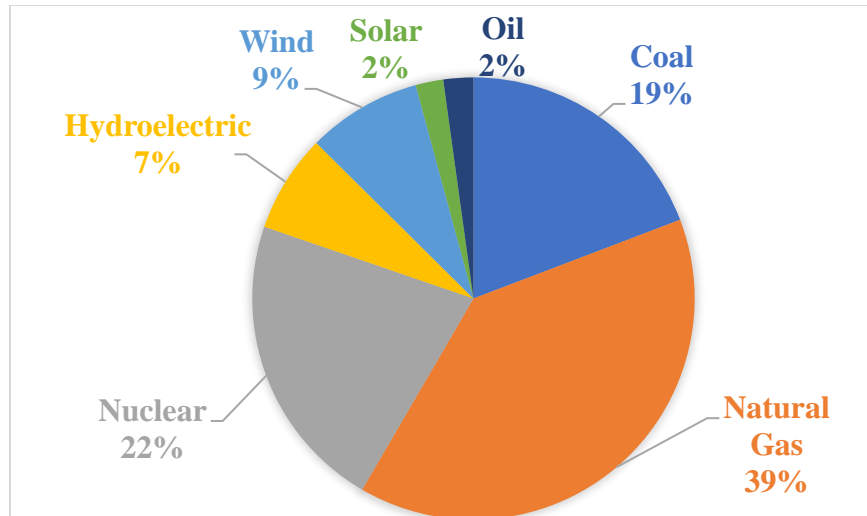
Figure 1-4: U.S. electricity generation by energy source in 2019
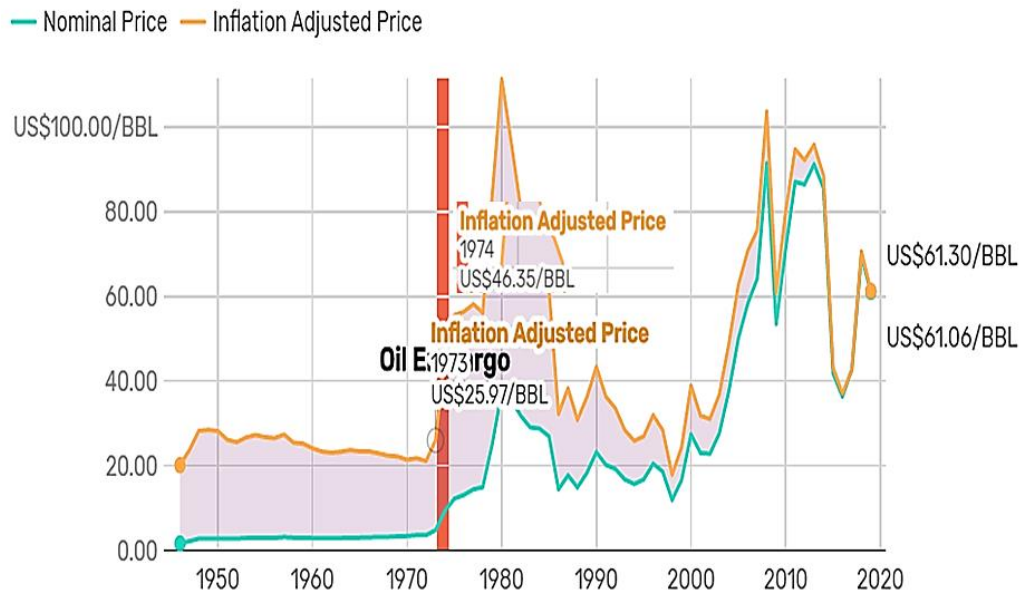
Figure 1-5: Oil Prices Per year

d) Pollution. Some of the most significant hidden costs of fossil fuels are from the air emissions that occur when they are burned. Unlike the extraction and transport stages, in which coal, oil, and natural gas can have very different types of impacts, *all* fossil fuels emit carbon dioxide and other harmful air pollutants when burned. These emissions lead to a wide variety of public health and environmental costs that are borne at the local, regional, national, and global levels. Furthermore, in terms of pollution, as per the Institute

9

for Health Metrics and Evaluation that the air pollution affects about 147 million of people either by death or being in a bad health condition.

1.3.2 Resources

As a response to the above-mentioned problems, the renewables are increasingly displacing fossil fuels in the power sector, offering the benefit of lower emission of carbon and other types of pollution. In 2019, renewable energy sources accounted for about 11% of total U.S. energy consumption and about 17% of electricity generation. With equal share in U.S. electricity generation, the biomass contributes with 2% of the total electricity generated. In nature, if biomass is left lying around on the ground it will break down over a long period of time, releasing carbon dioxide and its store of energy slowly. By burning biomass its store of energy is released quickly and often in a useful way. So, converting biomass into useful energy imitates the natural processes but at a faster rate. The biomass comes from a variety of sources, Figure 1-6, which includes:

- Wood from natural forests and woodlands
- Forestry plantations
- Forestry residues
- Agricultural residues such as straw, Stover, cane trash and green agriculture wastes
- Agro-industrial wastes, such as sugarcane bagasse and rice husk
- Animal wastes
- Industrial wastes, such as black liquor from paper manufacturing
- Sewage
- Municipal solid wastes (MSW)
- Food processing wastes

Biomass conversion systems reduces greenhouse gas emissions in two ways. Heat and electrical energy are generated which reduces the dependence on power plants based on fossil fuels. The greenhouse gas emissions are significantly reduced by preventing methane emissions from decaying biomass. Moreover, biomass energy plants are highly efficient in harnessing the untapped sources of energy from biomass resources and helpful in development of rural areas.
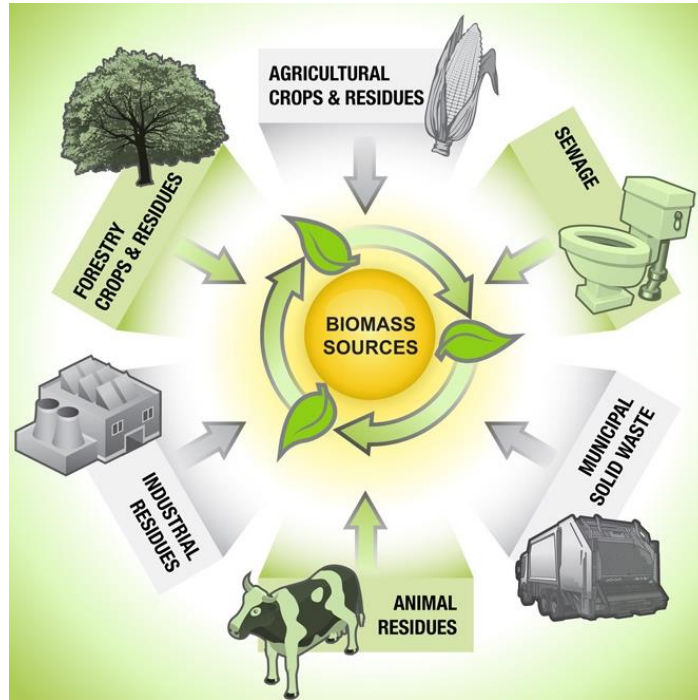
Figure 1-6: Biomass Sources

1.3.2.1 Agricultural Residues

Crop residues encompasses all agricultural wastes such as bagasse, straw, stem, stalk, leaves, husk, shell, peel, pulp, stubble, etc. Large quantities of crop residues are produced annually worldwide and are vastly underutilized. Rice produces both straw and rice husks at the processing plant which can be conveniently and easily converted into energy.

Significant quantities of biomass remain in the fields in the form of cob when maize is harvested which can be converted into energy. Sugar cane harvesting leads to harvest residues in

11

the fields while processing produces fibrous bagasse, both of which are good sources of energy. Harvesting and processing of coconuts produces quantities of shell and fiber that can be utilized.

Current farming practice is usually to plough these residues back into the soil, or they are burnt, left to decompose, or grazed by cattle. These residues could be processed into liquid fuels or thermochemically processed to produce electricity and heat. Agricultural residues are characterized by seasonal availability and have characteristics that differ from other solid fuels such as wood, charcoal, char briquette. The main differences are the high content of volatile matter and lower density and burning time.

1.3.2.2   Animal Waste

There are a wide range of animal wastes that can be used as sources of biomass energy. The most common sources are animal and poultry manure. In the past this waste was recovered and sold as a fertilizer or simply spread onto agricultural land, but the introduction of tighter environmental controls on odor and water pollution means that some form of waste management is now required, which provides further incentives for waste-to-energy conversion.

The most attractive method of converting these organic waste materials to useful form is anaerobic digestion which gives biogas that can be used as a fuel for internal combustion engines, to generate electricity from small gas turbines, burnt directly for cooking, or for space and water heating.

1.3.2.3   Forestry Residues

Forestry residues are generated by operations such as thinning of plantations, clearing for logging roads, extracting stem-wood for pulp and timber, and natural attrition. Harvesting may occur as thinning in young stands or cutting in older stands for timber or pulp that also yields tops

and branches usable for biomass energy. Harvesting operations usually remove only 25 to 50 percent of the volume, leaving the residues available as biomass for energy.

Stands damaged by insects, disease or fire are additional sources of biomass. Forest residues normally have low density and fuel values that keep transport costs high, and so it is economical to reduce the biomass density in the forest itself.

1.3.2.4 Wood Wastes

Wood processing industries primarily include sawmilling, plywood, wood panel, furniture, building component, flooring, particle board, moulding, jointing and craft industries. Wood wastes generally are concentrated at the processing factories, e.g., plywood mills and sawmills. The amount of waste generated from wood processing industries varies from one type of industry to another depending on the form of raw material and finished product.

Generally, the waste from wood industries such as saw millings and plywood, veneer and others are sawdust, off-cuts, trims, and shavings. Sawdust arises from cutting, sizing, re-sawing, edging, while trims and shaving are the consequence of trimming and smoothing of wood. In general, processing of 1,000 kg of wood in the furniture industries will lead to waste generation of almost half (45 %), i.e., 450 kg of wood. Similarly, when processing 1,000 kg of wood in sawmill, the waste will amount to more than half (52 %), i.e., 520 kg wood.

1.3.2.5 Industrial Wastes

The food industry produces many residues and by-products that can be used as biomass energy sources. These waste materials are generated from all sectors of the food industry with everything from meat production to confectionery producing waste that can be utilized as an energy source.

Solid wastes include peelings and scraps from fruit and vegetables, food that does not meet quality control standards, pulp and fiber from sugar and starch extraction, filter sludges and coffee grounds. These wastes are usually disposed of in landfill dumps.

Liquid wastes are generated by washing meat, fruit and vegetables, blanching fruit and vegetables, pre-cooking meats, poultry and fish, cleaning, and processing operations as well as wine making.

These waste waters contain sugars, starches, and other dissolved and solid organic matter. The potential exists for these industrial wastes to be anaerobically digested to produce biogas, or fermented to produce ethanol, and several commercial examples of waste-to-energy conversion already exist.

Pulp and paper industry are one of the highly polluting industries and consumes large amount of energy and water in various unit operations. The wastewater discharged by this industry is highly heterogeneous as it contains compounds from wood or other raw materials, processed chemicals as well as compound formed during processing. Black liquor can be judiciously utilized for production of biogas using anaerobic UASB technology.

1.3.2.6   Municipal Solid Wastes and Sewage

Millions of tons of household waste are collected each year with the vast majority disposed of in open fields. The biomass resource in MSW comprises the putrescible, paper and plastic and averages 80% of the total MSW collected. Municipal solid waste can be converted into energy by direct combustion, or by natural anaerobic digestion in the engineered landfill.

At the landfill sites, the gas produced, known as landfill gas or LFG, by the natural decomposition of MSW (approximately 50% methane and 50% carbon dioxide) is collected from the stored material and scrubbed and cleaned before feeding into internal combustion engines

14

or gas turbines to generate heat and power. The organic fraction of MSW can be anaerobically stabilized in a high-rate digester to obtain biogas for electricity or steam generation.

Sewage is a source of biomass energy that is very similar to the other animal wastes. Energy can be extracted from sewage using anaerobic digestion to produce biogas. The sewage sludge that remains can be incinerated or undergo pyrolysis to produce more biogas.

1.3.3 Thermochemical Conversion Process

The conversion process of biomass depends upon many factors, such as quantity and nature of feedstock, environmental regulations, the required energy. There are three major products usually produced from biomass: transportation fuel, heat/power generation and chemical feedstock. The first two types of products are energy related and could be produced from biomass through thermo-chemical technology. There are four different conversion processes available within thermo-chemical technology. These processes are combustion, gasification, pyrolysis and liquefaction. Figure 1-7 shows the temperature range for the thermochemical conversion processes. Pyrolysis and gasification of wastes are efficient solutions over direct combustion, as it can produce liquid/syngas fuels of medium to high heating value, which can be utilized with the currently available infrastructure for energy and power generation, and transportation. Thermochemical conversion methods such as gasification are industrially viable options compared to biochemical conversion methods such as anaerobic conversion due to the high reaction rates provided by gasification. Gasification is an efficient thermochemical decomposition of solid carbonaceous material to product gases of higher heating value compared to the solid precursor in the presence of gasifying agents such as steam, air, or CO_2. The major components of product gas are H_2, CO, CO_2, CH_4, and other higher hydrocarbons.
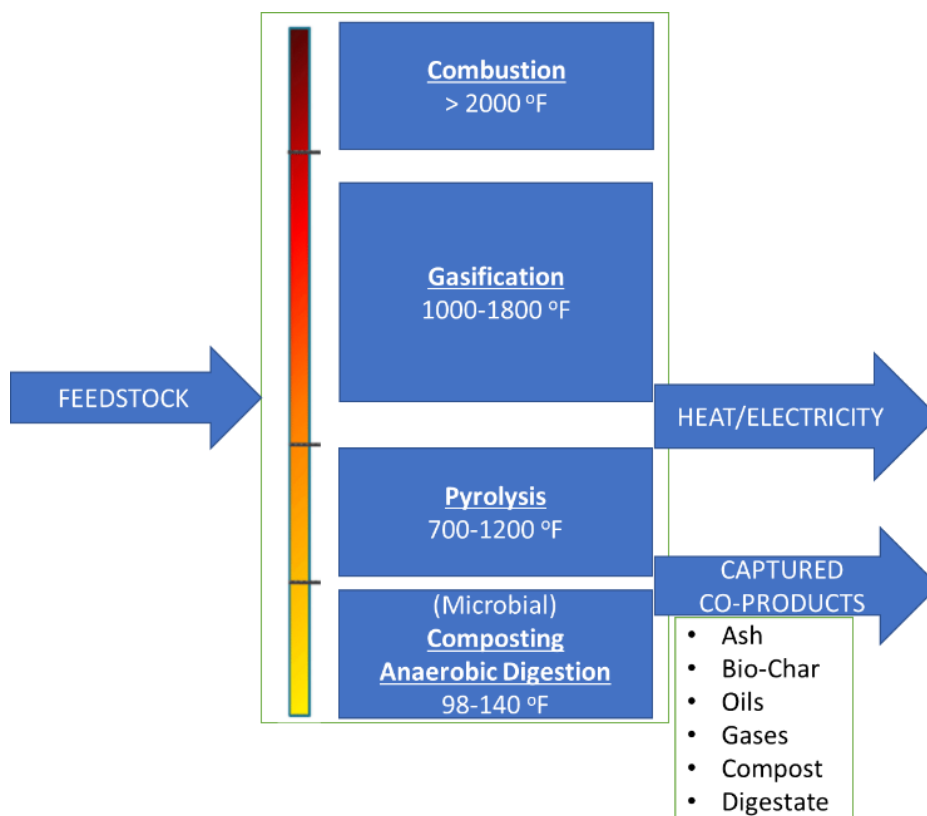
Figure 1-7: Overview of thermal conversion processes

Figure 1-8 shows different stages of a waste fuel particle undergoing during heat-up in a thermochemical gasification reactor. After feeding the particle it is dried and the humidity leaves the particle as steam. Beyond a temperature of about 200°C devolatilization occurs and gaseous components are released from the particle. These components are the main source for the undesired components in the product gas that is summarized later as tar. The amount of volatiles released can be very low (e.g., for hard coals below 10 wt.%) but also high (e.g., 75wt% - 85 wt.% for biomass) and can reach even 100 wt.% (e.g., for plastics). After the devolatilization stage of the fuel particle the so-called char remains. To convert char into a gaseous form a gasification agent is necessary. Above temperatures of about 700°C the kinetics of heterogeneous gasification reaction are high enough to observe a remarkable char gasification. The primary products from the heterogeneous gasification reactions are mainly permanent gases such as CO, H2, CO2, and CH4.

16

Finally, ash is produced that contains some residual char due to the reducing conditions in the gasification reactor; heat is necessary in all three stages of the gasification process.
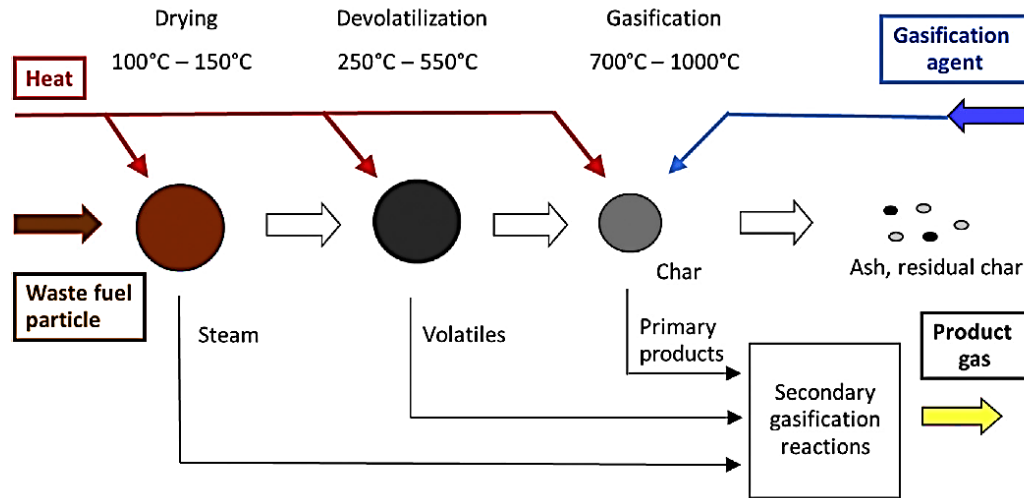
Figure 1-8: Gasification Process

In this study, a comprehensive study of the different factors will be carried out experimentally to determine the optimum conditions that would lead to faster conversion rates with less energy supplied.

1.4 Organization of Material

Chapter 1 gives a brief introduction to the gas turbine system with the identification of major challenges involved to improve the system efficiency as well as the life of turbine blades. In addition to a brief introduction of the importance of using biomass resources to solve critical problems that have been generated by the usage of fossil fuels.

Chapter 2 presents a literature review of the previous work done by researchers in the area of combustor, in particular the dilution zone in the combustor. Furthermore, a separate literature review of the optimum use of biomass resources and the techniques used for biomass energy conversion.

Chapter 3 gives a detailed description of the experimental setup used for both projects, the different steps used, the test procedures and the cases studied.

Chapter 4 discusses the results for the case studies in the dilution zone in the combustor with a comparison of various passive dilution techniques to come up with the optimum design that gives the most uniform temperature profile at the exit section. Detailed experimental cases considered, and their findings are explained in this chapter a long with a computational fluid dynamics model compared with the experimental results.

Chapter 5 presents the experimental results obtained for the optimum use biomass resources using different thermochemical conversion techniques. Several blends have been mixed together and compared based on several parameters to find the optimum operating conditions the best blend based on different chemical kinetics parameters.

Chapter 6 Conclusion and Future Work.

CHAPTER 2- LITERATURE REVIEW

2.1   Temperature Distribution along Gas Turbine Blades

The increase of turbine inlet total temperature is always a demand to improve the performance of a gas turbine in terms of the efficiency and power. Consequently, the continuous improvement of the gas turbines metallurgy makes it possible to operate with an inlet turbine temperature in the range of 1700 ^{o}C (Powel, 1991) [80]. In modern military jet engines like the Snecma M88 (Corde, 1991) [14] the turbine temperature is 1,590 ^{o}C. However, the challenges were not limited only on increasing the temperature but on how to manage the highly non-uniform flow fields exiting from the combustor. These non-uniformities include the pressure, velocity and, most importantly, temperature. As one of non-uniformities, the turbine inlet temperature distortion (hot streaks) grasps the attention of the researchers to study their immigration. Jenny et al. [45] studied the effect of hot steak migration on turbine blades. The results show that the hot streaks cause localized hot spots on the blade surface which lead to high heat loads and catastrophic failure of the blades. Furthermore, with the hot steak migration in a turbine stage, Basol et al (2011) [5] found numerically that tracking the hot streak migration led to a heat load redistribution in the rotor row in the spanwise direction. The study helps to facilitate the design of the combustor temperature profiles in circumferential direction to have an optimum heat load distribution on the rotor blade leading to an overall increased blade life. To model unsteady combustion hot streak migration, Busby et al (1999) [9] investigated the use inviscid limbed deterministic stresses is viable option to show the effect of hot streak on turbine blade tip and outer air seal loads.

Another study by Qureshi et al. (2012) [85] shows the effects of turbine inlet temperature distortion on the heat transfer and aerodynamic characteristics. The effect of a predominantly

radial temperature profile is a considerable reduction of time-averaged heat load on the rotor casing, roughly consistent with the change in adiabatic wall temperature expected at the wall. The effect is reduced deeper into the rotor passage because of additional mixing in the rotor. Roback and Dring (1993) [88] studied the effects of the hot streaks on turbine rotor airfoil surface temperature. They concluded that rectification of hot streams of fluid passage can produce a large difference in the adiabatic recovery temperature. Povey and Qureshi (2009)[78] introduced numerous definitions and terminologies used to describe and quantify temperature distortion in combustors using six combustor simulators. Saxer and Felici (1996) [92] provided a comparison between the time averaged solution and the steady-state solution, in which the circumferential variations introduced by the streak are cut off (but not the radial variations). The results show that the tangential temperature distortions at the rotor inlet have a stronger effect on the radial secondary flow than the streak radial variations. Hence, accurate predictions of temperature distributions in the presence of streaks of hot gas require any numerical procedure to account for unsteady as well as three-dimensional effects.

The developed two- and three-dimensional Navier- Stokes analyses by Rai et al (1990) [86] showed the redistribution of inlet temperature in a turbine. These analyses were used by Dorney et al. (1992) [20] who experimentally studied the effect of the hot streaks on the secondary flows and wall temperature of turbine rotor. The main purpose of the study was to understand the physical mechanisms that control hot streaks migration through a turbine stage that is leads to hot spots on the rotor high pressure surface. Furthermore, in the hot streak migration, Takahashi et al (1991) [99] found that the redistribution of the hot streak in the second stator passage was much different than rotor passage which shows that the periodic unsteadiness of hot streak migration.

The temperature profile along the turbine blades is like a parabola or a sinusoidal as demonstrated by Povey and Qureshi (2008) [77].

Butler [10] injected a heated carbon dioxide to trace the hot streaks migration. The energy transfer at the end wall of the turbine blade was decreased because of inlet temperature distortion as explained by (Povey et al (2007) [79] and Qureshi et al (2011) et al [84]) More studies were conducted to know the reason for this temperature distortion and what are the factors affecting the combustor exit flow fields through the dilution hole parameters. Haldeman and Walker (1977) [39] created and developed an empirical model to predict the temperature distribution based on scaling parameters such as diameters ratios, density ratios, and downstream distance of injection showed a great effect on jet penetration and temperature profiles. In addition, momentum flux ratios and the mixing length of opposed and offset rows of jets was studied by (Haldeman et al (1984) [40] and Gupta et al (2016) [31]).

Stevens et al (1988) [96] studied the effects of the jets in crossflow to show that the flow fields characteristics vary randomly from one jet to another where each jet has its own characteristics. This is responsible for the irregularity of the temperature at the combustor exit. More research was conducted to solve this irregularity in temperature to reduce the thermal stresses. Dai et al. (2014) [17] studied multiple jets in confined crossflow and compared the mixing quality of aligned and staggered holes configuration. The results showed that the staggered holes give more uniform temperature and velocity profile at the combustor exit. Hatch et al. (1995) [34] experimented with studying geometry and flowing influences on jet mixing in a cylindrical duct. The results showed that the depth of penetration for a fixed number of orifices achieves affects the mixture uniformity. In addition, the average depth of penetration to the center is desirable for the overall mixing standpoint.

Crocker and Smith (1995) [16] introduced an angel dilution jets to enhance the circumferential mixing at the expense of jet penetration. Another investigation conducted by Elgammal et al. (2016) [23] which is the insertion of a streamlined body to improve the mixing quality by diverting the hot stream towards the cold stream. To evaluate various dilution jet entry schemes, Norgen and Humenik (1968) [67] found that by enlarging and increasing the flush holes of rectangular shape both with and without external scoops helps in improving mixing conditions to provide good temperature profile. The jet to mainstream momentum flux ratio was studied by Holdeman et al (1973) [41]. It was observed that at a given momentum flux ratio the mixing conditions between the two streams is the best. In addition, it was found that the jet to mainstream momentum flux is an important parameter that influences the mixing quality where the mixing efficiency is increasing with the increase of flux ratio. For Witting et al (1984) [108], it was found that there is a large deviation between the experiment and correlation for higher differences in the momentum flux ratios for opposite jet injection.

Stevens and Carrotte (1988) [96] investigated experimentally the reasons behind the non-uniform temperature distribution of 16 heated jets injected into an annular cross flow. It was noticed that the distortion in temperature distribution is caused by the jet structure by the exit velocity profile. Liou et al (1991) [56] studied the turbulent mixing of two confined jets. It was found that the side-inlet-angle has a great effect on the mixing quality. As well it was found at a given Reynolds number and axial station, the mixing quality is increasing when the side inlet velocity is increasing which strengthen the results obtained from Holdeman et al (1973) [41] and Witting et al (1984) [108]. Hatch et al. (1995) [34] investigated the effect of momentum and orifice geometry on the mixing characteristics. It was found for the same number of orifices, the degree of jet penetration and mixing circumferential downstream of injection plane are coupled with the

momentum flux ratio. On the other hand, for the same momentum flux, it was found that increasing slot aspect ratio and increasing inlet jet angle with respect to mainstream direction are responsible for decreasing jet penetration. Experimental and numerical researches were carried out to explore the features of the dilution jets and manipulate the number of related variables to achieve the homogeneity required in mixing with the hot gasses. Previous experimentation about jets size and spacing with respect to a rectangular duct height was done at different r and density ratios, and results of dimensionless temperature with 3-D coordinates showed that superiority of r over density ratio for mixing profiles [40]. An earlier work for the same author with similar conditions deduced that better mixing outcome can be attained at each r from a specific spacing to duct height proportionality [95]. In 1990, a 3-D simulation of small dilution zone targeted reducing the non-uniformity "pattern factor" at the exit plane, and it was found that the pattern factor has non-linear relation with "jet spacing/ duct height" ratio and increase with jet inlet turbulence [42]. Experimental and empirical studies investigated the flow field in the dilution zone in a combustion chamber with single row of round-jets in a straight duct, then an extensive study included realities of a combustion chamber such as: variation in the main-stream temperature, jet shape and arrangement, and wall convergence streamwise. The investigations on the temperature distribution sustained the importance of momentum-flux ratio and jet-orifice spacing (especially when equals the dividing-radius to even annulus areas) to the mixing control, meanwhile the cross-section area contraction and jet diameter were not much effective to the required uniformity [38]. Other studies and patents were introduced to improve the design and performance of the dilution zone in various combustors [[55],[81]]. Finally, recent work by Gupta et al. on the exact test-rig in the dissertation tested the attachment of jet deflectors (i.e., guide vanes) on the holes to direct the jet into the crossflow with an angle varying from 0º (full penetration counter flow) to 90º (full swirl transverse

flow) [32]. Experiments on different Re gave the advantage to the 30⁰ orientation for generating 30% more temperature uniformity than staggered wall holes mixing chamber with 1% additional pressure drop. Another investigation conducted by Gupta et al. is the insertion of the streamlined body (American football) to divert the primary flow towards the inject jets. Following the same procedures of guide vanes experimentation accompanied with LES simulations, the streamlined body enhanced the mixing with a low-pressure drop [32].

Finally, Elgammal conducted some a comparative analysis of the shape and size of the streamlined body. The results showed that increasing the blockage ratio and the aspect ratio of the streamlined body attain uniform temperature distribution at the exit duct [22].

As an extension, the research discussed in this paper aims to optimize the position and the orientation of the guide vanes to have a better mixing quality, less pressure drop and less thermal stresses to the guide vanes.

2.2 Biomass Energy Resources

Energy consumption in the world is predominantly from fossil fuels for transportation and electricity generation [69]. Fossil fuels cause problems such as air pollution, greenhouse gases, and environmental issues from the extraction. Also, high price fluctuation and possible fuel depletion are a threat to the fossil-fuel-based economy. Furthermore, society is turning into energy consumption monitoring and low carbon practices [57]. Consequently, interest in alternative and renewable energy sources has been heightened. In 2020, the generation of electricity was 19% from renewable sources, and it is expected to take 36% of the share by 2050 [69]. Biomass raises as one of the alternatives to meet the increasing energy demand because it is abundant, carbon-neutral, and clean. Biomass is defined as every organic material that can be converted to energy. Biomass can be classified into first, second, and third-generation biomass. The first-generation

24

biomass converts carbohydrates and starches into biofuel (e.g., corn). The second generation includes agricultural, animal waste, and wood, while the third generation refers to algae [86]. To convert biomass into usable bioproducts with three main technologies: (1) Mechanical conversion, (2) biochemical conversion and, (3) thermochemical conversion [68][70]. In mechanical conversion, mechanical forces reduce the size of the biomass. This step usually prepares the fuel for combustion or another thermochemical process. The biochemical process uses microorganisms to degrade biomass. Among the technologies used for biological decomposition are Anaerobic digestion and hydrolytic fermentation. Anaerobic digestion produces mainly methane, while fermentation produces ethanol [11],[71]]. Thermochemical uses heat to promote chemical reactions that decompose the organic matter in the biomass, yielding bio-oils and/or Syngas (depending on the temperature and atmosphere) [89], Pyrolysis uses an inert atmosphere such as (Nitrogen or Argon) to decompose the biomass in a reactor at elevated temperatures, the products of Pyrolysis are bio-oils, non-condensable gases and biochar. While gasification uses controlled amounts of oxygen to partially oxidize the fuel, producing Syngas and ashes [104].

There are three main technologies for Pyrolysis reactors, batch reactors, moving bed, reactors with movement caused by mechanical forces and reactors when the movement I caused by fluid flow (fluidized bed) [63]. The gas yield depends on several factors: (1) type of biomass, (2) particle size, (3) heating rate, (4) Temperature and residence time [65]. This study aims to review recent advances in the Pyrolysis of feedstock from the perspective of the kinetics and product yields.

2.2.1 Pyrolysis Process

Pyrolysis is a thermochemical process that decomposes the livestock in the absence of oxygen. Pyrolysis happens at medium temperatures (300-800°C) or high temperatures (800-1300°C) [70]. Pyrolysis products are (1) bio-oil (tar), (2) non-condensable gases (or Syngas) that is a mix of

different gasses such as H_2, CH_4, CO, C_2H_X, C_3Hx, and (3) char. The yield of each of these products depends on several factors, such as the kind of feedstock, temperatures, heating rates, and residence time [29]. According to the operating conditions, Pyrolysis can be classified as slow, fast, or flash Pyrolysis [72].

Slow Pyrolysis uses low heating rates (usually less than 10°C/s) and long residence times (from 5-30 min) [36]. Hussein showed that low hearing rate and high residence time promotes the completion of chemical reactions [44], giving as a result higher yields of Syngas and biochar. Vieira et al. [105] optimized slow Pyrolysis parameters for a fixed bed reactor. Results showed that the optimal conditions were given for the longest residence time and the slowest heating rate (5°C/min and 120 min).

Fast Pyrolysis uses heating rates higher than 100°C/s and residence times from 0.5 to 2 seconds. Fast Pyrolysis has the advantage of low residence time, reducing the overall cost of the process [116]. Besides, biochar yields are much lower in fast Pyrolysis compared with slow Pyrolysis reducing the solids handling. The main product of fast Pyrolysis is bio-oils.

Flash Pyrolysis uses heating rates greater than 500°C/s and residence times of less than one second. This technology requires special reactor configuration and very small particle size to ensure temperature uniformity [2].

Abundant research compares the yields of each technology. Yuan et al. (2017) [116] compares the biochar yields of fast and slow Pyrolysis of walnut shells, showing that the mechanism of biochar formations is similar in slow and fast Pyrolysis, but the yields of biochar in slow Pyrolysis are much higher than the yields of biochar in fast Pyrolysis. Al Arni (2018) [2] studied the conversion of bio-oil from sugarcane bagasse, finding that slow Pyrolysis produces more Syngas

and less bio-oil compared to fast Pyrolysis. Pyrolysis follows three main steps: drying, Primary Pyrolysis, and secondary Pyrolysis [102].

e) Drying

In the drying step, the moisture on the biomass is removed, moisture in livestock varies between 5-20% [21]. Biomass drying is mainly done to reduce the volume of the biomass and increase the efficiency of the thermochemical process. Reed et al. [87] showed that high moisture reduces the value of the fuel. The removal of moisture for biomass is usually done by thermal drying. However, thermal drying can be an expensive process, such as fuel's value, and energy cost from drying must be a trade-off. Researchers have focused on modeling drying processes to optimize drying conditions for biomass [27][33]. Studies conclude that small particle size and low heating rates are the most effective way to dry

f) Primary Pyrolysis

Primary Pyrolysis happens at temperatures between 250-600°C [65]; the chemical reactions are associated with the thermal cracking of Hemicellulose, Cellulose, and Lignin. Gaur et al. (1995) [26] compiled the degradation for different kinds of biomass, including the independent three components (Hemicellulose, Cellulose, and Lignin) using Thermal Gravimetrical Analysis (TGA). Gaur showed that Hemicellulose and Cellulose decompose at a faster rate than Lignin. Also, the peaks of degradation occur at temperatures between 270,340 and 380°C, respectively. Pyrolysis of biomass occurs in different sets of competitive reactions (such as char formation, depolymerization or methanation) [58]. Yang et al. (2007) [114] showed that the degradation of Hemicellulose and Lignin is highly exothermic for temperatures below 500°C; after that temperature, the endothermic reactions are dominant, and the degradation of Hemicellulose and Lignin become highly endothermic. The opposite behavior was observed for Cellulose. For

temperatures below 400°C the degradation of Cellulose was highly endothermic. However, after 400°C the exothermic reactions dominate the decomposition of Cellulose.

g) Secondary Pyrolysis

Secondary Pyrolysis occurs at temperatures from 600°C to 1,400°C. This stage further decomposes the products (tars) from the primary Pyrolysis, yielding Syngas, and char. Several publications [103] showed that hydrogen formation is promoted at higher temperatures, which increases the heating value of the Syngas. In addition, the char formed in the primary Pyrolysis can work as a catalyzer increasing the total degradation at higher temperatures

2.2.2 Gasification

Gasification is an efficient thermochemical decomposition of solid carbonaceous material to produce gases of higher heating value compared to the solid precursor in the presence of gasifying agents such as steam, air, or CO_2. The major components of product gas are H_2, CO, CO_2, CH_4, and other higher hydrocarbons. Undesirable by-products containing a mixture of heavy aromatic hydrocarbon residues, referred to as tar, are also formed, which must be further pyrolyzed or reformed to enhance the Syngas yield. The factors that affect the composition of Syngas evolved from gasification are Gasifying agent, temperature, feedstock composition, and other reactor operational parameters affect the composition of Syngas evolved from gasification. Production of homogeneous fuel (Syngas as intermediate) from heterogeneous biomass is a combination of sources including chicken manure, poultry litter, biomass, solid wastes, and coal makes it an attractive solution over direct combustion of these low-value heterogeneous feedstocks providing feed flexibility along with versatility. Abundant literature is available on the effects of using different catalysts, gasifiers, and favorable temperatures on biomass gasification [54]. Eq. 2-1 to

28

Eq. 2-5 show the major governing reactions (considering C to represent the biomass) that occur during gasification [37].

$$\text{Char Oxidation: } C + O_2 \Longrightarrow CO_2 \qquad (2\text{-}1)$$

$$\text{Boudouard Reaction: } CO_2 + C \rightleftharpoons 2CO \qquad (2\text{-}2)$$

$$\text{Water-gas shift Reaction: } CO + H_2O \rightleftharpoons CO_2 + H_2 \qquad (2\text{-}3)$$

$$\text{Water-Gas Reaction: } C + H_2O \rightleftharpoons CO + H_2 \qquad (2\text{-}4)$$

$$\text{Thermal Cracking: } C_nH_m \Longrightarrow C + C_xH_y + H_2 \qquad (2\text{-}5)$$
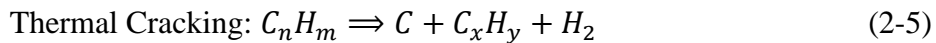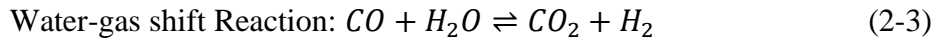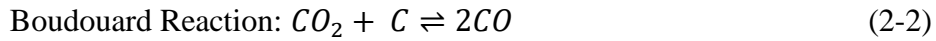
Figure 2-1 show that the United States consume about 9 billion chicken a year. The average chicken produces 2.5 Lb. of dry manure throughout the grow out period. With an average calorific value 10 MJ/kg of the chicken manure, that is equivalent to 60 million barrels of crude oil.
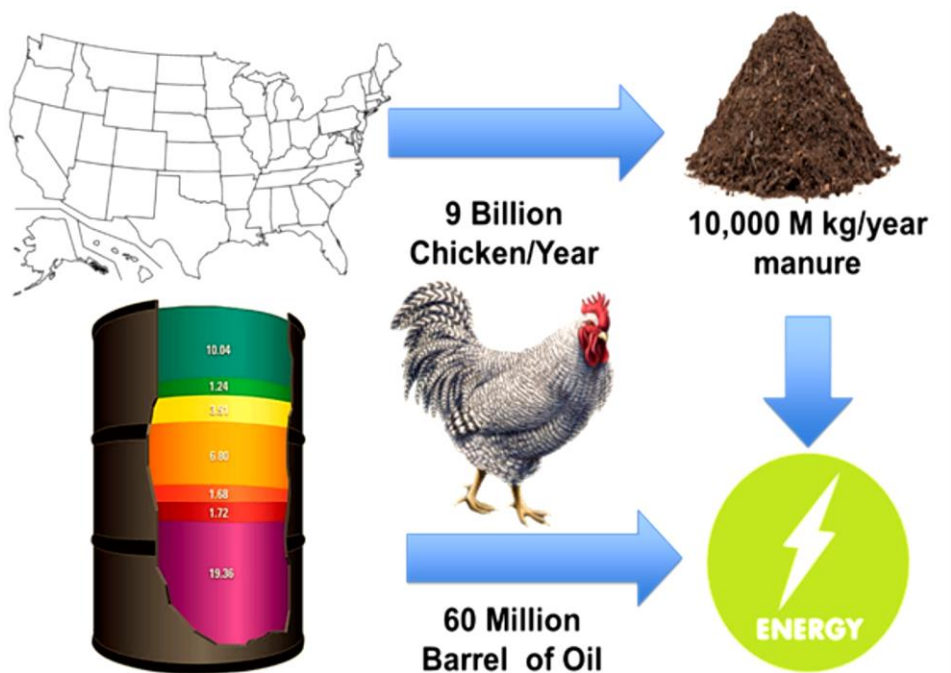
Figure 2-1: available energy in chicken manure produced by chicken consumed in the United States per year

Chicken droppings, waste beddings, waste food, and feathers from the coops form the major source from poultry litter. This biomass has high nitrogen content due to proteins and amino acids, high phosphorus, and ash content, making poultry litter a low-grade feedstock that is different from

other conventional biomasses such as wood. Such differences endeavor the motivation for an investigation into the pyrolytic behavior of chicken litter [52]. One of these differences investigated from thermal gravimetric analysis (TGA) was the start of decomposition at lower temperatures compared to coal, wherein the maximum weight loss rate was observed at 643 K [19]. The TGA results on the Pyrolysis of chicken litter showed three stages of weight loss, unlike woodchips Pyrolysis, which occurs in two stages because of lignocellulose content. Three stages of chicken litter decomposition observed from the TGA corresponding to the decomposition of Cellulose and Hemicellulose with a peak at a temperature less than that of wood chips, followed by manure and Lignin decomposition and the last stage of residual char devolatilization. This is unlike TGA of wood chips Pyrolysis, which showed only two stages [52]. Higher manure content assisted in the faster decomposition of waste litter. An increase in temperature increased Syngas yields, and decreased liquid and char yields [48]. CO2 yields increased due to decarboxylation of minerals carbonates in the ash at temperatures above 973 K until a stable value above 1273 K [1]. Highly viscous bio-oils produced from fast Pyrolysis of chicken litter had less acidity and higher heating value compared to bio-oils from hardwood due to the decomposition of protein content in a chicken litter into hydrocarbons [46].

Although the high inorganic content in the chicken litter can provide fertilizing capabilities, and catalytic activity in Syngas production, it causes handling difficulties due to the low fusion temperature of inorganics present since the chicken litter ash contains high amounts of Ca, Na, and K. Such high amounts of ash content (>20%) in a chicken litter with phosphorous and potassium oxides makes it an efficient fertilizer even after gasification [25]. The gas evolution from inorganic matter in manure, such as decarboxylation of carbonates and the low melting points of its constituents, induces error into the modeling of product gases from high temperature gasification

and Pyrolysis if ash is considered inert as in conventional models [82]. Chicken litter gasification was demonstrated by blending with coal and found no change in the heating value of product gas [53]. The ultimate analysis showed enough oxygen present in a chicken litter to gasify its carbon contents; such a method was called "auto gasification" [110]. This investigation also found ineffective availability of carbon to react with oxygen due to reactions with other hydrocarbons and water-gas reaction, causing oxidation of CO evolved to form CO_2. Use of catalysts in steam gasification of chicken manure in a fluidized bed at temperatures around 873 K produced Syngas rich in H_2 content and total gas yields with the addition of $Ni-Al_2O_3$ catalyst [111]. Supercritical gasification of chicken manure was also investigated [76],[112]. The abundant literature on biomass, although helpful in assessing chicken litter, concrete understanding of the differences with biomass, and effects of other gasifying parameters, is still lacking and much desired.

Using steam as the gasifying agent is known to generate a higher quality Syngas with high amounts of hydrogen content [[50],[59],[94]]. The high latent heat required for evaporation makes steam the most expensive gasifying agent, and thus long reaction time is undesirable. On the other hand, air, which is the cheapest agent generates the lowest quality Syngas and fastest reaction rates. Using a mixture of air (oxygen) and steam as the gasifying agent provides the benefit of improved Syngas quality while the exothermic reaction of air boosts the reaction rates. Steam can be injected at later stages in gasifiers [6] to reform the Syngas and improve its quality, or it can be mixed with air at the early stages of the gasification [3], to give even improved concentrations of hydrogen. The concentration of oxygen in the gasifying agent plays an important role in the quality of Syngas evolved and the rates of reaction. Thus, the oxygen concentration needs to be optimized to seek for the most feasible reaction conditions [115].

2.2.3 Co-Pyrolysis and Co-gasification

Co-Pyrolysis and Co-gasification are a viable option to enhance the performance of the thermochemical processes. Depending on the biomass mixed (and the ratio), synergetic effects can promote the Syngas yield, the energy of activation, or degradation rate. Guo et al. 2010 [30] demonstrated that the extractives in singular biomass could improve the thermal degradation of the biomass components (Hemicellulose, Cellulose). Mallick et al. (2018) [60] showed that the binary conversion of the biomass, depending on the ratio, can be considered as an additive equation.

Research has focused on mixing lignocellulosic biomass with coal [13],[24]. Results show that some biomasses can produce positive synergetic effects increasing the yield of volatiles without affecting the process. He et al. 2019 [35] mixed cotton and coal, results showed that the rate of decomposition increased for the co-Pyrolysis blends compared to the biomasses standalone.

Mixtures of lignocellulosic biomasses have been largely studied. Another common path is to mix lignocellulosic biomass with plastics. Burra et al. [8] studied the co-Pyrolysis of pinewood with plastic waste. Results show non-synergetic effects between the two biomasses. The best performance was obtained by mixing pinewood with BPC. Hossain et al. (2017) [43] studied the co-Pyrolysis of a solid tire with rice husk to show the possibility of getting liquid products that are comparable with petroleum fuels. However, these liquid products are only produced if the Pyrolysis conditions are correctly selected. Costa et al. (2014) [15] investigated mixing the rice husk with plastic waste using different pressures and residence time; an enhance in the biomass conversion was observed. Also, the best performance was obtained for lower pressure, high temperatures, and short residence times, or low-pressure low temperature and high residence time.

Co-gasification targets to promote reactions that yield hydrogen to increase the quality of the produced Syngas. Similarly, to Pyrolysis, mixtures of lignocellulosic biomasses have been largely studied. Ng et al. (2017) [66] studied air gasification of chicken manure, and woody biomass, an increase on the lower heating value (LHV) of the Syngas was accounted to the properties of chicken manure (softer, smaller size and loosely packaged). Dayananda et al. (2013) [18] experimentally studied the co-gasification of chicken manure and rice husk. Results show that the mixing ratio of 70% chicken manure and 30% rice husk produced the Syngas with the highest energy value. Seçer [93] studied the efficiency of co-gasification of biomass hydrolysates (products from hydrolysis), lignocellulosic biomass, and coal. Results conclude that biomass hydrolysates produce more hydrogen than the other biomasses because hydrolysis breaks down the structure of the biomass in smaller monomers, leading to higher Syngas yields. Co-gasification yields higher CO_2 due to the higher oxygen on biomass. However, this CO_2 is consumed on further reactions such as Boudouard reaction, which is later converted into hydrogen in other consecutive reactions (water-gas shift reaction).

The main objective of this thesis is to explain the chemical kinetics of the thermochemical conversion process for different biomass species. Consequently, it helps in explaining and gives a better understanding of some of the complicated thermochemical processes, such as co-Pyrolysis. Due to the mass production of these biomass species (chicken manure and cow manure), the chemical kinetics of different thermochemical processes were studied.

CHAPTER 3- EXPERIMENTAL SETUP AND PROCEDURES

3.1 Combustor Experimental Setup

Figure 3-1&Figure 3-2 display the experimental setup of the combustor simulator. The figure shows the main components of the experiment; fan, control panel, dampers, electrical heaters, the measurements location, and the test section (dilution section). The total flow, 1.73 m^3/s is supplied by a forced draft electrical fan coupled to 3 HP motor. With the help of the first damper the total flow can be controlled while the second damper is responsible for regulating the total flow rate into two streams: Primary stream (Hot stream) and Secondary stream (Cold stream). Downstream the second damper, the primary stream is heated by four sets of electrical heaters: two sets of $2 \times$ 1950 W each, and another two sets of 2×3700 W each. All heaters are distributed in the center duct (D_p= 40 cm). The outer duct (D_s=60 cm), where the secondary stream is kept always at room temperature, is insulated with cladding to minimize heat exchange between the two streams. Figure 2 shows the full dimension details of the combustor model.

1. Exit velocity measurements
2. Exit temperature measurements
3. Dilution section
4. Inlet temperature measurements
5. Inlet velocity measurements
6. Electrical heaters, 6a. Heaters arrangement
7. Damper locations, 7a. Internal view
8. Fan
9. Control panel
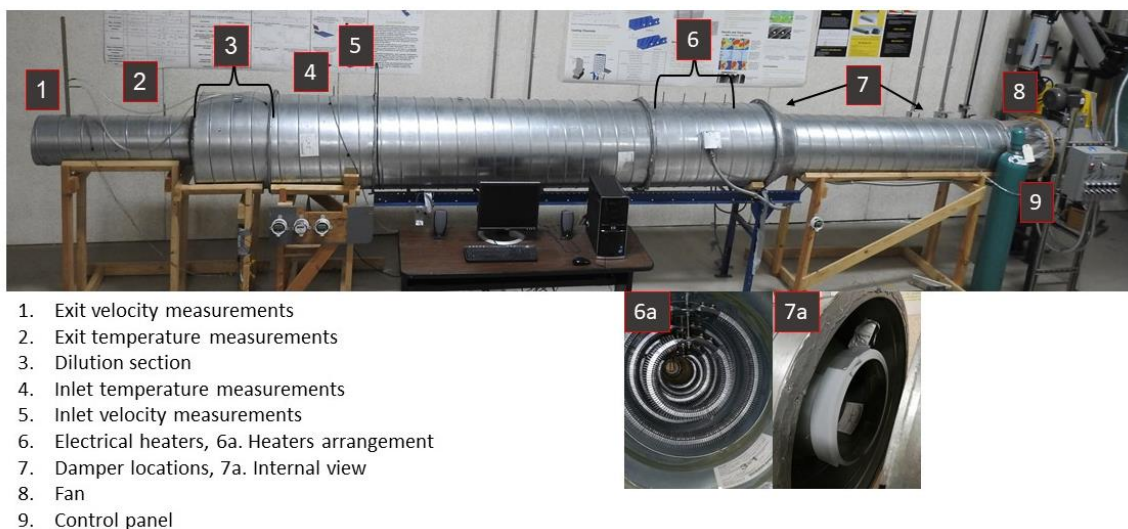
Figure 3-1: Experimental Setup

Figure 3-2: Dimension details of combustor model (All dimensions are in mm)

3.1.1 Experimental Setup Components

3.1.1.1 Fan

The fan is required to supply a pressure of 248 Pa at a 1.727 m³/s flow rate, Figure 3-3a. After the fan, there is a damper that is used to control the flow rate through the whole combustor as shown in Figure 3-3b.

Figure 3-3: (a) Fan installed on the fixture, (b) Volume dam per, and (c) Heater.

3.1.1.2 Control Panel

The control panel shown in Figure 3-4 is used to select the number of heaters to be operated depending on the primary air temperature required. The ambient air forms the secondary cooling air which is insulated from the hot primary air and flows into the test section through the dilution holes

Figure 3-4: Control panel for all the heaters.

3.1.1.3 Electrical Heaters

As shown in Figure 3-5 four sets of smaller (1950 W, 240 V and 0.225 m radius) and larger (3700 W, 240 V and 0.368 m radius) circular fin- strip heating elements were connected to provide approximately the required 19 kW of heat supply which is needed according to Eqn. (3-1). All these heaters can be controlled manually through the control panel.

Figure 3-5: Four Sets of heaters

$$E = m_\infty C_p \Delta T = \rho_\infty Q C_p \Delta T \qquad (3\text{-}1)$$

3.1.1.4 Pitot tubes

A set of two pitot tubes were installed in the experimental facility - one at the entry to the test-section and the other in the exit section at 0.2 m distance away from the test-section outlet. The static and dynamic pressure ca be read by using Fluke device, Figure 3-6.

Figure 3-6: Fluke Handheld Micro-manometer

3.1.1.5 Thermocouples

Thermocouples were used to monitor temperatures in the primary (or mainstream) flow, secondary (or diluent) flow and in measuring the temperature field at the exit of the combustor simulator. The primary inlet temperature was measured using 6 thermocouples zip tied equally at 3.8 cm to a threaded rod to record the temperatures along 42 a radial line, shown in Figure 3-7. One thermocouple was used in the annulus region to measure the inlet temperature of the diluent air. At the exit of the combustor simulator, 6 thermocouples zip tied equally at 2.5 cm to a threaded rod were utilized to collect the exit temperature data. All the temperature measurements in this study were made using 30-gage type 'K' thermocouples provided by the Modine Manufacturing Company in Milwaukee.
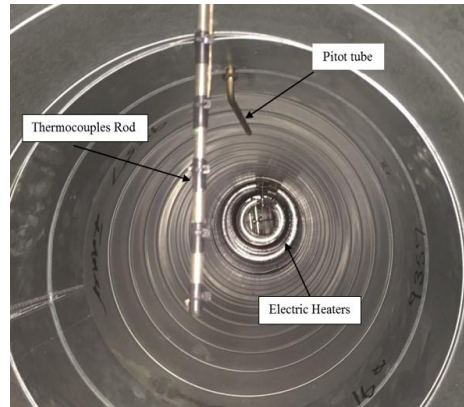
Figure 3-7: Thermocouples Array

The measuring devices are installed before and after the test, section to measure the inlet and exit flow parameters; temperature, velocity, and static pressure for the temperature Ni-Cr K-type thermocouples of ±2.2 °C standard uncertainty. Six sensors are spaced linearly by 3.8 cm, along the radius of the primary duct, and one sensor is used to measure the cold air temperature. The thermocouples are connected to 8 channel thermocouple input USB data acquisition module. Through the calibrated software, InstaCal[TM] the temperature readings can be displayed on the computer with sensor accuracy ±0.25°C. In terms of the velocity and pressure measurements, a sliding pitot-static tube is installed and connected to FLUKE®992 differential pressure flow meter with determined accuracies ±2.5% in velocity and ±1% + 1 Pa in pressure. The same set of devices is installed at the exit duct; the only difference is the radial spacing between the thermocouples, which is 2.5 cm starting from the center. To minimize the random error, all the readings were taken three times at the same condition within a short time, then the final value is averaged.

3.1.2 Test Section

Figure 3-8 shows the detailed dimensions of the staggered dilution holes in the test section. The staggered holes are arranged into Four rows. The two rows with larger holes of diameter 5 cm were located at 5 cm and 15 cm, respectively from the entrance to the cylindrical portion of the

test section. While the rows of smaller holes with diameter of 2.5 cm were positioned at 5 cm and 10 cm, respectively from the entrance to the conical frustum portion. Each row consisted of 16 holes equally distributed circumferentially, thus making a total of 64 dilution holes in the test section. The second row was staggered with respect to the first one.

Figure 3-8: Dilution Section Setup

3.1.3 Test Procedure

The fan is used to supply the total flowrate which is split into two main streams, primary and secondary air streams (Dilution stream) by damper. The primary stream is heated by four sets of electrical heaters while the secondary stream is kept at room temperature and directed through dilution holes via the secondary duct into the test section. Both streams are mixed in the test section (Dilution section). The temperature difference between the two streams was controlled by the numbers of heaters working through the control panels. Because of symmetry all the measurements were recorded along radial line before and after the test section.

3.2 Numerical Simulation

STAR-CCM+ 11.04 was used to simulate all the experimentally obtained results, seven cases, based on Finite Volume (FV) solver. For the volume meshing, the polyhedral cells were selected as they are more adaptive to the geometry; cylinder, swirling flow, and responsive in the situations of flow components change. Besides, the hexagonal prism layers mesh is applied to the wall surfaces to activate the calculations of accurate boundary layer modeling including the viscous sublayer for the turbulence model (low y+ ~1), Figure 3-9. Moving forward to the test section where the jet holes and guide vanes edges, Figure3-10 shows finer cell to capture the physics of swirl, tumble, wake region, and stagnation. Because of the large aspect ratio between the test section diameter and the guide vanes, the total number of cells chosen are 10million with ten prism layers on the solid surfaces to efficiently model the viscous sublayer. In addition, the 10 million cells are needed for the geometry surface quality and to fill the gaps compared to coarser mesh.
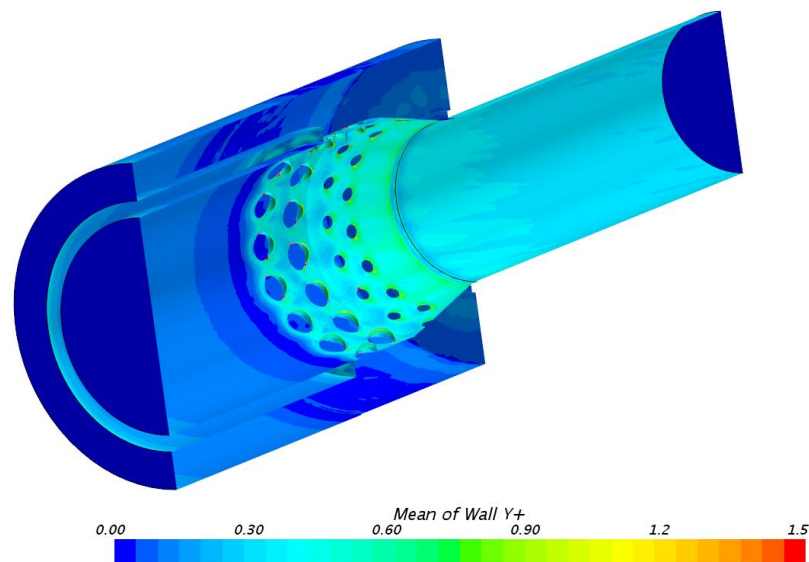
Figure 3-9: Y^+ Distribution over the test section
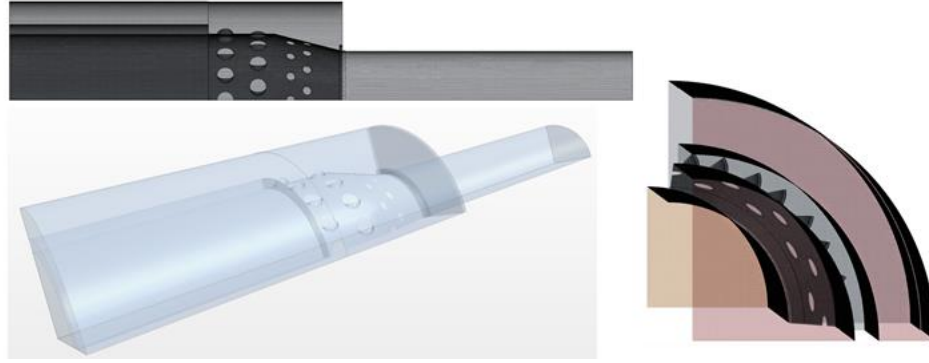
Figure3-10: Meshed Domain

Based on the experimental measurements, the boundary conditions were defined by the axial velocity and average temperature at the inlet for both streams (Primary and Secondary) and by pressure for the mixture at the outlet. The non-slip and adiabatic conditions were applied for the duct walls. Constant properties were assumed to be constant over the cross sections. The integral of the mass flux over the cross-section equation, Eq. (3-2), is used to determine the mean velocity, axial velocity. The simplified steady flow thermal energy equation, Eq. (3-3), is used to determine the average temperature. The ideal mixture velocity and temperature were calculated by using the Mass and energy conservations' equation, as shown in Eq. (3-4) and (3-5).

$$\dot{m} = \int_{A_c} \rho v(r,x) dA_c \approx 2\pi\rho \int_0^R v(r,x)r\,dr = \rho V_a A_c \qquad (3\text{-}2)$$

$$\dot{q} = \int_{A_c} \rho v C_p T dA_c = \dot{m} C_p T_{avg} \qquad (3\text{-}3)$$

$$AV_a|_P + AV_a|_S = AV_a|_m \qquad (3\text{-}4)$$

$$AV_a T_{avg}|_P + AV_a T_{avg}|_S = AV_a T_{avg}|_m \qquad (3\text{-}5)$$

3.2.1 Case Studies

All the locations on the combustor have been tested to achieve the best uniformity. Starting with internal guide vanes, Figure 3-11-Figure 3-12 show four different orientations of the internal guide vanes concerning the primary stream at the different locations. Each case has been conducted

at two different flowrates: full and half flowrate. The Reynold number was calculated for each

case based on the primary stream velocity (5 m/s & 2.5 m/s) with an inner diameter 0.4 m.
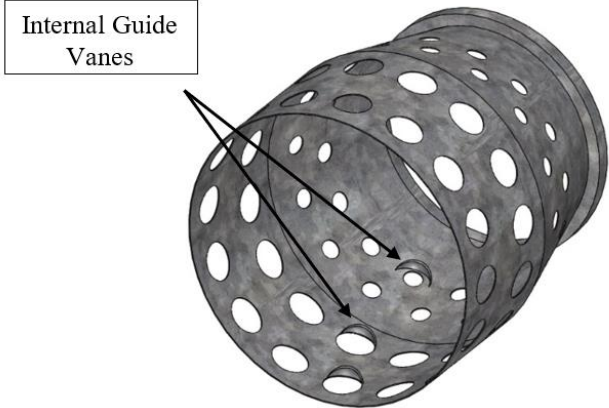
Figure 3-11: Internal Guide Vanes' Locations

a) 0º   b) 30º

c) 60º   d) 90º
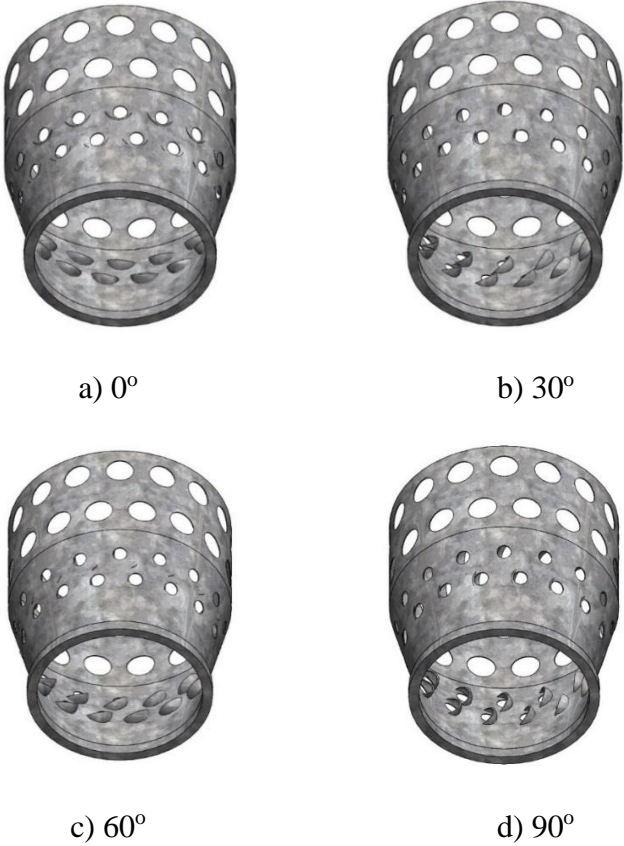
Figure 3-12: Four different orientations for the internal guide vanes on small holes
a) 0º b) 30º c) 60º d) 90º

42

a) 0° b) 30°

c) 60° d) 90°
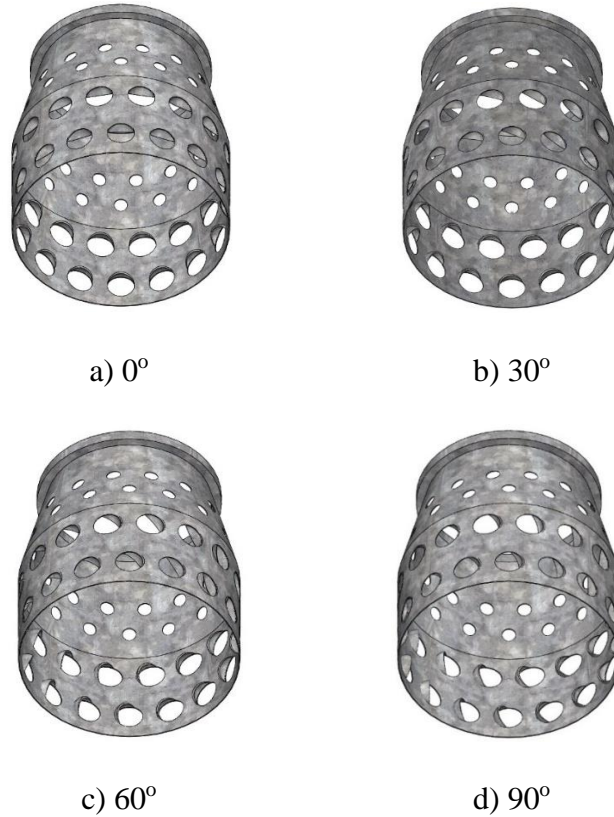
Figure 3-13: Four different orientations for the internal guide vanes on large holes

Based on the decision made from the previous results, another location, External Guide Vanes, have been studied the numerically and experimentally to be compared with the internal guide vanes at 3 different orientations as shown in Figure 3-14. The angle considered is with respect to the primary and secondary stream flow. The cases can be represented as follow:

1. Internal Guide Vanes with 0° orientation (0° INGV)

2. Internal Guide Vanes with 30° orientation (30° INGV)

3. Internal Guide Vanes with 90° orientation (90° INGV)

4. External Guide Vanes with 0° orientation (0° EXGV)

5. External Guide Vanes with 30° orientation (30° EXGV)

6. External Guide Vanes with 90° orientation (90° EXGV)
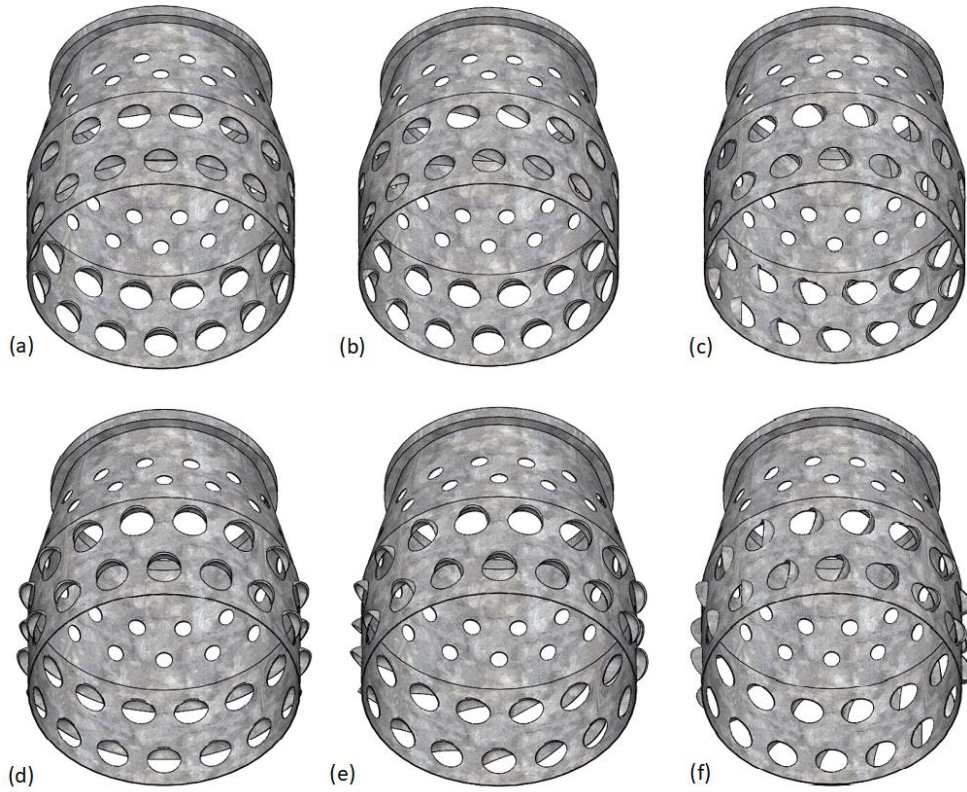
Figure 3-14: Guide Vanes at two different locations; Internal Guide Vanes (a) 0º, (b) 30º, (c) 90º. External Guide Vanes (d) 0º, (e) 30º, (f) 90º

Figure 3-15 shows all the proposed cases to enhance the thermal uniformity at the combustor exit. Four different angles were tested at Two different flow rates. The angle considered is for the primary and secondary streamflow. The cases can be represented as follow:

a) Standard Staggered Holes (SH)

b) $\Theta = 10º$

c) $\Theta = 20º$

d) $\Theta = 30º$

e) $\Theta = 45º$

(a)
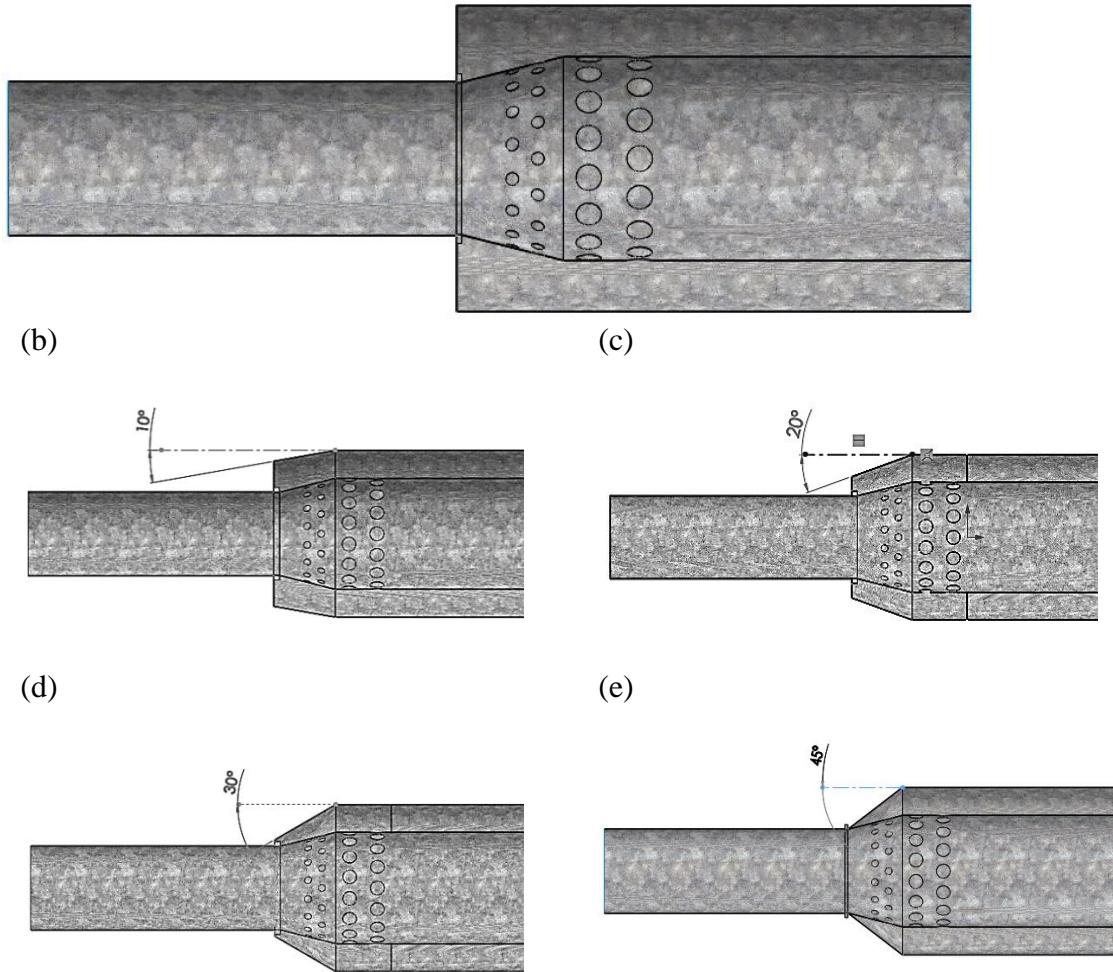
Figure 3-15: Proposed case studies for the combustor design a) Traditional Design b) 10-degree angle, c) 20 degree, d) 30 degree, e) 45 degree.

Since the large eddies contain most of the turbulence energy and are responsible for most of the momentum transfer and turbulent mixing, the turbulence model selected for these cases is Large Eddy Simulation (LES). The governing equations for LES are Navier-Stokes equations which are derived from the fundamental conservation laws for mass, momentum, and energy. The time step was 10^{-4} s, which was enough to satisfy low convective Courant number.

Evaluation Criteria

The evaluation criteria are divided into three sections to be able to select the proper technique, and they are as follow:

a) Temperature distribution

b) Total Pressure drops

c) Thermal stresses on Guide Vanes

Starting with the temperature distribution, since it is challenging to get the same actual temperature difference between the primary (hot) and secondary (cold) streams, dimensionless numbers were used to evaluate/compare the proposed techniques. In this paper, for all cases, the maximum temperature for the primary stream was below 400 K. Equation (3-6) is used to determine the equilibrium mixture fraction which relates the temperature difference between the equilibrium temperature and the secondary stream to the maximum temperature difference. The equilibrium mixture temperature, ideal mixture temperature, is determined from Eq. (3-7) (i.e.,$T_{avg}|_m = T_{eq}$) while the primary and secondary stream temperatures were measured using thermocouples.

$$f_{equil} = \frac{T_{eq} - T_s}{T_p - T_s} \qquad \text{3-6)}$$

Similarly, with replacing the equilibrium mixture temperature with the actual measured temperature at a local radial point, the actual mixture fraction can be obtained from eq. 6

$$f_{.} = \frac{T_m - T_s}{T_p - T_s} \qquad \text{(3-7)}$$

Based on equation 5 and 6, the uniformity factor (χ) can be calculated from eq. (3-8) to see how far the actual mixture fraction from the equilibrium mixture temperature. The smaller the value of (χ), it means that the actual exit temperature is close to equilibrium temperature (i.e., more uniform temperature distribution). The normalized mixture fraction is another valuable number,

eq. (3-9), to show the radial temperature deviation from the equilibrium value. The flatter

normalized mixture fraction curve, more uniform temperature distribution.

$$\chi = \frac{\sum |(f - f_{equil}).dr|}{R} \qquad (3\text{-}8)$$

$$f^* = \frac{f - f_{eq}}{f_{eq}} \qquad (3\text{-}9)$$

The total pressure drop across the test section cannot be neglected as it indicates the total

power loss from the turbine or the overall rise in the power consumption from the compressor to

get the same net power output. Finally, the thermal stresses on the guide vanes will be part of the

evaluation as it will affect their life span. shows a summary of the proposed techniques in this

thesis.

Table 3-1 shows a summary of the proposed techniques in this thesis.

Table 3-1: Tested Case Studied

Guide Vanes				Combustor Design			
Orientation	Internal Guide Vanes		External Guide Vanes	10º	20º	30º	45º
	(INGV$_s$)	(INGV$_L$)	(EXGV$_L$)				
0º	x	x	x				
30º	x	x	x	x	x	x	x
60º	x	x	-				
90º	x	x	x				

3.3 DTG Experimental Setup

Figure 3-16 shows the Differential Thermal Gravimetry (DTG) apparatus, which is used

simultaneously to perform the Thermogravimetric (TGA) and Differential Thermal Analysis

(DTA). The device is consisting of three main parts. The first part is the electric furnace, which

supplies the required heat of reaction and can be controlled to generate different heating rates and

then maintain the reaction at a constant desired temperature. The second part is the measurement

system, which consists of rods that are each fitted with thermocouples; then, both rods are connected to a sensitive balance mechanism. One of the detector rods is used as a reference/control, and it carries an empty sample cell, while the other rod is used to measure the changes of mass and temperature of the active sample cell relative to the control cell. The third part of the device is the autosampler, which is a robotic system capable of loading and unloading the samples on the detectors automatically. The weight difference between the two detectors, obtained by the delicate balance, indicates the sample weight. The difference between the voltage readings of the two sensors is measured for the differential thermal analysis. Any dry non-corrosive gas agent can be used with the device. The measurable range of the mass is ±500 mg, with a resolution of 1 µg and ±1% accuracy. The device can provide up to 1500 °C with ±1 °C uncertainty. The thermocouples used here are Pt-10%pt/Rh thermocouples. The measurable range for the differential thermal analysis is 1000 µV with ±1% µV accuracy and noise level less than 1 µV.

(a)   (b)
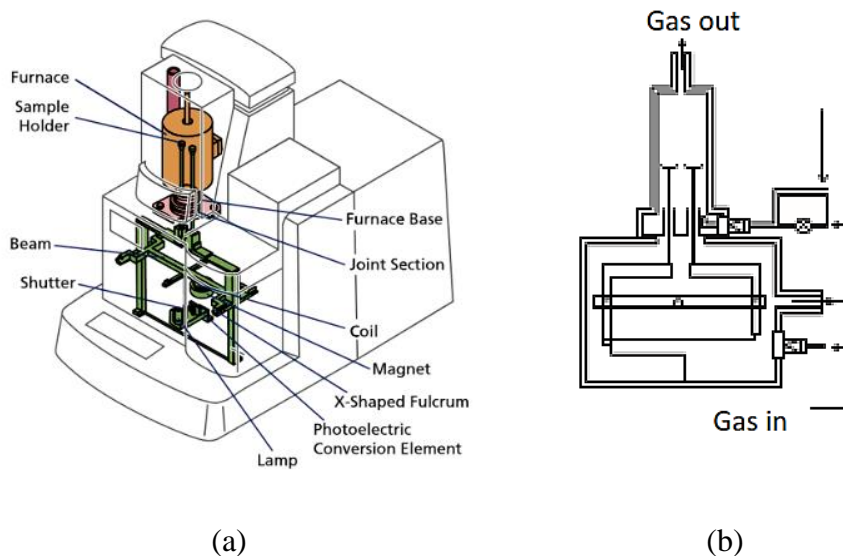
Figure 3-16: The Shimadzu DTG-60AH; (a) Main device components, (b) Gas flow through the device

To minimize the effect of gas turbulence on the readings, a regular calibration was performed on the device all over the temperature range and operating gas flow rate. Alumina pans were used for all case studies. Equation (3-10) is used to calculate the extent of reaction, while its rate is calculated by using Eq. (3-11). The Arrhenius rate expression was used as the first step of any kinetics model [107]. To calculate the activation energy, the following procedure was followed; equations (3-12) and (3-13) were combined to get equation (3-15), then by taking the natural log, Eq. (3-13) through (12) are used to calculate the activation energy where Eq. (3-13) and (3-14) are combined to get eq (3-15). Equation (3-16) is obtained by taking the natural log of Eq. (3-15), where the activation energy E_a and the exponent constant A can be obtained.

$$\alpha = \frac{w_0 - W_t}{w_0 - w_f} = \frac{v_t}{v_f} \tag{3-10}$$

$$\frac{d\alpha}{dt} = \frac{(\alpha_t - \alpha_{t-1})}{\Delta t} \tag{3-11}$$

$$k(T) = A \exp\left(\frac{-E_a}{RT}\right) \tag{3-12}$$

$$\frac{d\alpha}{dT} = \frac{k(T)}{\beta} f(\alpha) = \frac{A}{\beta} \exp\left(\frac{-E_a}{RT}\right) f(\alpha) \tag{3-13}$$

$$\frac{d\alpha}{dT} = k(T)(1 - \alpha)^n \tag{3-14}$$

$$\frac{d\alpha}{dT} = \frac{k(T)}{\beta} f(\alpha) = \frac{A}{\beta} \exp\left(\frac{-E_a}{RT}\right)(1 - \alpha)^n \tag{3-15}$$

$$ln\left(\frac{\frac{d\alpha}{dT}}{(1-\alpha)^n}\right) = \ln\left(\frac{A}{\beta}\right) - \left(\frac{E_a}{RT}\right) \tag{3-16}$$

3.3.1 OPERATION CONDITIONS

Chicken manure used in this study was dried chicken manure fertilizer of irregular form, with sizes ranging from 1 to 3 mm. The apparent density of particles measured from fluid immersion was 1.5 g.ml^{-1}. The ultimate and proximate analysis, along with the higher heating value (HHV) of the sample is given in Table 3-2

Table 3-2: Proximate and ultimate analysis of chicken manure and Cow Manure [64],[75]]

	Chicken Manure	Cow Manure
Proximate analysis (wt.% dry)		
Volatile content	65.56	62
Ash Content at 550 ºC	21.65	23
Fixed Carbon	12.8	15
Ultimate analysis (wt.% dry)		
Carbon	35.59	35.2
Hydrogen	4.57	3.1
Nitrogen	4.98	2.2
Sulfur	1.45	0.7
Oxygen	35.52	33.3
HHV (in MJ/kg)	13.15	16

3.3.2 Case Studies

Three different thermochemical conversion processes were tested with two different livestock manures. Figure 3-17 shows a schematic drawing for all the case studies with some of the operation conditions.

Table 3-3 shows 32 case study where each case was repeated at least two times to minimize random errors and the device was calibrated to minimize systematic errors.
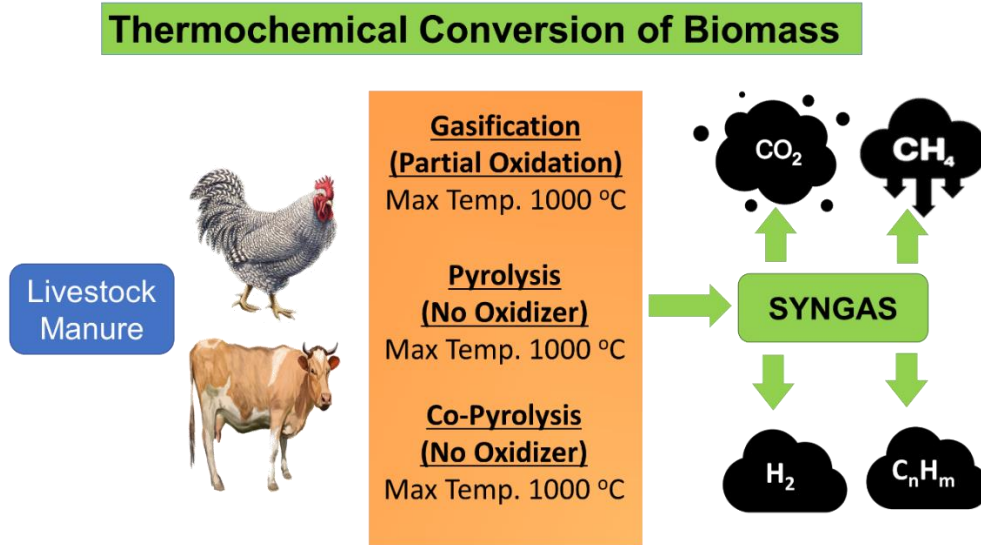
Figure 3-17: Schematic Drawing of the case studied

Table 3-3: Total Case Studied by DTG

Tested Sample	Technique	Gas Agent	Heat Rate (ºC/min)

			5	10	15	20	25	30	35	40
Chicken Manure	Pyrolysis	N2	√	√	√	√	√	√	√	√
Cow Manure										
Chicken + Cow Manures	Co-Pyrolysis	N2	√	√	√	√	√	√	√	√
Chicken Manure	Gasification	CO2	√	√	√	√	√	√	√	√
		Air	√	√	√	√	√	√	√	√
Cow Manure	Gasification	CO2	√	√	√	√	√	√	√	√
		Air	√	√	√	√	√	√	√	√
Sheep + Cow Manures	CO-Gasification	Air	√	√	√	√	√	√	√	√

CHAPTER 4- COMBUSTOR EXPERIMENTAL RESUTLS AND DICUSSION

4.1 Experimental and Numerical Study on the Use of Guide Vanes in the Dilution Zone

Effect of changing Internal Guide Vanes Location and Orientation. Increasing the angle decrease the depth while increasing the swirl. Both the depth and the swirl action are expected to give a positive effect to the mixing of primary and secondary flows, consequently achieving the temperature uniformity. Based on Eq. 3-5, Table 4-1 shows the uniformity factor for each case. Overall, it can be observed that the internal guide vanes on large holes at all orientations give a lower uniformity factor compared to the other location, on small holes. The 30° orientation on the large holes gives the lowest uniformity factor at both flow rates compared to different directions. The $0°$ guide vanes should give maximum penetration of the current secondary (or dilution) flow into the primary flow while the $90°$ guide vanes should provide the maximum swirl. It can be observed that 90° gives the highest uniformity factor at the two different flow rates and locations. For all cases, the uniformity factor of 60° doesn't differ much more from that one obtained from the 90° except only one case at half open damper on the small holes, as the uniformity factor for each case is 0.241 and 0.274 respectively.

Table 4-1: Comparison between internal guide vanes on small holes and on large holes based on the Uniformity Factor (χ) at two different flow rates

Damper Angle	Guide Vanes Orientation							
	0°		30°		60°		90°	
	Small	Large	Small	Large	Small	Large	Small	Large
Fully Open (Re= 1.1x10^5)	0.271	0.266	0.308	0.228	0.311	0.304	0.328	0.316
Half Open	0.242	0.227	0.183	0.133	0.241	0.253	0.274	0.262

(Re= 0.55x10^5)									

The normalized mixture fraction gives the same results obtained from the above table. Figure 4-1 shows, for full flowrate, the 30° INGVL gives the more flatten curve around the horizontal axis which reflects the more uniform temperature distribution followed by the 0° INGVL and 0° INGVs. It can be observed that 90° INGVs is the worst case regarding the normalized mixture fraction. In Figure 4-2, for half flowrate, the 30° INGVL gives the most flatten curve around the horizontal axis and thus the radial temperature distribution is uniform.
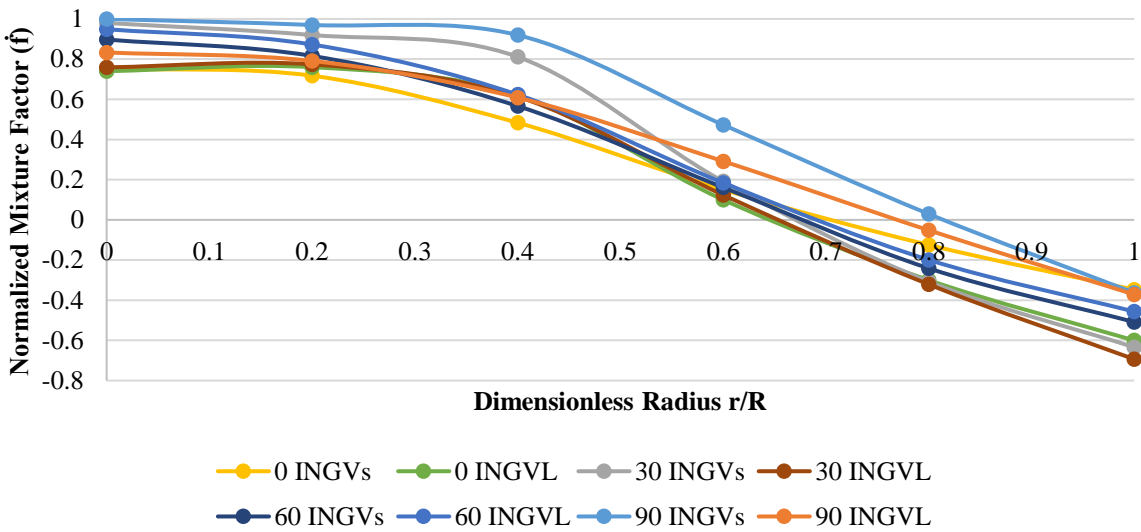
Figure 4-1: Radial distribution of the normalized mixture fraction, full flowrate
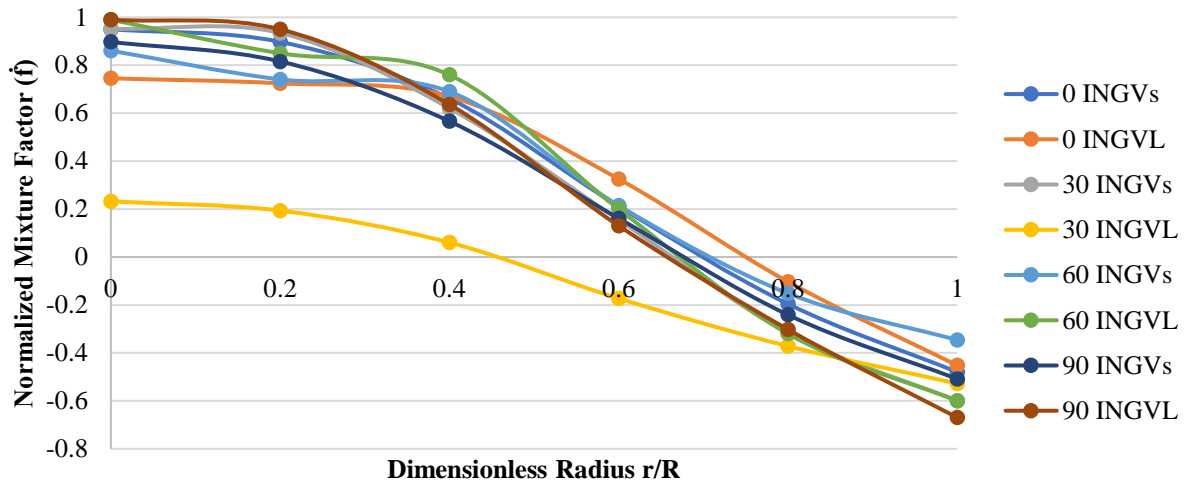
Figure 4-2: Radial distribution of the normalized mixture fraction, half flowrate

4.1.1 Mesh Independence and Validation

The validation and grid sensitivity analysis for computer simulation results is carried out based on the experimentally obtained data. The temperature and velocity profiles were used for the mesh independence and validation at two different cases. The total number of cells tested ranged from 6×10^6 to 12×10^6 with 2×10^6 step. For the axial velocity profile, Figure 4-3 show the axial velocity distribution at the combustor exit. A significant deviation can be observed from the 6M mesh (coarse mesh) compared to the experimental work. Increasing the total number of cells improves the results to be close to the experimental data but at the expense of the computational time. The 10M cells are the closest to the experimentally obtained results with a maximum average error of 11% for the velocity. For the temperature profile, it can be observed from Figure 4-4 that the experimental temperature near the center almost identical to the numerical one with a maximum error of 5% when moving to the wall. These maximum errors only occur near the wall. Three main reasons can explain these discrepancies. First, the experimental velocities are lower than the numerical one due to the flow losses at the joints. Second, the adiabatic wall condition is considered for the simulation that overestimated the temperature values, which, consequently, has

54

a great effect on the uniformity factor. In addition, the heat loss to the surrounding in the experiments, including radiation and natural convection, was not accounted for in the simulation. Third, the error generated from the measuring devices which already mentioned in the experimental setup section.

(a)   (b)
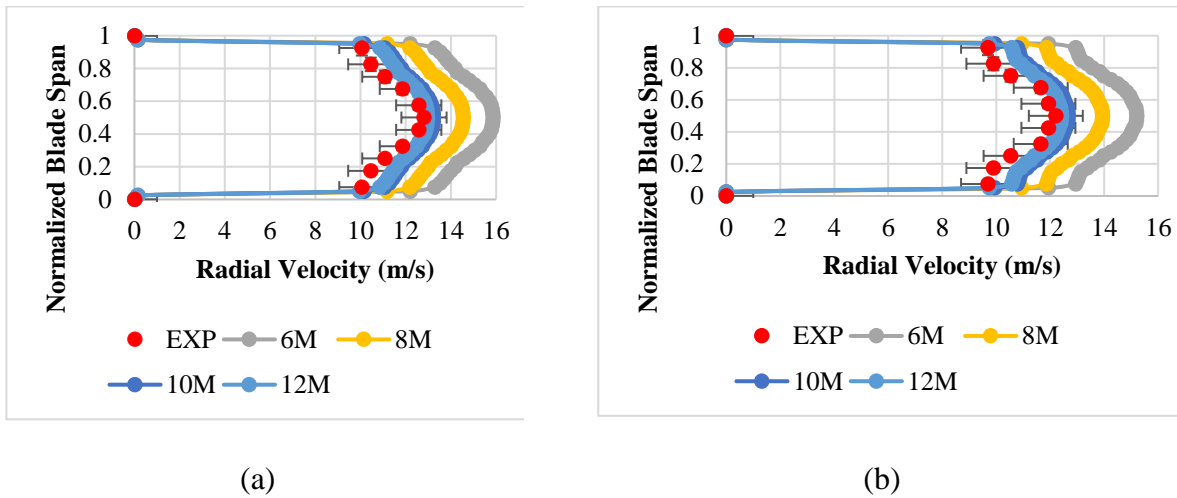
Figure 4-3: Mesh independence test of Radial velocity at combustor exit for (a) 0° INGV, (b) 30° INGV

(a)   (b)
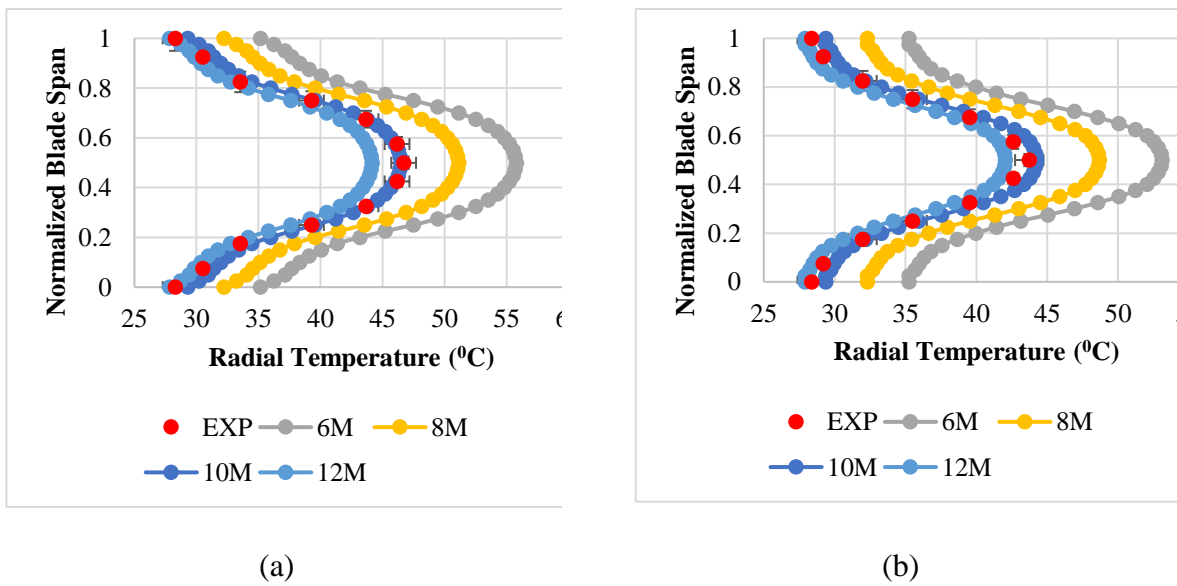
Figure 4-4: Mesh independence test of Radial temperature at combustor exit for (a) 0° INGV, (b) 30° INGV

55

4.1.2 Experimental and Numerical Outcomes

All cases were tested experimentally and numerically to make sure that the results are consistent and applicable. Two Reynolds number, 1.0×10^5 and 0.76×10^5, were tested to show the performance of the proposed techniques at high and low Reynold number. Since the depth of penetration and swirling are the two major factors affecting the mixing quality, the 0° guide vane should give the maximum penetration while the 90^0 gives the maximum swirl.

Temperature Distribution. Based on Eq. 3-8, it can be seen from Figure 4-5 that the external guide vanes give the lowest uniformity factor compared to the internal guide vanes installed at the same angle, experimentally and numerically, except for the 90° there is no significant difference. Taking the staggered holes as a reference, it can be observed that the 30° EXGV gives a 16% lower uniformity factor than the staggered holes while the internal guide vanes with the same angel give 13% only. For the 0° orientation compared to the staggered holes, the uniformity factor is lower by 10% and 6% for the external and internal guide vanes, respectively.

	SH	EXGV 0	EXGV 30	EXGV 90	INGV 0	INGV 30	INGV 90
EXP	0.313	0.282	0.262	0.320	0.294	0.272	0.314
NUM	0.298	0.278	0.258	0.310	0.282	0.268	0.310
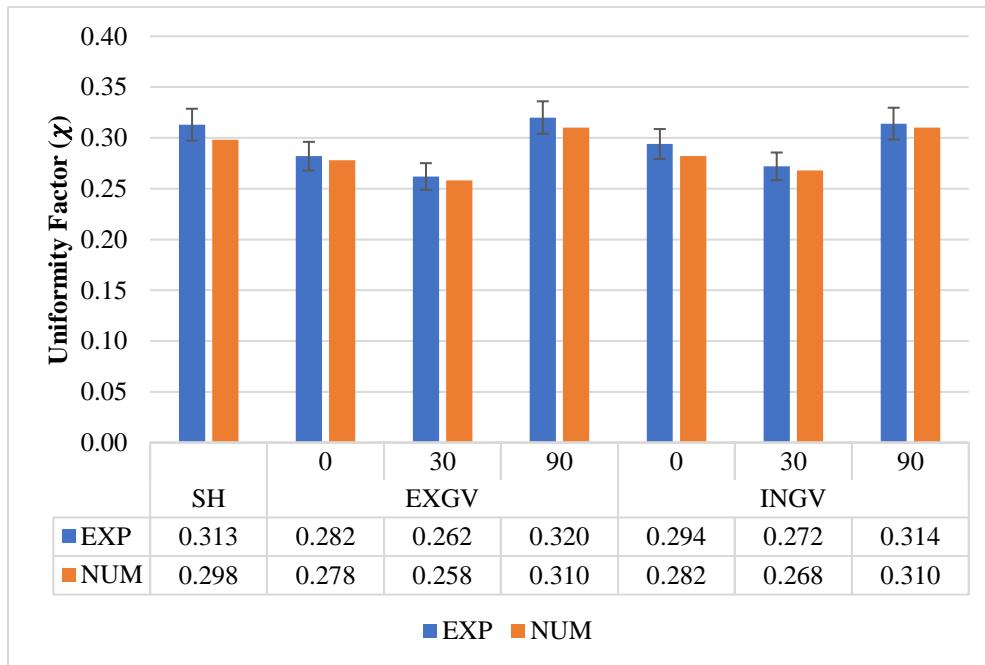
Figure 4-5: Uniformity Factor for different cases tested at Re=1.0 x10^5

In Figure 4-6, Reynold number is 0.76×10^5, the uniformity factor is reduced for all cases compared to the full flowrate (i.e., Re=1.0×10^5). The main reason for this reduction is the more residence time available inside the dilution zone due to lower flow rate conditions, which provided enough time for the mixing of the primary hot air and the cooler dilution air. For instance, the 30° EXGV at low Reynold number gives 34% lower than its corresponding at high Reynolds number, which means more uniform temperature distribution at the combustor exit. Also, at this flow rate, it gives about 25% more uniform temperature flow than the staggered holes while the 30° INGV gives 13% only. For the 0^0 orientation, the highest depth of penetration, the external guide vanes have a uniformity factor of 0.216 while internal guide vanes are higher with 5%. Still, the 90° is the worst case at both locations.

	SH	EXGV 0	EXGV 30	EXGV 90	INGV 0	INGV 30	INGV 90
EXP	0.231	0.216	0.173	0.221	0.227	0.201	0.243
NUM	0.221	0.206	0.165	0.216	0.218	0.192	0.232
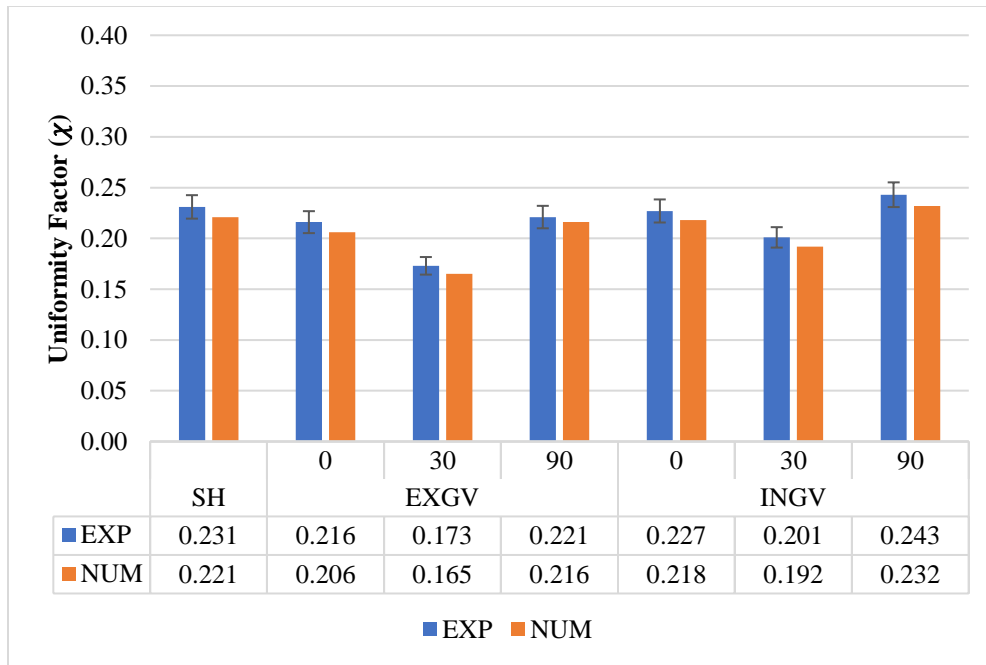
Figure 4-6: Uniformity Factor for different cases tested at Re=0.76×10^5

The radial distribution of the normalized mixture fraction at two different flow rates is shown in Figure 4-7 and Figure 4-8, which is given by Eq. (3-9) at the combustor exit for all cases. The more deviation of the mixture fraction from the equilibrium mixture fraction, the more is the non-

uniform temperature distribution. It can be observed that the temperatures are higher at the center of the combustor exit and decrease towards the wall. The good mixing between the hot and cold streams would result in more uniform flow conditions in the radial direction. The results obtained from the uniformity factor can be reflected clearly on the normalized mixture fraction. Figure 4-7 shows that the 30° EXGV has the flatter curve around the horizontal axis, which means that the radial temperature distribution is close to the equilibrium temperature followed by the 30^0 INGV. The 90^0 INGV is the worst case where the central temperature is the highest temperature among all other cases, which means poor mixing between the hot and cold streams. In addition, at the same guide vane orientation, it can be observed that the external guide vanes give a flatter curve compared to the internal ones. Figure 4-8 shows the normalized mixture fraction at low Reynold number. Taking the best two cases at each location, 30° EXGV, and 30° INGV, it can be depicted that the 30° EXGV gives the best result in terms of the temperature distribution.
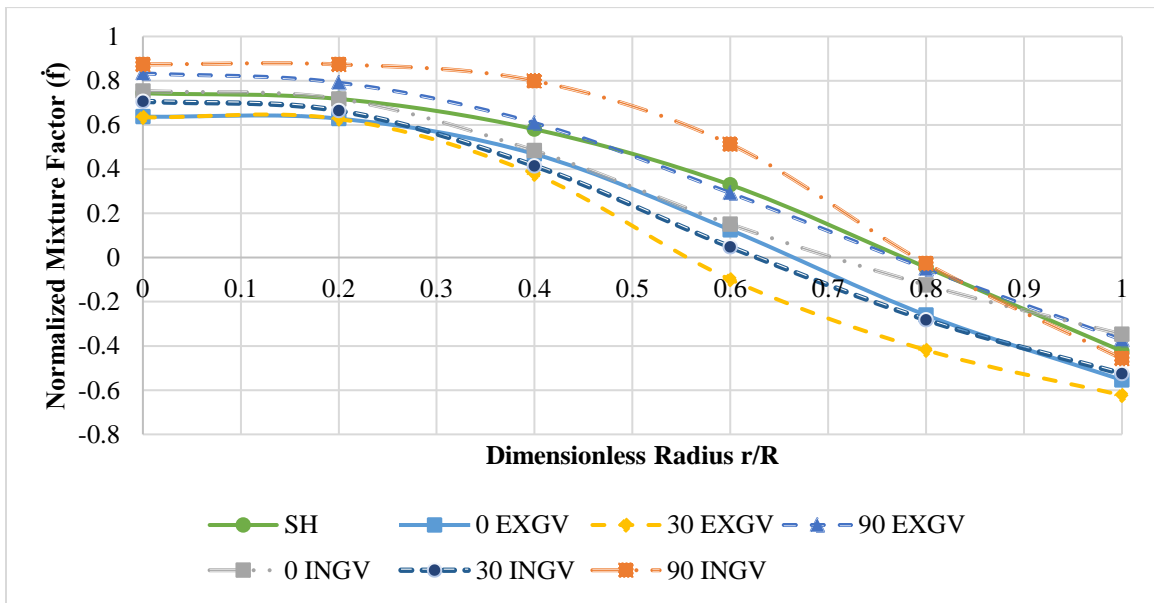
Figure 4-7: Normalized mixture fraction for different cases at Re= 1.0×10^5
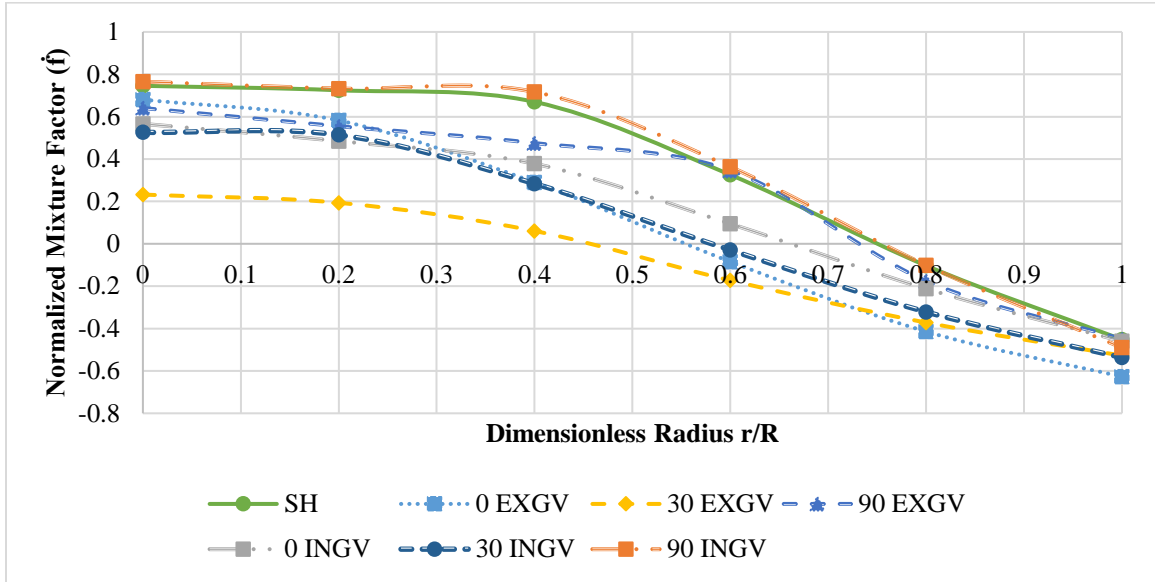
Figure 4-8: Normalized mixture fraction for different cases at Re=0.76×10^5

Figure 4-9 shows a significant explanation for these results. The external guide vanes are forcing the cold stream to penetrate the dilution section to be mixed with the hot stream. Consequently, a better mixing compared to the internal guide vanes, which are introducing a lesser amount of the cold flow. This is reflected in the temperature distribution at the combustor exit where the internal guide vanes give a higher interior temperature at the combustor exit.

(a)

(b)

(c)

(d)

(e)   (f)

Mean of Temperature (C)
21.800   26.292   30.784   35.276   39.768   44.260
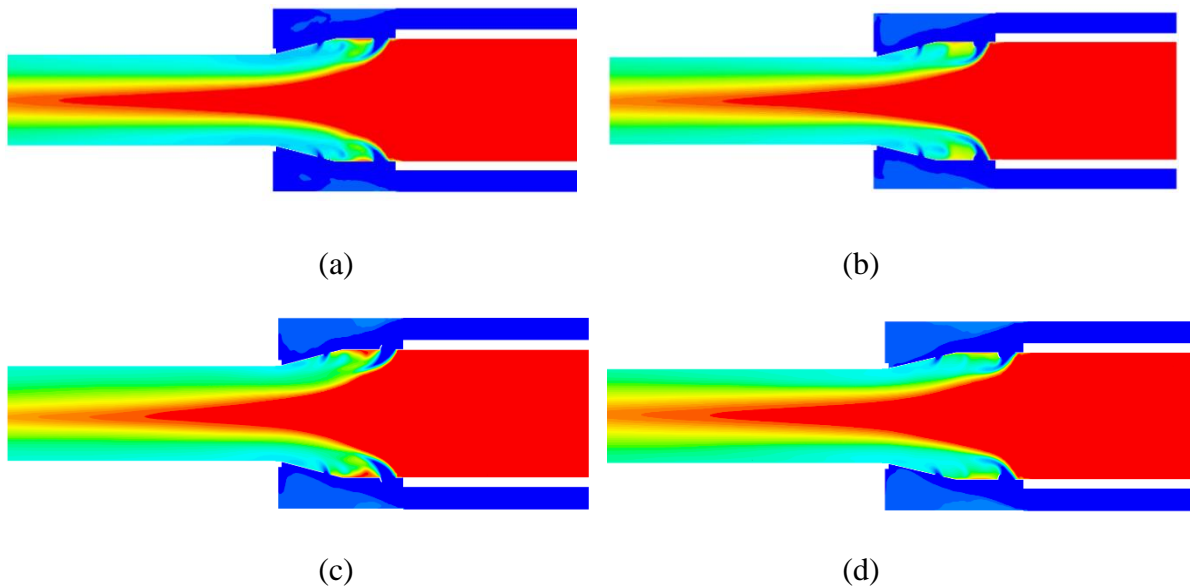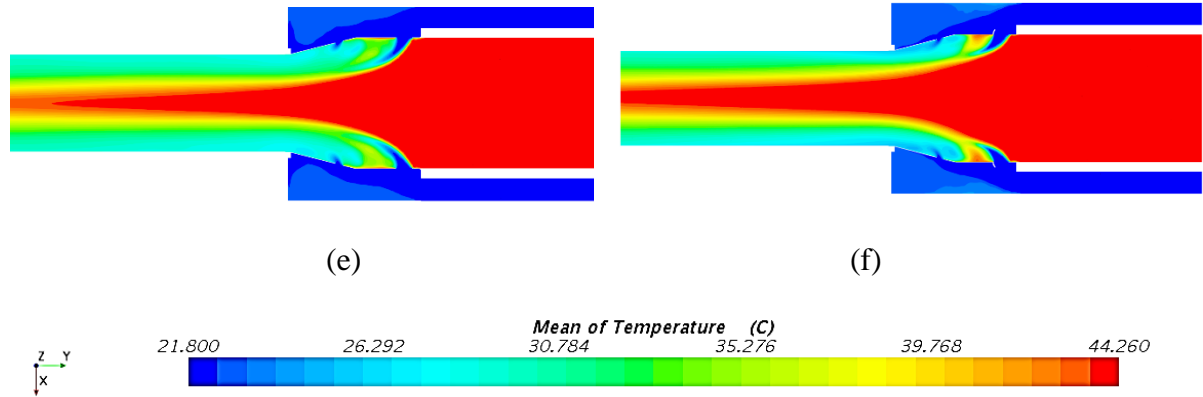
Figure 4-9*: Average radial temperature distribution at combustor exits using guide vanes (a) 0°
EXGV, (b)0°INGV, (c) 30° EXGV, (d) 30°INGV, (e) 90°EXGV, (f) 90°INGV*

Pressure Drop. Table 4-2 shows the average pressure loss for the proposed techniques. It can

be noticed that, for all cases, the external guide vanes give less pressure drop compared to the

internal ones. The plausible reason for this lesser pressure is that the internal guide vanes are facing

the primary stream, which is considered the big portion of the total flow rate. Taking the staggered

holes as a reference, the 30° INGV gives the highest average pressure drop with 9.3% higher than

the staggered holes. The 30° EXGV gives 4.7% higher than the staggered holes. However,

compared to 30° INGV, which is the best case for the internal guide vanes in terms of temperature

distribution, the 30° EXGV is almost half the pressure drop.

Table 4-2: Pressure loss data for the case studies

Primary flow inlet Reynolds number	Pressure Loss %						
		EXGV			INGV		
	SH	0°	30°	90°	0°	30°	90°
1.0×10^5	44.7	43.6	46.8	40.6	45.9	48.9	46.3
0.76×10^5	48.0	47.4	50.3	45.7	46.6	52.5	49.0
Avg. Pressure Loss (%)	46.4	45.5	48.6	43.1	46.3	50.7	47.7

Thermal Stresses on Guide Vanes. Since the primary goal of improving the mixing quality

is to protect the turbine blades from the thermal stresses caused by the non-uniform temperature

distribution, it is recommended to have the same concept with any proposed techniques. Figure

4-10 shows the temperature distribution over the external and internal guide vanes. This scene was expected as the external guide vanes are located on the outer diameter of the combustor and exposed to the cold stream. On the other side, the internal guide vanes are facing the hot gases which means that they are subjected to temperature fluctuation. This kind of fluctuation in temperature will reduce their life span and affect their geometry. Consequently, this will be reflected in the mixing process over time and maintenance cost.

(a)   (b)
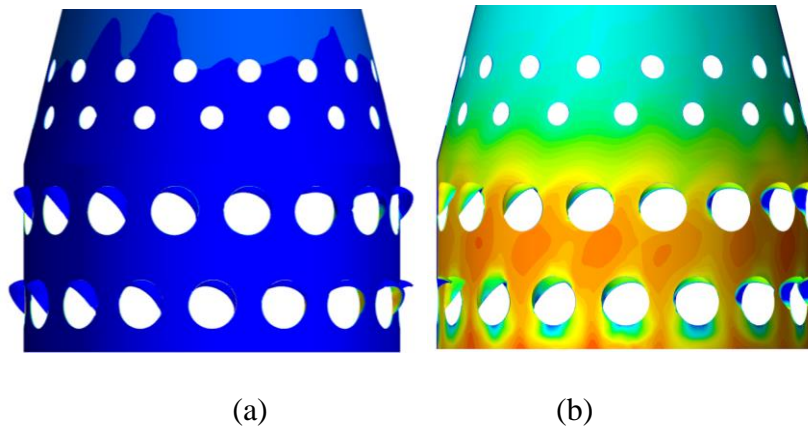
Figure 4-10 Temperature distribution on the guide vanes a) External Guide Vanes,
b) Internal Guide Vanes

4.2 Experimental and Numerical Study on the Effect of Annular Combustor Design

Temperature Distribution. The uniformity factor at two different flow rates is shown in Figure 4-11 & Figure 4-12. It can be observed in both figures that increasing the angle of the outer surface helps in pushing the secondary stream to penetrate the test section and reduces the uniformity factor. At the two different flow rates, the 30 and 45 degrees gave a uniformity factor of 0.202 and 0.205 at full flow rates, respectively, Figure 4-11, while at the half flow rate, they give 0.059 and 0.058, respectively, Figure 4-12. Comparing those results to the standard design staggered holes, the uniformity factor is reduced by 50%. The 10 degrees did not significantly affect the staggered

holes, while the 20 degrees gave a uniformity factor of 0.273, which is almost 22% compared to
the basic design.

	SH	10	20	30	45
NUM	0.310	0.310	0.273	0.202	0.205
EXP	0.326	0.329	0.281	0.208	0.209
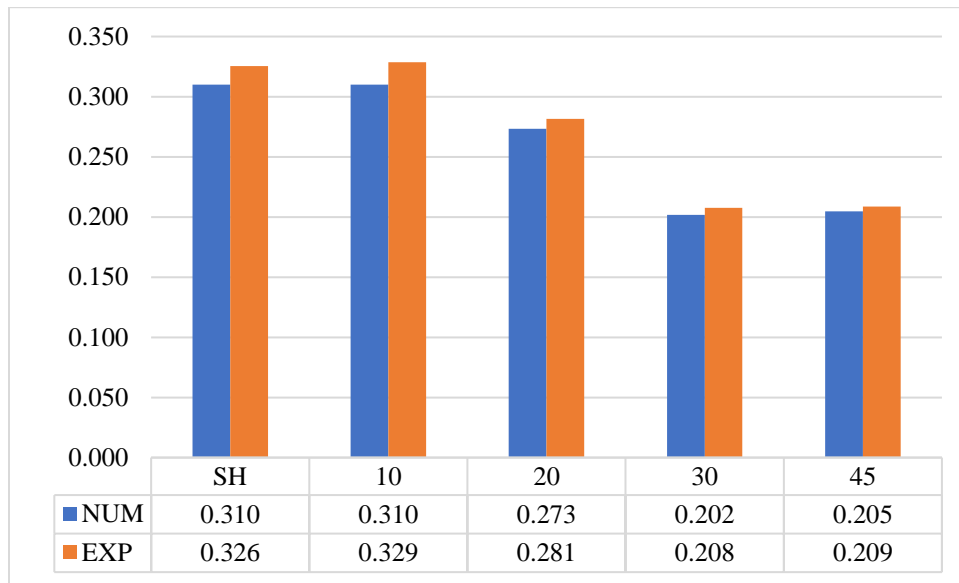
Figure 4-11: Uniformity factor for different cases tested at Re $= 1.0 \times 105$

	SH	10	20	30	45
NUM	0.095	0.080	0.076	0.059	0.058
EXP	0.100	0.084	0.078	0.061	0.059
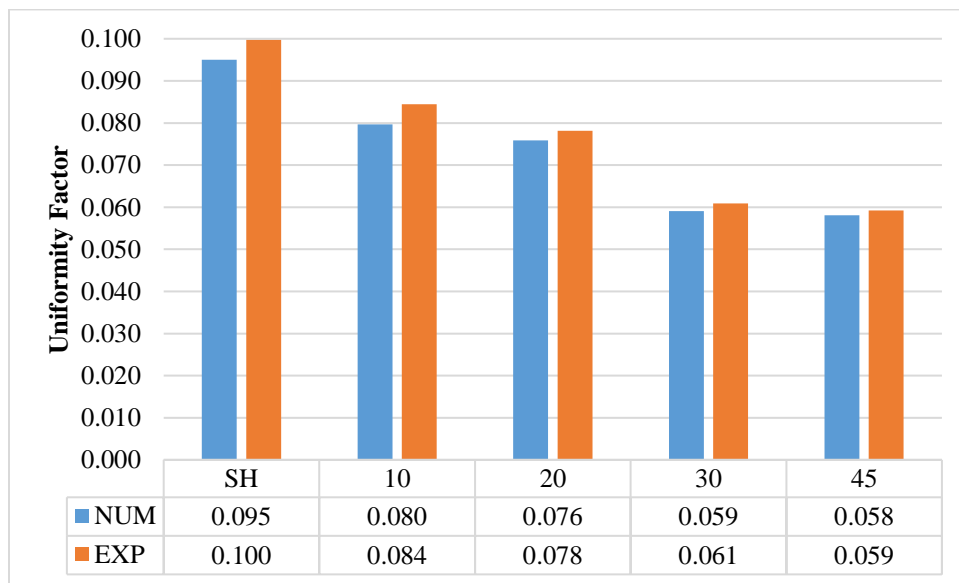
Figure 4-12: Uniformity factor for different cases tested at Re $= 0.76 \times 10^5$

To visualize the temperature distribution at different locations, the normalized mixture
fraction was graphed in Figure 4-13 & Figure 4-14. At zero normalized mixture fraction along the
horizontal axis, the exit combustor temperature is equal to the uniform temperature which is

obtained from the first law of thermodynamics for mixing two streams. As long as the curve is flatter around the horizontal axis, the exit temperature is close to the uniform temperature. In both flow rates chosen in Figure 4-13 and Figure 4-14, the 10-degree angle deviated from the other 4 cases. A plausible reason behind that increasing the angle in this case did not direct much of the secondary stream to penetrate the holes rather than increasing the eddies in the area between outer and inner surface of the test section. These eddies caused a back pressure on the secondary stream, which blocked it from penetrating the test section holes. As expected, the 30 and 45 degrees achieved the most flattened curve along the horizontal axis, which means that the average measured temperature is close to the equilibrium temperature.
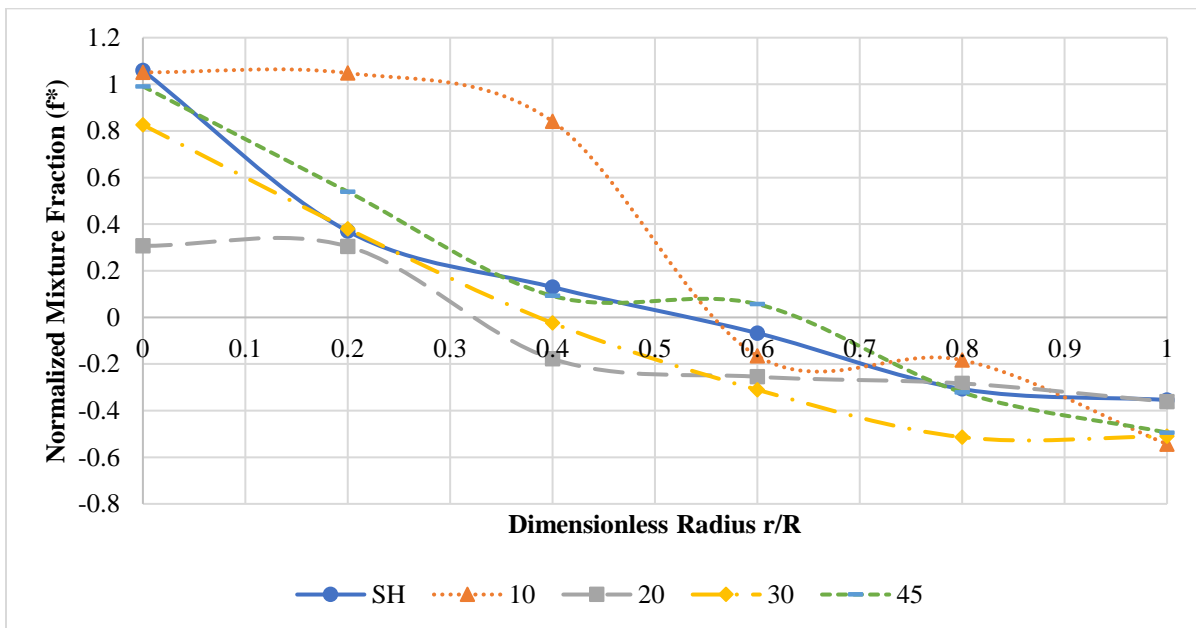
Figure 4-13: Normalized mixture fraction for different cases tested at Re $= 1.0 \times 10^5$
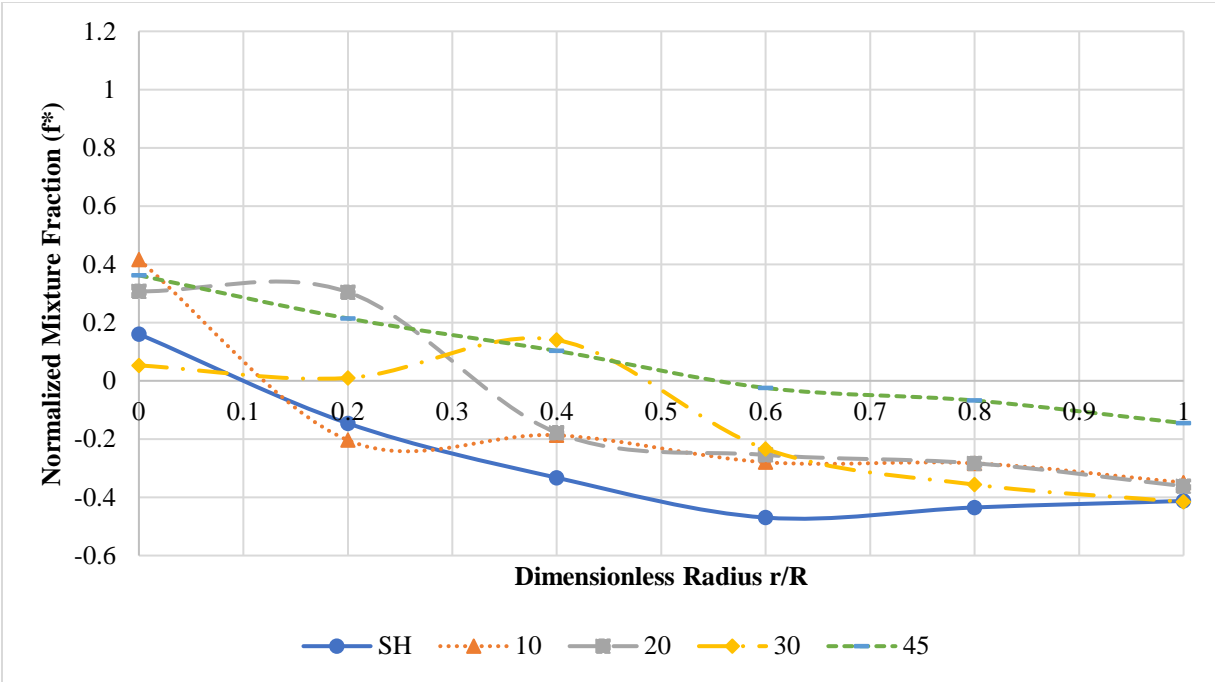
Figure 4-14: Normalized mixture fraction for different cases tested at Re $= 0.76 \times 10^5$

The numerical simulation helps explain these results through Figure 4-15, where the temperature distribution is visualized for each case at the two flow rates. More cold air is being pushed from the secondary stream to the primary stream for the full flow rates if the angle is increased. Furthermore, the hot spots are reduced at 45°, which means better mixing quality than all other cases. At lower Reynolds number, although the maximum temperature is higher compared to high Reynolds number, the temperature profile at the exit section is more uniform. Still, the 30 and 45 degrees achieved the uniform temperature.
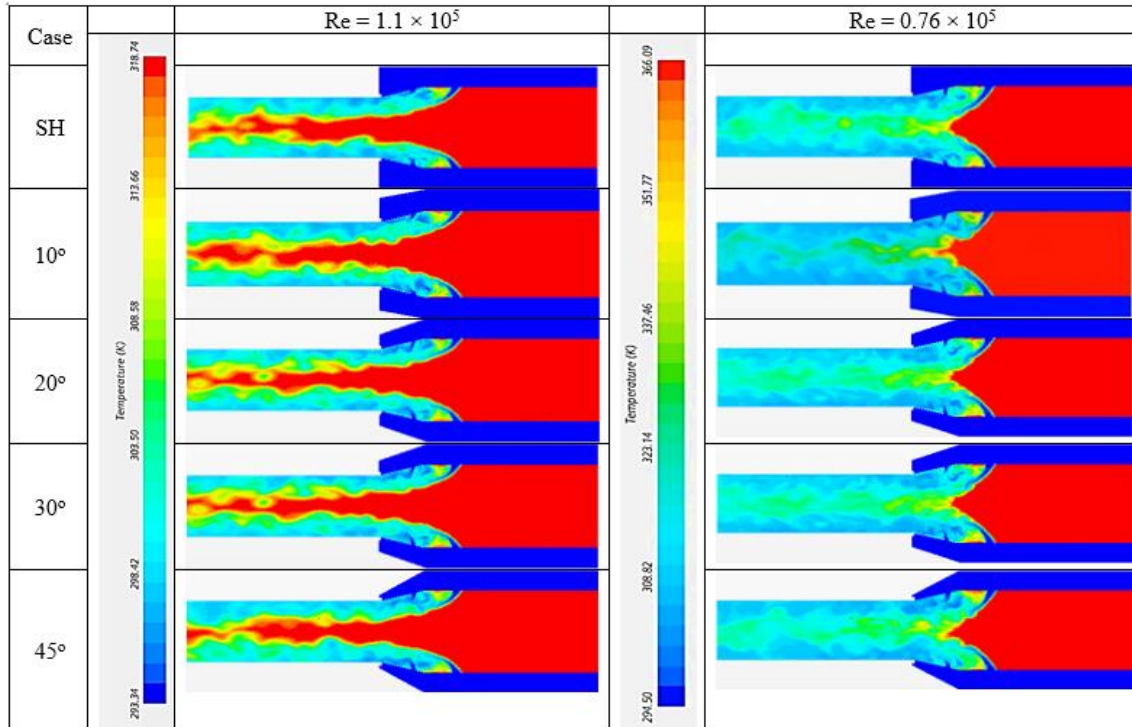
Figure 4-15: Temperature distribution at combustor exit for different angles compared to staggered holes at two different Rynoldns numbers

Pressure Drop. Table 4-3 shows the average pressure drop at the proposed case studies. Overall, taking the staggered holes as a reference, all the pressure drops obtained are not that much lower/higher than the basic design, which means that the modification in the combustor design would not affect the generated power from the gas turbine. The lowest average pressure drop goes for the 10 degrees with 0.7% lower than the staggered holes, while the 30 degree has the highest pressure drop of 45.6%. The 20 and 45 degrees have a similar pressure drop of 44.6 and 44.3%, which is 1.2% and 0.5% higher, respectively, than the basic design.

65

Table 4-3: Pressure drop percentage at proposed case studies

Primary flow inlet Reynolds number	Pressure Loss %				
	SH	10°	20°	30°	45°
1.0×10^5	40.6	45.7	43.8	43.5	46.8
0.76×10^5	47.0	40.4	45.3	47.8	41.8
Avg. Pressure Loss (%)	43.8	43.1	44.6	45.6	44.3

CHAPTER 5- BIOMASS ENERGY RESOURCES WITH LIVESTOCK MANURE

Three thermochemical processes were investigated: Pyrolysis, Gasification, and Co-Pyrolysis.

5.1 Pyrolysis of Chicken manure

The thermo-gravimetric and differential thermal analyses were conducted for the chicken manure using Nitrogen as gas agent with eight different heating rates from room temperature up to 1000ºC. The three main components in the chicken manure are Hemicelluloses, Cellulose, and Lignin. The thermal degradation of Hemicelluloses is known to peak at 240ºC, Cellulose at 380ºC, while Lignin has more of a steady degradation with a small peak at high-temperature 600-800ºC [78]. Figure 5-1 shows the extent of reaction of chicken manure at different heating rates when Nitrogen is used. It can be observed that all heating rates had the same trend with the increase of the temperature, the extent of reaction increases. In addition, when the heating rate increased, the progress of the extent of reaction seems to be delayed to a higher temperature. Furthermore, the figure shows that the faster the heating rate, the more delayed is the progress of each reaction with respect to temperature. The main reason is that increasing the heating rate does not allow enough time for each reaction to be completed before increasing the temperature. Another plausible reason can be the response of the measuring device. This delay can be observed as well when using different gas agents. This kind of behavior was also observed for wood [113]. The Pyrolysis reaction was best represented by dividing the decomposition into three mainstages. The first stage begins with the start of thermal cracking up to 250ºC. The second stage with a faster reaction between 250-350ºC. Finally, the third stage with a steady reaction from 350ºC to the end of the

67

reaction. These three distinct stages were used to find the kinetics of the reaction. Starting from 350°C and up to 700°C, the thermal degradation is a complicated overlap between the three main components (Hemicellulose, Cellulose, and Lignin) decomposition, and the effect of heating rate on the extent of reaction is more significant compared to the other temperature ranges. At the end of each reaction, a residual mass that failed to react either because of insufficient activation energy or the absence of suitable reacting media was leftover.
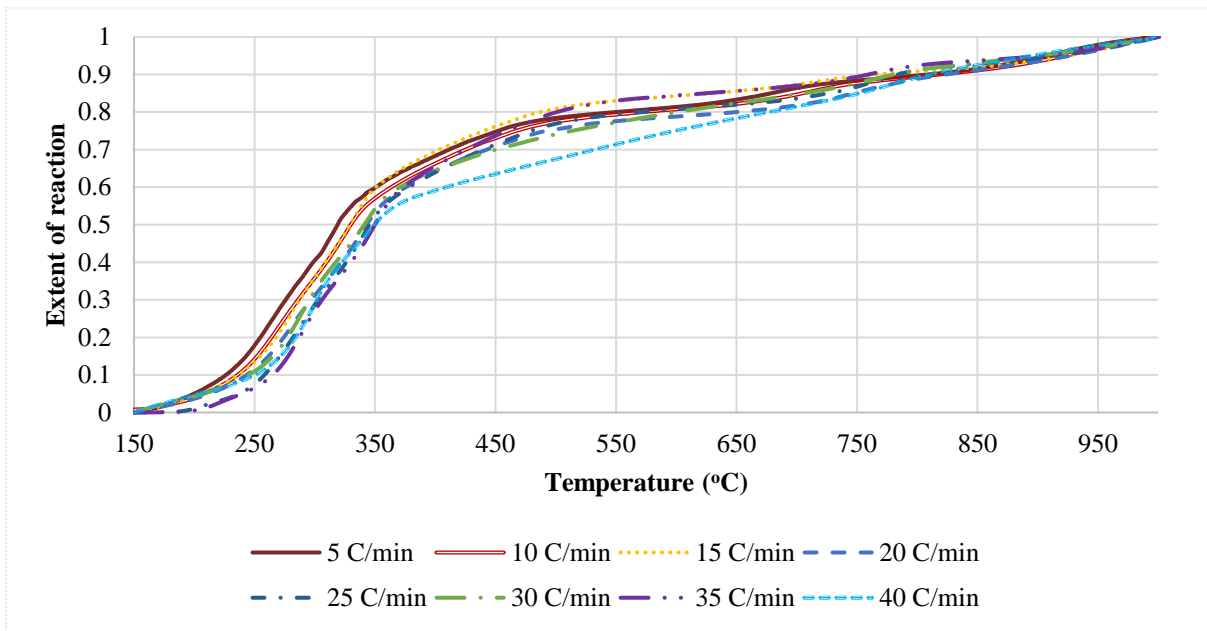
Figure 5-1: The extent of the reaction of chicken manure at different heating rates

The rate of change of the extent of reaction of chicken manure with the temperature at different heating rates is shown in Figure 5-2. Similar to Figure 5-1, it can be observed that the trend is the same for all tested heating rates. At 150°C for the low heating rates, all the moisture content has evaporated from the sample. For the highest two heating rates, 35 and 40°C/min, two peaks take place near 150°C due to the evaporation of any moisture in the sample. The main reason is that the heating rate is faster than the evaporation rate of the moisture content.

For all heating rates, the first two peaks are within the temperature range of 250-350°C, then the third peak started to occur at 670°C for the lowest heating rates (5°C /min). It can be observed that the peak value is increased with the increase in the heating rate, as well as the temperature at which the peak occurs. Starting with 5°C/min, the first peak took place at 255°C, and after increasing the heating rate, the temperature at which peak occurs is increased as well to reach 298°C for the heating rate of 40°C/min. The same scenario for the second peak, where it is 320°C, 325°C, 335 °C, 345°C, and 343°C for the heating rates 5, 15, 20, 30, and 40°C /min, respectively. The three peaks are indications for the three main components: Hemicellulose, Cellulose, and Lignin, respectively. The values obtained in this study are matching the values obtained by Yang et al. for determining the degradation temperature range of these main three components.
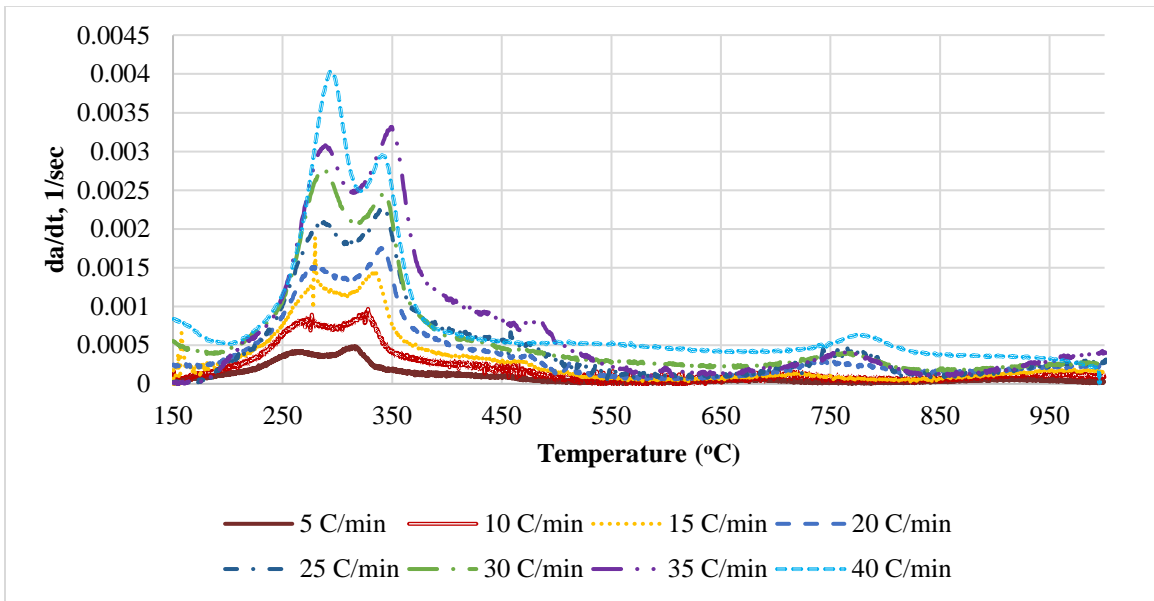
Figure 5-2: Rate of Change of the extent of reaction with the temperature at different heating rates

Kinetics of Reaction: Table 5-1 shows the activation energy and the Arrhenius constant at different heating rates. For the temperature range from 250 to 360°C, it can be observed that the

average activation energy is 91 kJ/mole and the average value for log A= 14.5 sec^{-1}. For the range

greater than 360 °C, the average activation energy is 75.6 KJ/mole while log A=10 sec^{-1}

Table 5-1: Kinetic parameters for Nitrogen Pyrolysis with different heating rates

β (°C/min)	n	Log(A/β)	Ea (kJ/mole)
5 (250-360°C)	5	14.9	84
5 (>360°C)	5	10.9	63.1
10 (250-360°C)	5	15	88.1
10 (>360°C)	5	11	65.1
15 (250-360°C)	5	15.3	89.6
15 (>360°C)	5	11.2	69.0
20 (250-360°C)	5	15.6	93.2
20 (>360°C)	5	11.4	72.3
25 (250-360°C)	5	16	95.8
25 (>360°C)	5	11.7	76.4
30 (250-360°C)	5	16.5	96.5
30 (>360°C)	5	11.8	80.9
35 (250-360°C)	5	16.8	98.3
35 (>360°C)	5	11.9	84.5
40 (250-360°C)	5	17	87.8
40 (>360°C)	5	11.9	99

Differential thermal analysis (DTA): Figure 5-3 shows the DTA variation with the temperature at different heating rates. For all the heating rates, it can be observed that the trend is the same for all the heating rates. The reaction is relatively steady except for a large peak downwards for the faster heating rate cases by activating the endothermic reaction due to the quick breakdown of Cellulose and Hemicelluloses below 350°C. With the increase in the heating rate, the magnitude of the peaks increases. The more massive peak is a result of a fast increase in the temperature of the control (empty) pan, while the active pan is enduring high rates of endothermic reactions hindering the sample temperature increase. Consequently, for 30°C/min and higher, the trend looks different from the other cases.
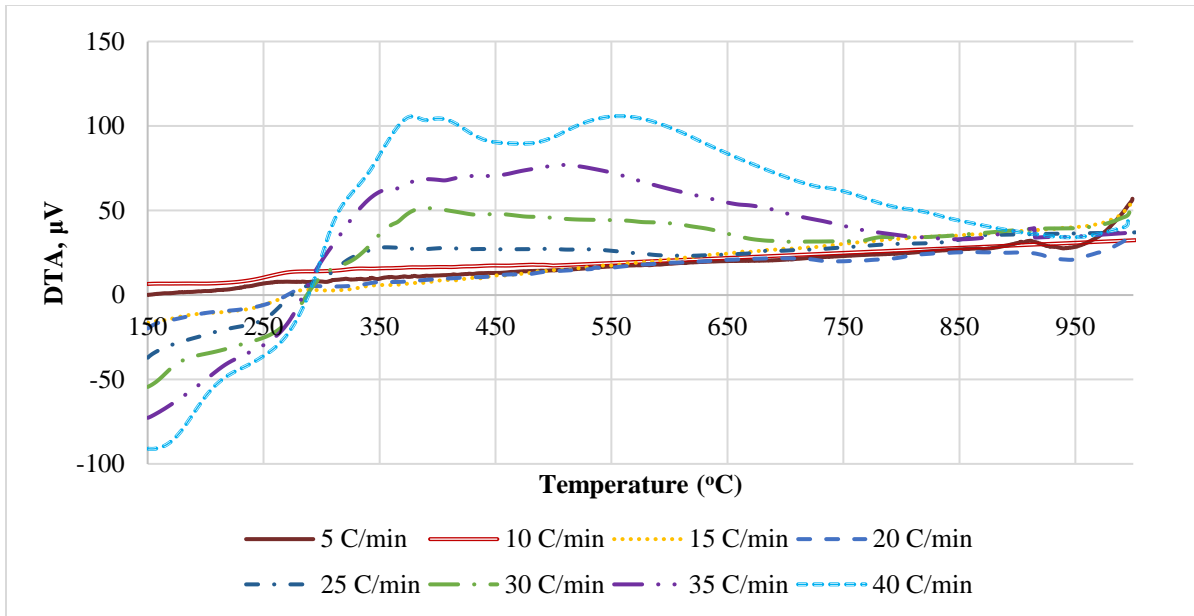
Figure 5-3: The change of the DTA with the temperature at different heating rates

5.2 Pyrolysis of Cow Manure

Figure 5-4 shows the extent of the reaction for the cow manure at eight different heating rates. It can be observed that all the heating rates have the same trend and increasing the heating rates responsible for delaying the extent of the reaction to a higher temperature. The Pyrolysis reaction was best presented by dividing the decomposition into four main stages. First stage up to 255°C, which represents the thermal cracking. A second faster reaction from 255 to 315°C. Then from 315 °C to 745 °C represents the thermal degradation of the three main components: Hemicellulose, Cellulose, and Lignin.
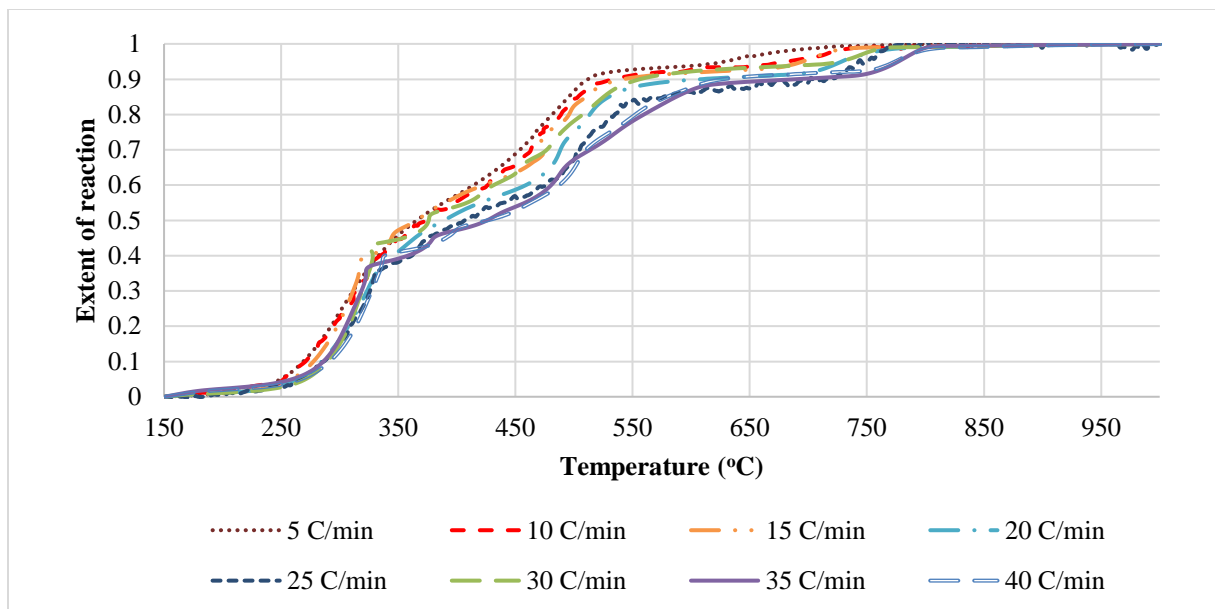
Figure 5-4: Extent of Reaction variation with temperature for cow manure at different

heating rates

The degradation temperature of the three main components can be obtained from Figure 5-5 The first peak represents the Hemicellulose degradation. For all the heating rates, the first peak occurs at 321°C. At 475 °C the thermal degradation of the Cellulose takes place for the lower heating rates and 500 °C for the 40 °C/min. A plausible reason for the small fluctuation between 350 °C and 500 °C is the degradation of impurities such as bedding. Relatively more minor bumps appear at 760°C for 35 and 40°C/min., which is due to the degradation of the low residuals of Lignin after combustion.

Figure 5-5: The rate of change of the extent of reaction with the temperature for cow

manure at different heating rates

Figure 5-6 shows the DTA variation with the temperature at different heating rates. All

heating rates are following the same trend. All the heating rates are exothermic, which means that

the reaction is self-sustainable. For the higher heating rates, the sharp decline after the first peak

implies that the reaction turns into endothermic. The main reason is that the faster heating rate

does not allow enough time to thermal equilibrium besides the heat transfer limitation. Based on

this conclusion and for figures clarity, the 5 °C/min is used to compare between the chicken manure
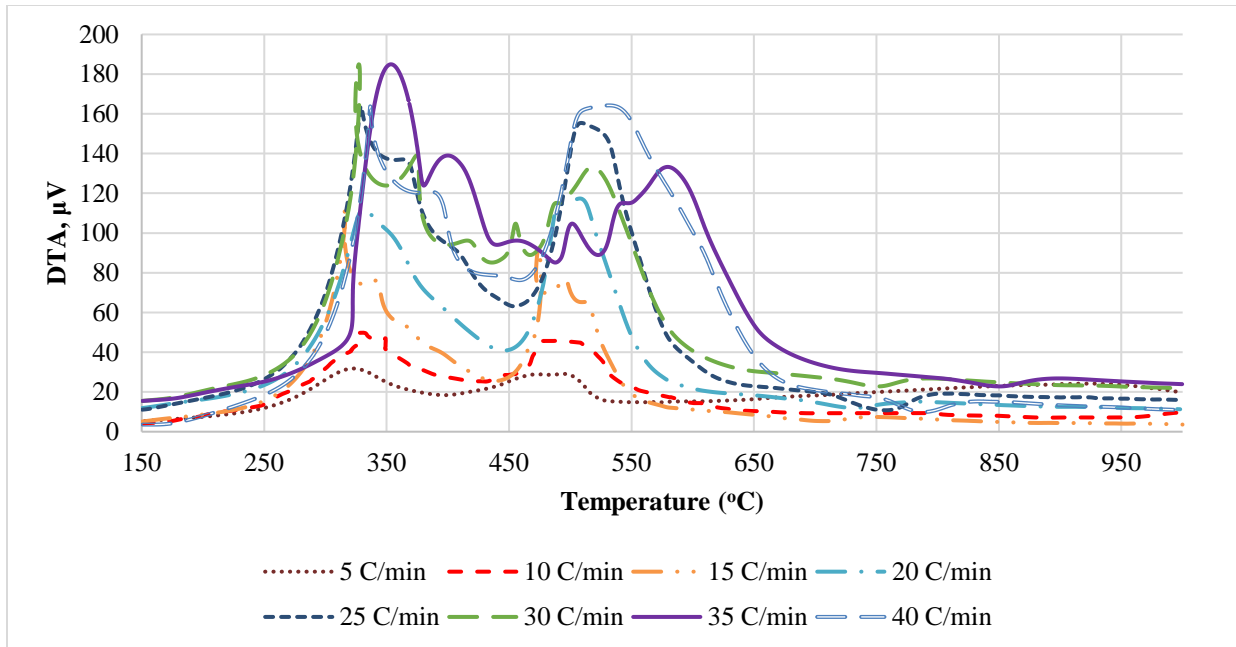
and cow manure.

Figure 5-6: The change of the DTA with the temperature for cow manure at different

heating rates

5.3 Gasification of Chicken Manure

5.3.1 Air Gasification

In this case, the air was used as a gas agent. As a result, the chemical reactions were not only limited to the Pyrolysis process but also gasification to take place because of the incomplete combustion of the gases and fixed carbon in the presence of O_2. With the same as nitrogen Pyrolysis, the same parameters were studied at the same heating rates. The same remarkable results obtained with case A, as seen in Figure 5-7, where all different heating rates had the same trend. As the temperature increases, the extent of reaction increases. When the heating rate increased, the progress of the extent of reaction seems to be delayed to a higher temperature. For the gasification part, the reaction can be divided into five main stages. The first stage takes place, starting from the thermal cracking up to 250°C. A faster second reaction between 250-350°C, then from 350 to 450°C another fast stage with a mild slope compared to the previous region. The fluctuation in

temperature between 450 and 600°C is because of the self-ignition. Right after 600°C, the extent of reaction is more than 95%, and the reaction tends to be very slow.

Figure 5-7: The extent of the reaction of chicken manure at different heating rates

Again, three significant peaks can be shown in Figure 5-8; 255, 340, and 500°C. As expected, the magnitude of the peak is increased as the heating rate increased as well as the temperature at which the peak occurs. As shown in the figure, for 5°C/min, the first peak occurs at 255°C. For 10 °C/min one can see that the first peak is shifted to the right (higher temperature) as well, and the peak value is higher. For 40 °C/min, the peak value is 0.005 sec^{-1}, which is the highest peak, and it happened at 293 °C, and so on. The increase in the peak value is resulting from the faster change in temperature. The characteristics of Hemi-Cellulose and Cellulose can be seen on the first two peaks. Another indication of self-ignition can be seen from the temperature fluctuation between 350°C and 450°C, which was already observed in Case A. a tiny bump appears at 680°C for 35 and 40°C/min., which is due to the degradation of the low residuals of Lignin after combustion.

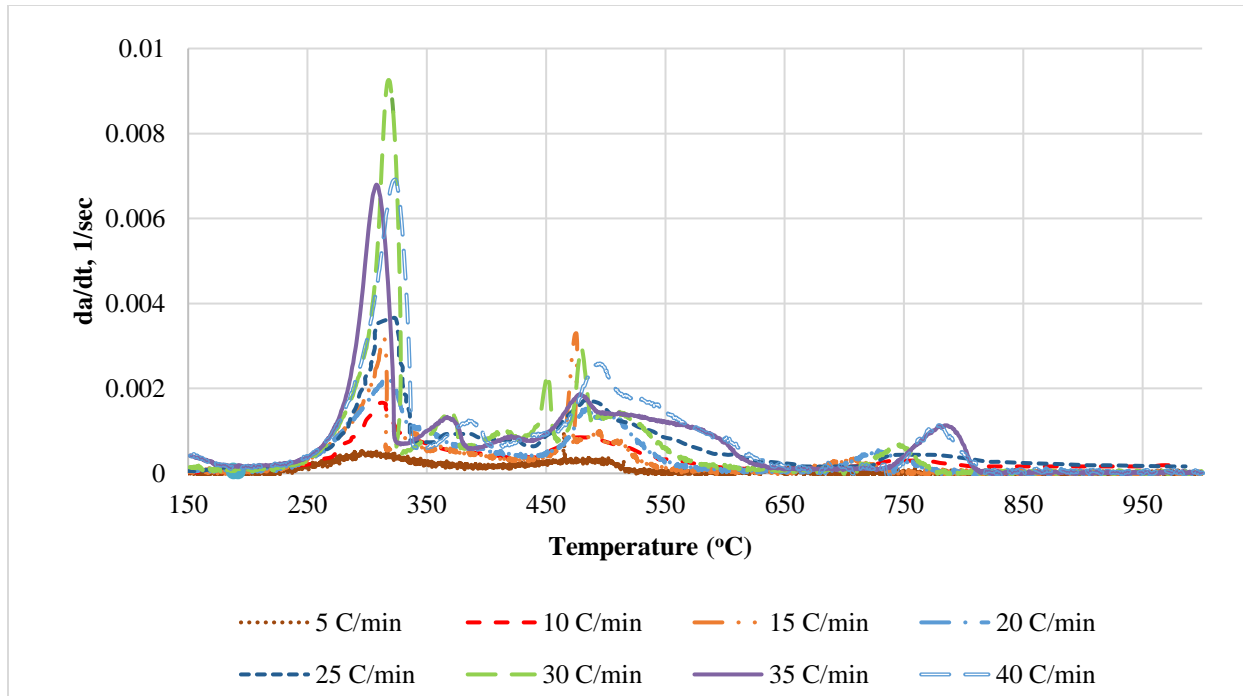Figure 5-8**:** The rate of change of the extent of reaction with the temperature

at different heating rates

Kinetics of reaction (TGA). The values for the Arrhenius equation constant and the activation

energy are shown in Table 5-2. Even though the reaction appeared more complicated than the N_2

Pyrolysis case, single kinetic reaction constants were calculated for the whole conversion reaction

where the average activation energy is 68.4 KJ/mole and the average log A=9.3 sec^{-1}.

Table 5-2**:** Kinetic parameters for Air gasification with different heating rates

β (°C/min)	n	Log(A/β)	a (kJ/mole)
5	3	11.2	70.3
10	3	10.1	66.7
15	3	10.1	64.5
20	3	10.9	70.8
25	3	10.3	67.6
30	3	10.9	70.3
35	3	10.3	67.9
40	3	10.2	69.0

Differential thermal analysis (DTA). In Figure 5-9, the same peaks are formed at the same

temperatures obtained from the previous two Figure 5-7 and Figure 5-8 and these peaks indicate

the thermal degradation of the Hemicellulose, Cellulose, and self-ignition. The fact that these peaks are positive (upwards) is due to the oxidation of some of the evolving gases rendering the reaction as exothermic. After 700ºC no significant reaction was recorded, and the weight of the sample was stable.
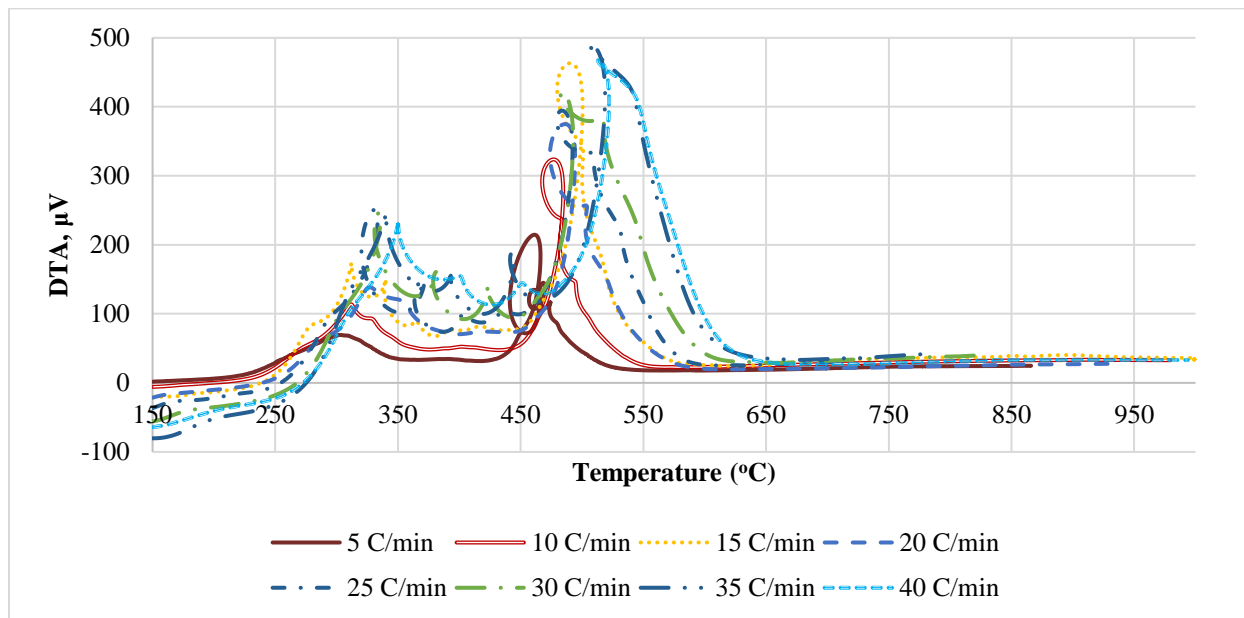
Figure 5-9: The change of the DTA with the temperature at different heating rates

5.3.2 Carbon Dioxide Gasification

The extent of reaction. Another gasification case was studied when CO_2 is used. In this case, as shown in

Figure 5-10, the four stages of the gasification reaction are as follows; start of thermal cracking up to 250ºC, the faster reaction between 250-360ºC, steady reaction from 360 to 700ºC, and finally, a quick reaction at 700ºC to the end of the reaction. These four distinct stages were used to find the kinetics of the reaction.

77
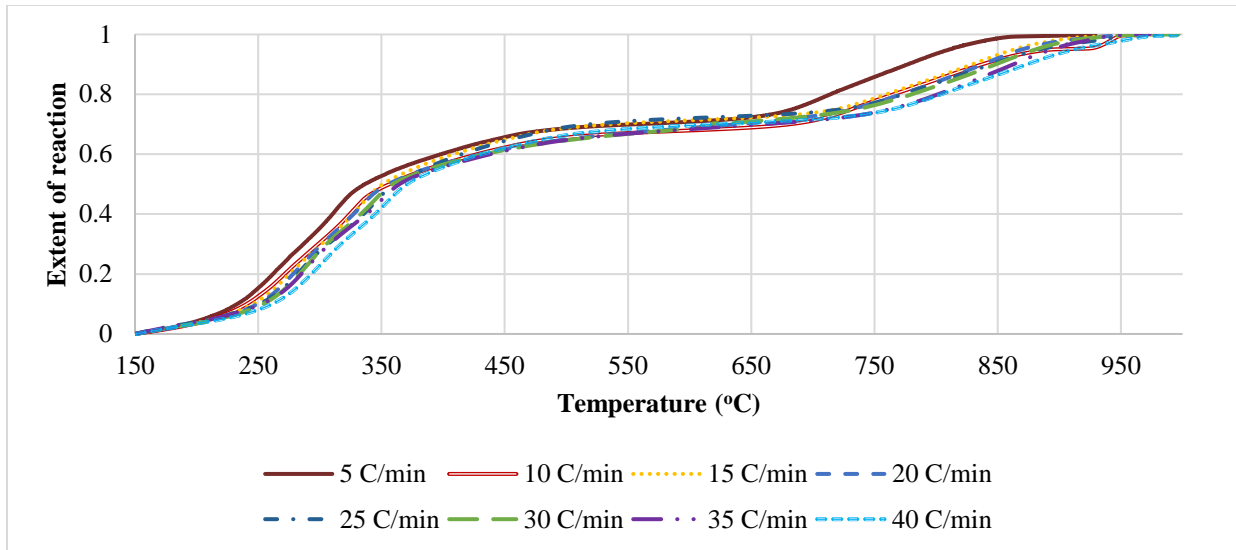
Figure 5-10: The extent of the reaction of chicken manure at different heating rates

In Figure 5-11 three significant peaks can be observed close to the following temperature: 250°C, 360°C, and $700-800^{\circ}$C. The first two peaks are characteristics for Hemicellulose and Cellulose, while the third peak ($700-800^{\circ}$C) is an overlap between the peak for Lignin and the peak for the Boudouard reaction between fixed carbon and CO_2, respectively. The peak value increases with the heating rate due to the faster increase of the temperature with time.
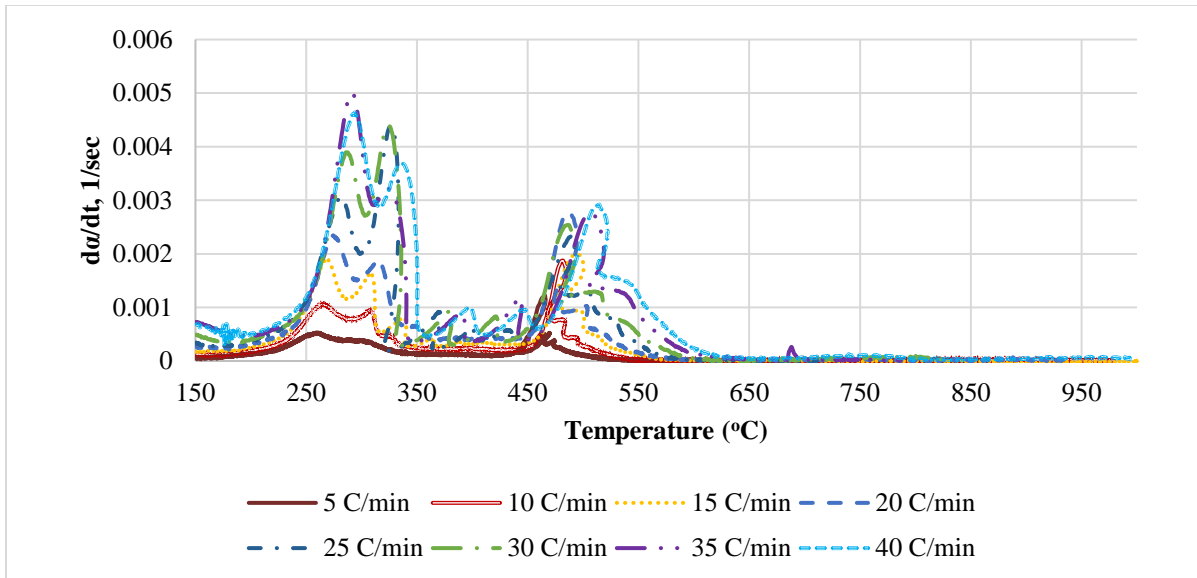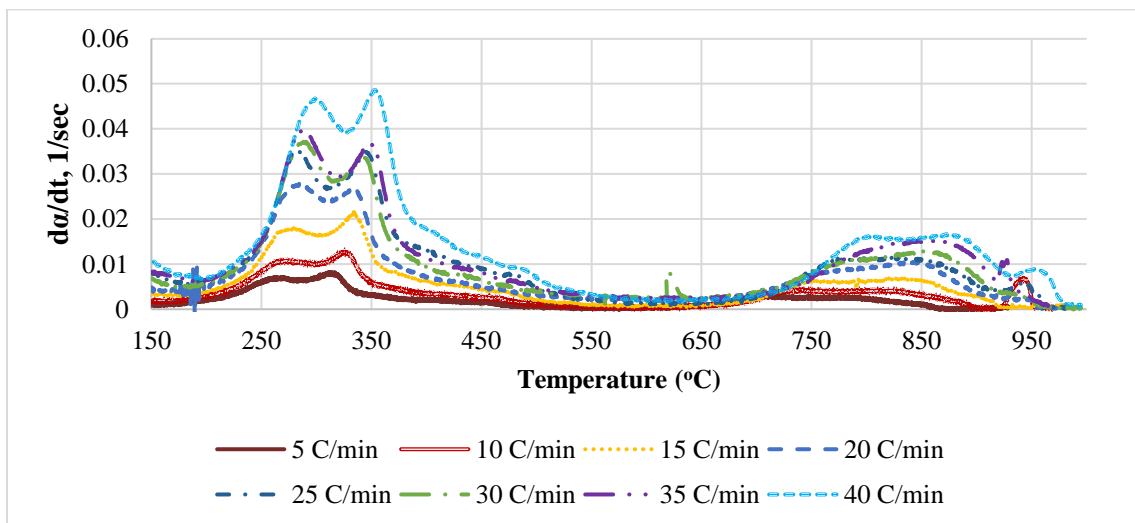

Figure 5-11: Rate of Change of the extent of reaction with the temperature at different heating rates

78

Kinetics of reaction (TGA). Table 5-3 shows the values of the Arrhenius equation constant and the activation energy. For the range 250-360°C, the average value for Ea= 59.6 kJ/mole and the average value for log A= 9.8 sec^{-1}, for the range 360-630°C, the average value for Ea= 34.9 kJ/mole and the average value for log A= 4.8 sec^{-1} , and for > 630°C, the average value for Ea= 547.6 kJ/mole and the average value for log A= 68 sec^{-1}

Table 5-3: Kinetic parameters for Carbon Dioxide gasification with different heating rates

β (°C/min)	n	Log(A/β)	Ea (kJ/mole)
5 (250-360°C)	5	9.8	63.2
5 (360-630°C)	5	4.3	39
5 (>630°C)	5	72.5	575.5
10 (250-360°C)	5	8.9	60.2
10 (360-630°C)	5	5.0	38.7
10 (>630°C)	5	68.1	523
15 (250-360°C)	5	9.1	61.5
15 (360-630°C)	5	3.5	32.9
15 (>630°C)	5	68	556
20 (250-360°C)	5	8.9	61.3
20 (360-630°C)	5	3.8	34.8
20 (>630°C)	5	67.3	551
25 (250-360°C)	5	8.0	57.1
25 (360-630°C)	5	3.0	305
25 (>630°C)	5	66.5	549
30 (250-360°C)	5	8.7	60.3
30 (360-630°C)	5	3.0	33.3
30 (>630°C)	5	68.1	561.5
35 (250-360°C)	5	8.0	56.4
35 (360-630°C)	5	2.9	32.6
35 (>630°C)	5	63.6	544.7
40 (250-360°C)	5	7.5	56.4
40 (360-630°C)	5	3.7	37.6
40 (>630°C)	5	62	519.7

As shown in Figure 5-12, the reaction is relatively steady from 350 to 700 °C with an exothermic reaction where the DTA values are positive. The endothermic reactions took place below 350°C due to the fast breakdown of Cellulose and Hemicelluloses, and another endothermic reaction of CO_2 with the fixed carbon in the chicken manure at a temperature greater than 700°C.

After 700°C, when the heating rate increases, the curve started to drop sharply, which means that the reaction is endothermic. Also, the magnitude of the peak increases. Comparing the different heating rates, after 700 °C, one can observe that, for 5°C/min, the reaction is exothermic, where the curve goes up, while for the 40°C/min, it sharply goes down. The faster rate of change in temperature does not allow enough time for thermal equilibrium between the reference and sample, and thus the peak value appears larger.

In terms of mass residual, Figure 5-13 shows the average mass residual for the three gas agents. The average residual mass in the case of N_2 Pyrolysis is 25% of the total mass, and it is independent of the heating rate, while for the air gasification and CO_2 gasification, the average residual mass is 23% and 19%, respectively.
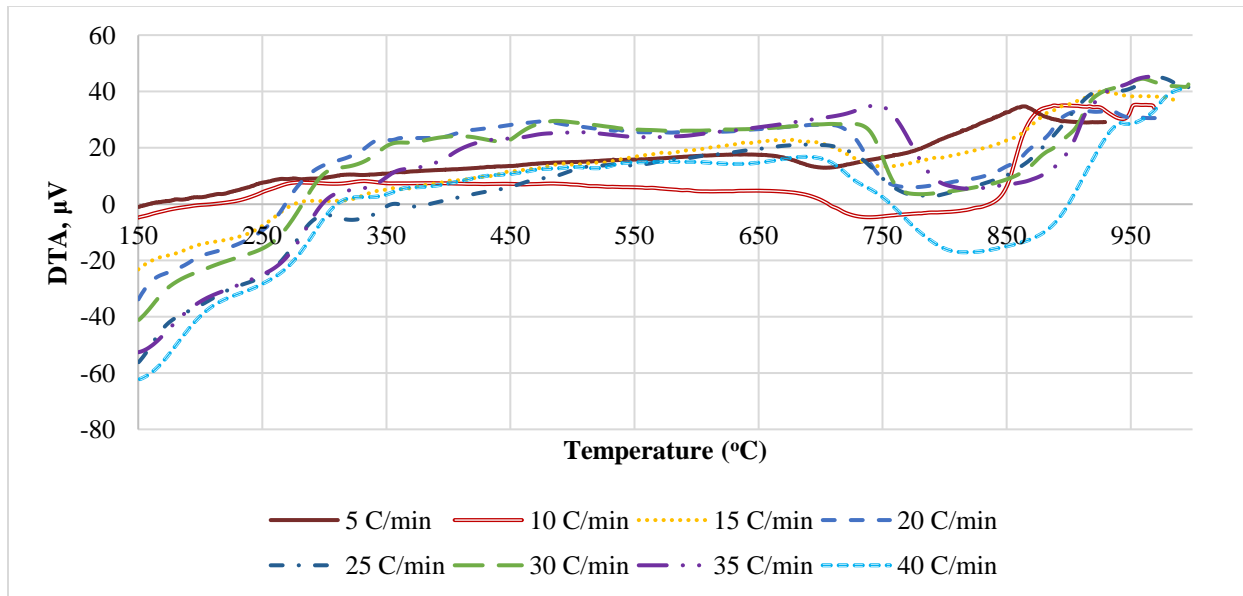
Figure 5-12: The change of the DTA with the temperature at different heating rates
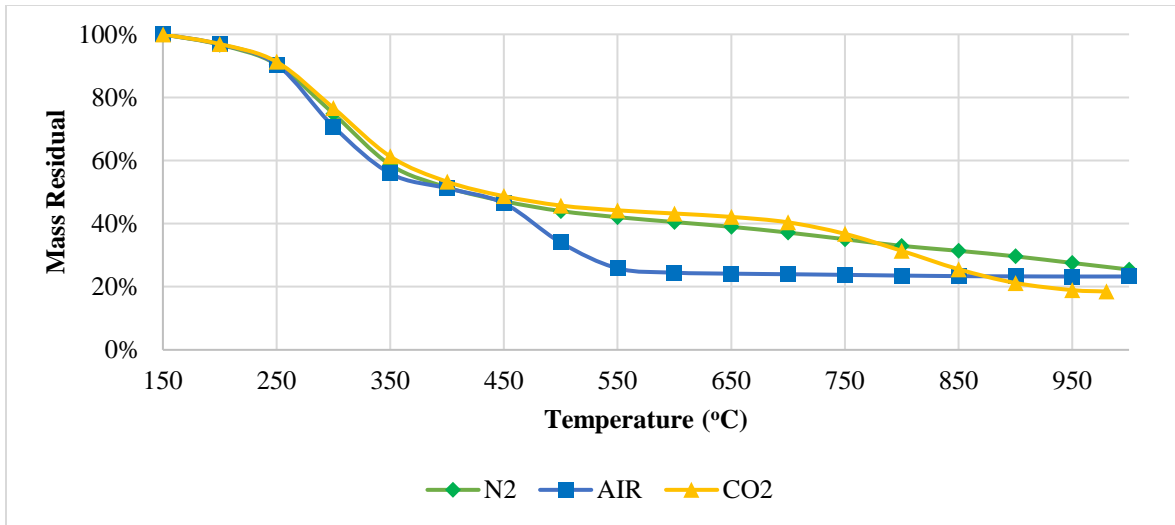
Figure 5-13: Mass residual change versus temperature for the three tested gas agents.

5.4 Gasification of Cow Manure

5.4.1 Air Gasification

In this case, the air was used as a gas agent. As a result, the chemical reactions were not only limited to the Pyrolysis process but also gasification to take place because of the incomplete combustion of the gases and fixed carbon in the presence of O_2. With the same as nitrogen Pyrolysis, the same parameters were studied at the same heating rates. The same remarkable results obtained when nitrogen was used, as seen in Figure 5-14, where all different heating rates had the same trend. As the temperature increases, the extent of reaction increases. When the heating rate increased, the progress of the extent of reaction seems to be delayed to a higher temperature. For the gasification part, the reaction can be divided into five main stages. The first stage takes place, starting from the thermal cracking up to 250°C. A faster second reaction between 250-350°C, then from 350 to 450°C another fast stage with a mild slope compared to the previous region. The fluctuation in temperature between 450 and 600°C is because of the self-ignition. Right after 600°C, the extent of reaction is more than 95%, and the reaction tends to be very slow.

Figure 5-14: The extent of the reaction of Cow manure at different heating rates

Again, three significant peaks can be shown in Figure 5-15; 302, 500, and 745°C. As expected, the magnitude of the peak is increased as the heating rate increased as well as the temperature at which the peak occurs. As shown in the figure, for 5°C/min, the first peak occurs at 302°C. For 10 °C/min one can see that the first peak is shifted to the right (higher temperature) as well, and the peak value is higher. For 35 °C/min and 40 °C/min, the peak value is 0.0037 sec⁻¹, which is the highest peak, and it happened at 344 °C, and so on. The increase in the peak value is resulting from the faster change in temperature. The characteristics of Hemi-Cellulose and Cellulose can be seen on the first two peaks. A tiny bump appears at 680°C for 35 and 40°C/min., which is due to the degradation of the low residuals of Lignin after combustion.
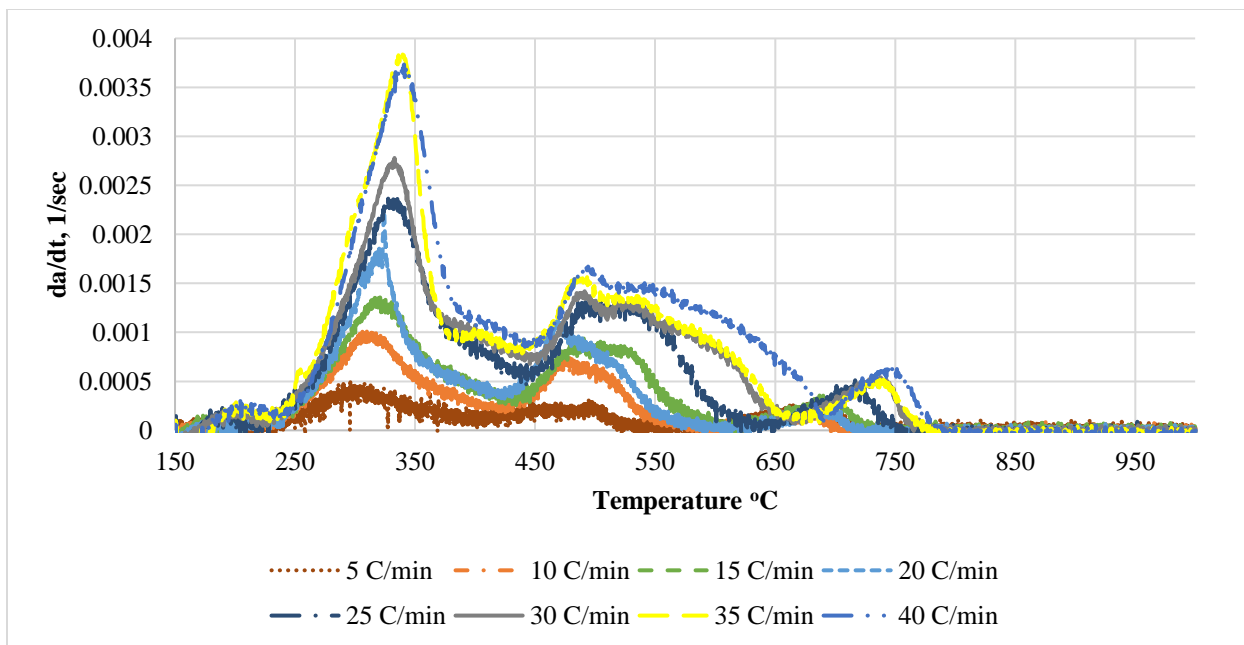
Figure 5-15: The rate of change of the extent of reaction with the temperature

*Differential thermal analysis (DTA).*Figure 5-16, the same peaks are formed at the same temperatures obtained from the previous two Figure 5-14 and Figure 5-15 and these peaks indicate the thermal degradation of the Hemicellulose, Cellulose, and self-ignition. The fact that these peaks are positive (upwards) is due to the oxidation of some of the evolving gases rendering the reaction as exothermic. After 700°C no significant reaction was recorded, and the weight of the sample was stable. The 5 c/min gives the most stable exothermic reaction among all other cases.
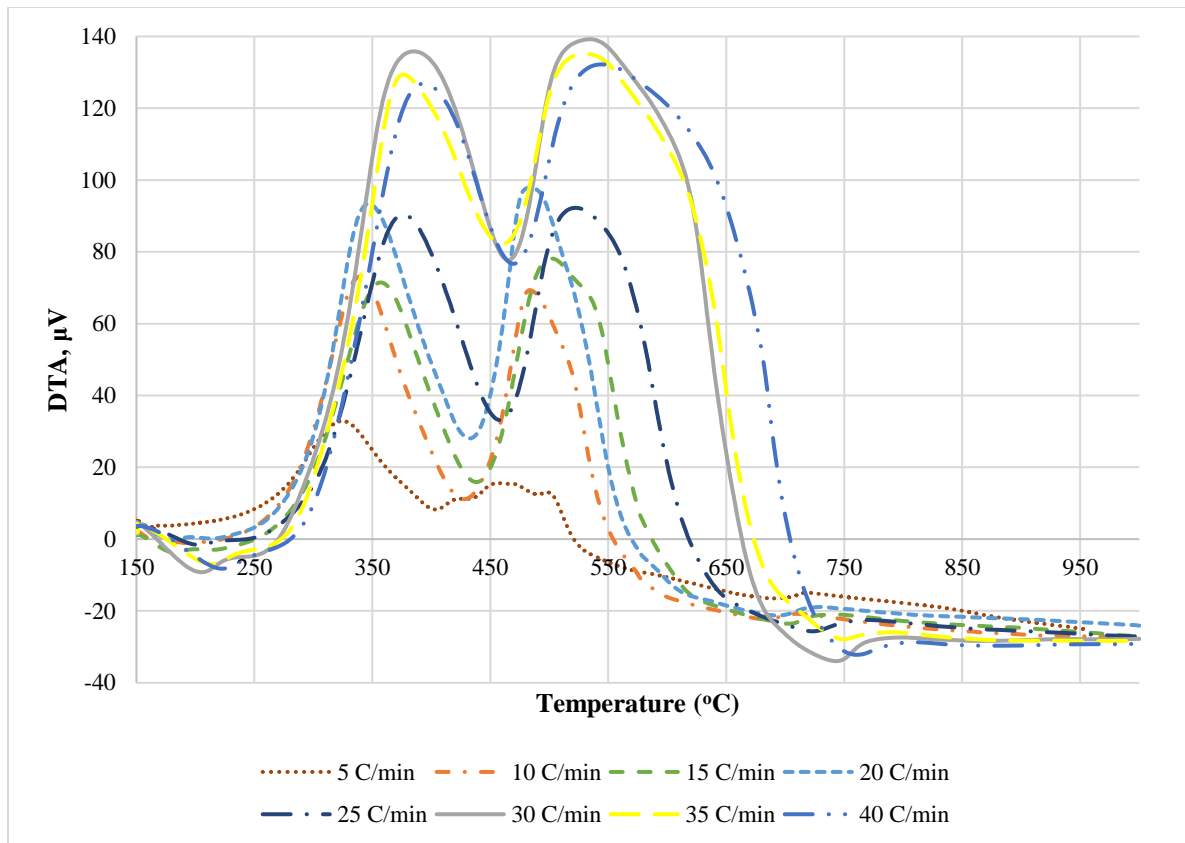
Figure 5-16: The change of the DTA with the temperature at different heating rates

5.4.2 CO2 Gasification

The extent of reaction. Another gasification case was studied when CO_2 is used. In this case, as shown in Figure 5-17, the four stages of the gasification reaction are as follows; start of thermal cracking up to 250°C, the faster reaction between 250-450°C, steady reaction from 450 to 750°C, and finally, a quick reaction at 750°C to the end of the reaction. These four distinct stages were used to find the kinetics of the reaction.
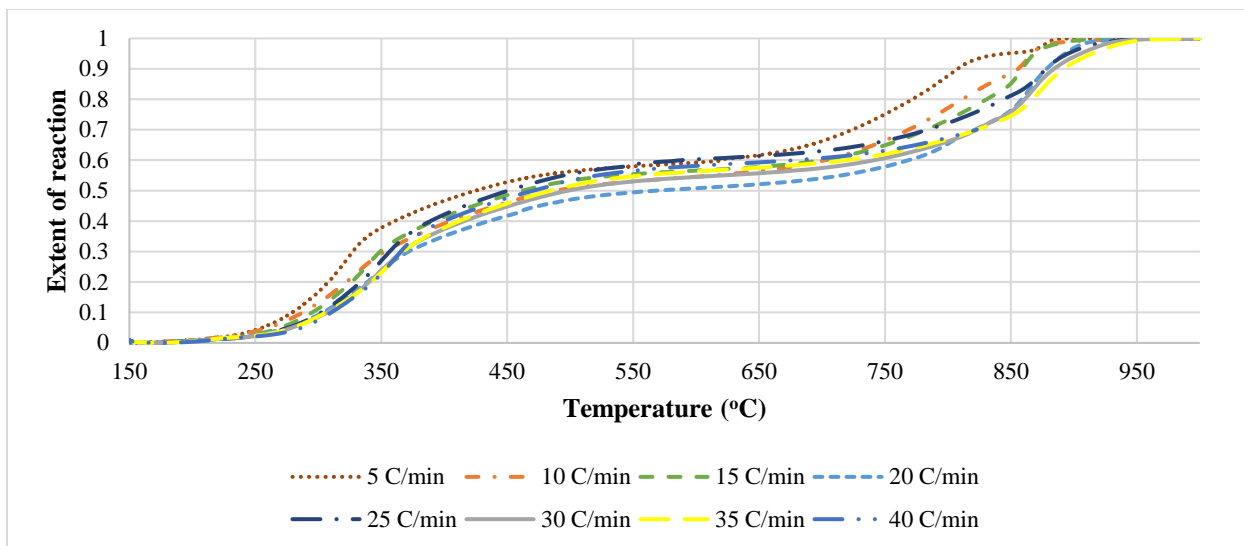
Figure 5-17: The extent of the reaction of Cow manure at different heating rates

As expected from the pyrolysis process that the first peak will be higher than the second peak. In Figure 5-18 three significant peaks can be observed close to the following temperature: 330°C, 460°C, and $760\text{-}880^{\circ}$C. The first two peaks are characteristics for Hemicellulose and Cellulose, while the third peak ($760\text{-}880^{\circ}$C) is an overlap between the peak for Lignin and the peak for the Boudouard reaction between fixed carbon and CO_2, respectively. The peak value increases with the heating rate due to the faster increase of the temperature with time.
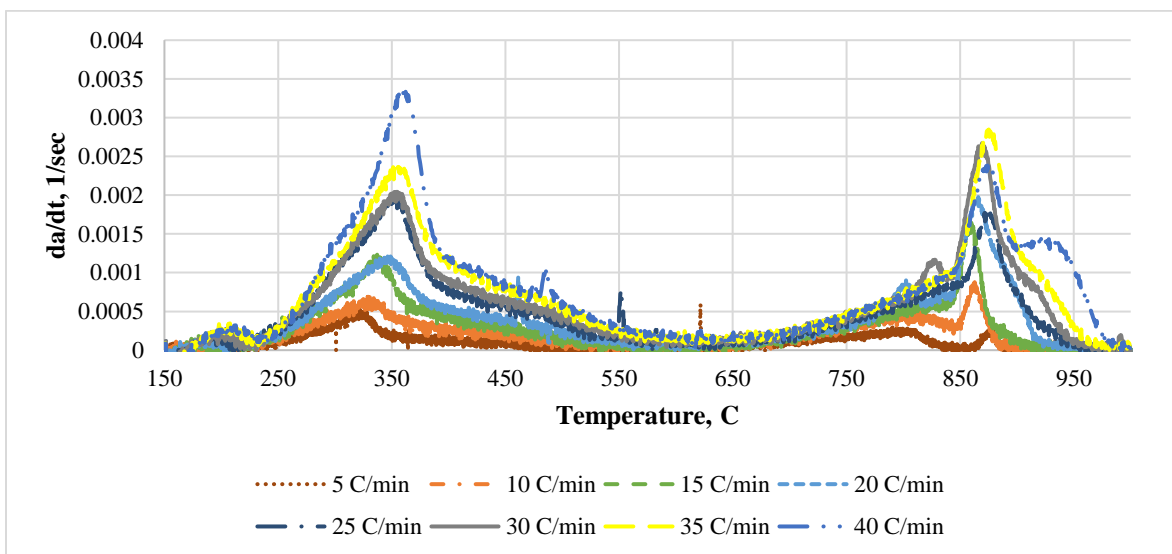
Figure 5-18: The change of the DTA with the temperature at different heating rates

As shown in Figure 5-19, the reaction is relatively steady from 150 to 350 °C with hardly exothermic reaction where the DTA values are positive. The endothermic reactions took place after 350°C due to the fast breakdown of Cellulose and Hemicelluloses, where the endothermic reaction took place for the rest of the experiment. After 750°C, when the heating rate increases, the curve started to drop sharply, which means that the reaction is endothermic. Also, the magnitude of the peak increases. Comparing the different heating rates, after 750 °C, one can observe that, for 5°C/min, the reaction required less heat, where the curve goes less down compared to other curves. The faster rate of change in temperature does not allow enough time for thermal equilibrium between the reference and sample, and thus the peak value appears larger.
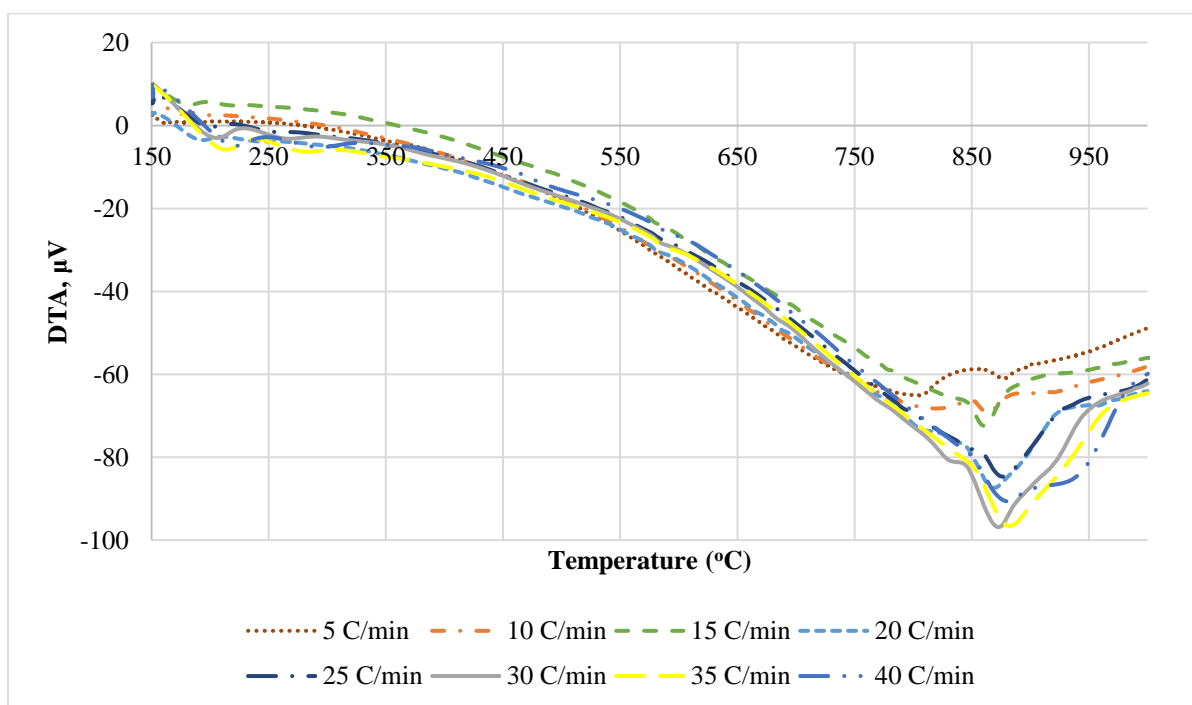
Figure 5-19: The change of the DTA with the temperature at different heating rates

5.5 Co-Pyrolysis

5.5.1 Co-Pyrolysis of Chicken and Cow manure

The two livestock manures have been mixed at four different ratios: 20%, 40%, 60%, and 80% cow manure of the total mixture weight. The same three parameters are used to give a better idea of the chemical kinetics for the mixture of thermal degradation. Starting with the extent of reaction. Figure 5-20 shows that the 40% and 60 % cow manure give a slower weight consumption compared to 20% and 80% cow manure. Figure 5-21 shows that the extent of reaction rate is increasing with increasing the cow manure percentage, which was expected as it approaches the cow manure characteristic to stand alone.
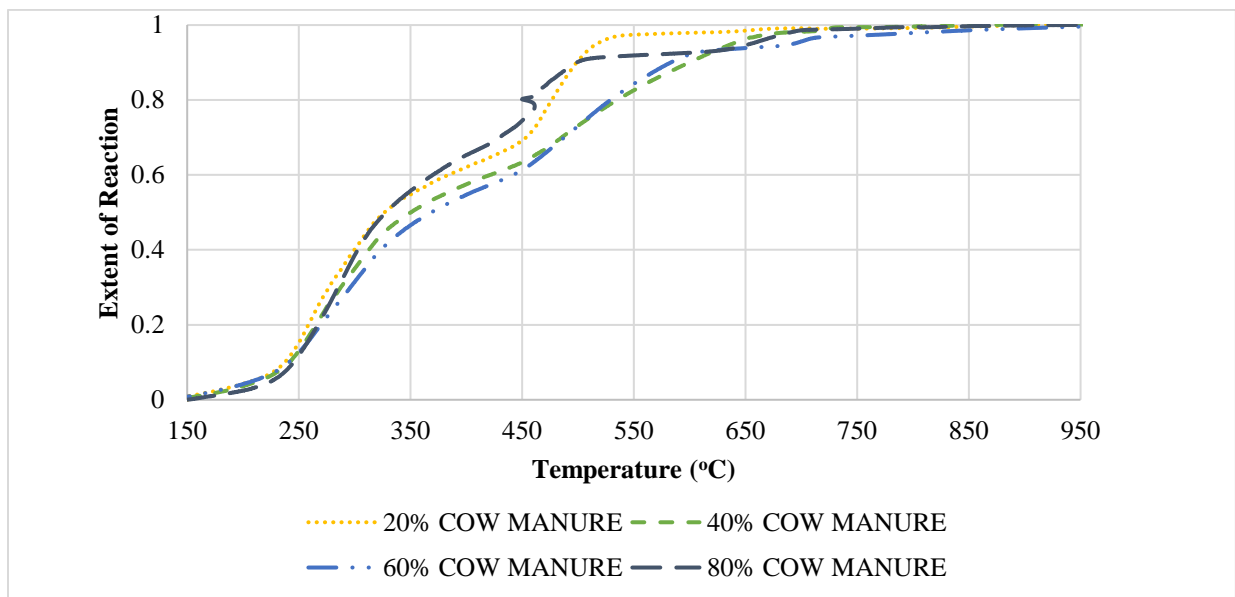
Figure 5-20: Extent of reaction variation with the temperature at different cow manure percentage
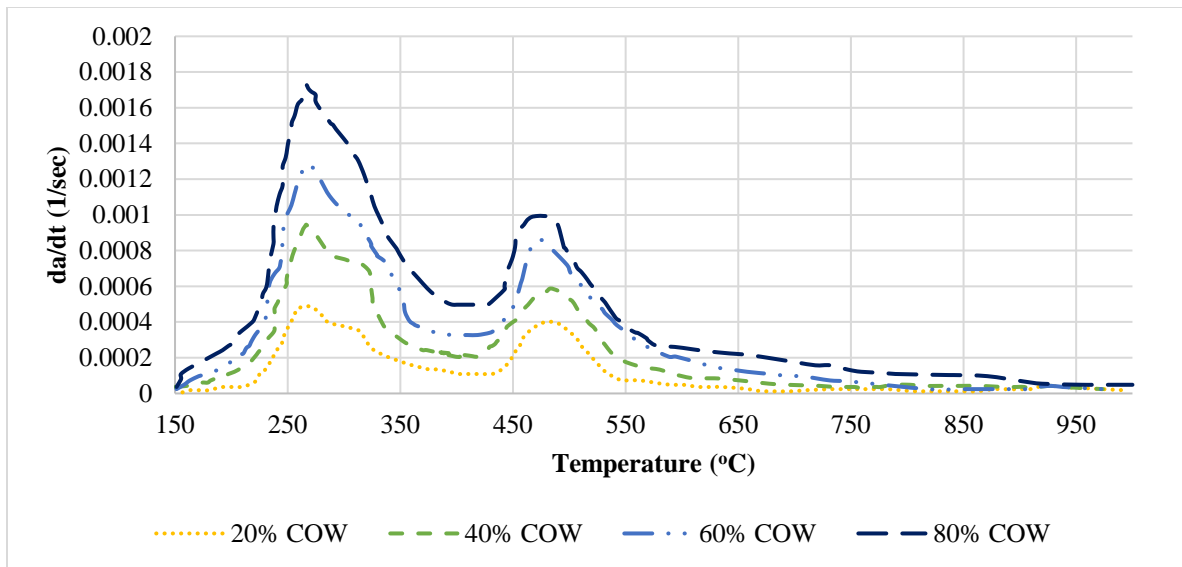
Figure 5-21: The rate of change of the extent of reaction with the temperature at different

cow manure percentage

Regarding the DTA, from Figure 5-22 it can be noticed that all the tested samples are exothermic except for the 60% cow manure, whose reaction turns into an endothermic reaction after 620 °C, which means further energy is needed to complete the Pyrolysis process. Several reasons for the inconsistency in the trend with 60% cow manure in comparison with other cases. The first one could be the bedding of cow manure (some wood straws). Another reason, as can be seen, increasing the cow manure percentage makes the reaction tends to be endothermic, and this is mainly because of the protein and amino acids that need a large amount of energy to be lost. In general, the thermal degradation of the cow manure is hard to predict because of the variation of its components. All these reasons could participate in this discrepancy. Overall, it can be observed that the 40% cow manure gives a stable exothermic reaction to the end of the process.
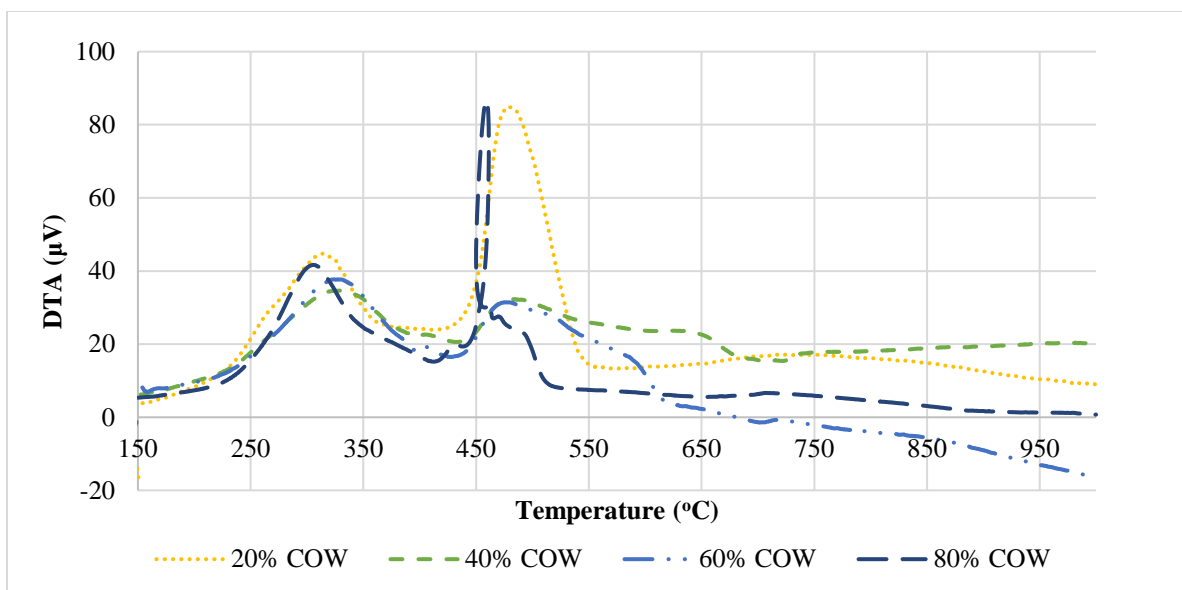
Figure 5-22: The change of the DTA with the temperature at different cow manure percentage

5.5.2 Evolved Gas Analysis

The main three components of most of the biomass species is Hemi-Cellulose, Cellulose and Lignin. Each of those elements has a decomposition temperature and the lignin has the highest temperature exceeding 800 °C. When the pyrolysis temperature is below this temperature, the residual mass is not only ashes. Sample was loaded in a metal mesh sample holder contained inside by quartz tube and quartz woo to keep sample in place. Two furnaces were used one for purge gas heating and the next one for pyrolysis. Both heated to 900 °C before the sample was loaded. Gases from the reactor were cooled using ice bath and pumped for analysis. Gases were acquired for the first 4 minutes using sampling gas bottles to analyze later and the next duration was analyzed online using Agilent 3000 microGC. MicroGC was calibrated using refinery gas standard. Each case has been implemented three times to reduce random errors.

5.5.2.1   Evolved Gas Analysis Data Processing:

To detect the N_2, H_2, O_2, CO, CO_2, CH_4, C_2H_2, C_2H_4, C_2H_6, and C_3H_8 the analyzer was calibrated. Any higher gaseous hydrocarbon existing will be insignificant quantity that is why it

they not included. The N2 flow rate is used as a tracer gas because it is an inert gas, and it will leave the reaction with the same mass as the inlet value. This known quantity will be used to calculate all other gases quantities using the measured concentrations from the gas analyzer. The energy rate for each gas x ($\dot{E}_x$) can be calculated by multiplying the mass flow rate by the heating value of each gas.

$$\dot{E}_x = \dot{m}_x \times HV_x \quad\text{...(5-1)}$$

The accumulated energy produced can be calculated by integrating the instantaneous energy rate with time

$$E_x = \left(\dot{E}_{x,l} - \dot{E}_{x,l-1}\right) \times \Delta t \text{.................................(5-2)}$$

The efficiency of conversion can be evaluated in two terms: carbon conversion efficiency and energy conversion efficiency. The carbon conversion efficiency, eqn. 5-3, is used to determine how much carbon is being converted compared to the carbon content in the biomass sample tested. where η_c is the carbon conversion efficiency.

$$\eta_c = \frac{m_{c,gas}}{m_{c,biomass}} \times 100\% \text{...(5-3)}$$

While $m_{c,gas}$ is the total carbon content of all the exhaust gases. This mass can be calculated by using eqn. (5-4).

$$m_{c,gas} = \sum_{i=1}^{x}\left(\dot{m}_{x,l} - \dot{m}_{x,l-1}\right) \times \Delta t \times f_x \text{ ....(5-4)}$$

Where f_x is the fraction of carbon by mass in each gas, for example $f_{CO} = 0.43, f_{CO2} = 0.27, f_{CH4} = 0.75, f_{C2H2} = 0.92, \dots\dots etc.$

With the same concept the energy conversion efficiency can be calculated by dividing the total energy extracted from each gas over the total energy in the biomass tested, eqn. (5-5)

$$\eta_E = \frac{\sum_{x=1}^{n} E_x}{m_{manure} \times HV_{manure}} \text{.................................(5-5)}$$

The dominate equation in the pyrolysis process is the thermal cracking, eqn. (5-6) as the nitrogen is the only gas that is used as an agent.

$$C_nH_m \rightleftharpoons C + C_xH_y + H_2 \ldots\ldots\ldots\ldots\ldots\ldots\ldots\ldots\ldots(5\text{-}6)$$
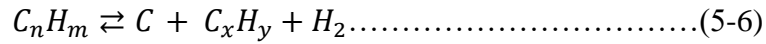
Other components should be taken into consideration which present in the biomass species such as amino acids, fats, and other components which are characterized by the presence of carboxylic groups (C=O-OH). When these groups are broken, they generate CO2.

The evolved gas analysis for the pyrolysis of the chicken manure at 900 ºC is shown in Figure 5-23. It can be observed that the CO_2 is produced at the highest flow rate and the same for the CH_4 among all the other hydrocarbons followed by C_2H_4 and H_2 then C_2H_6. Once the CH_4 starts to decay after 3 minutes from the reaction the formation of the CO and H_2 starts to increase this is because of the thermal cracking of the methane at this high temperature. Once the thermal cracking of the methane occurs the formation of all the other hydrocarbons starts to increase.
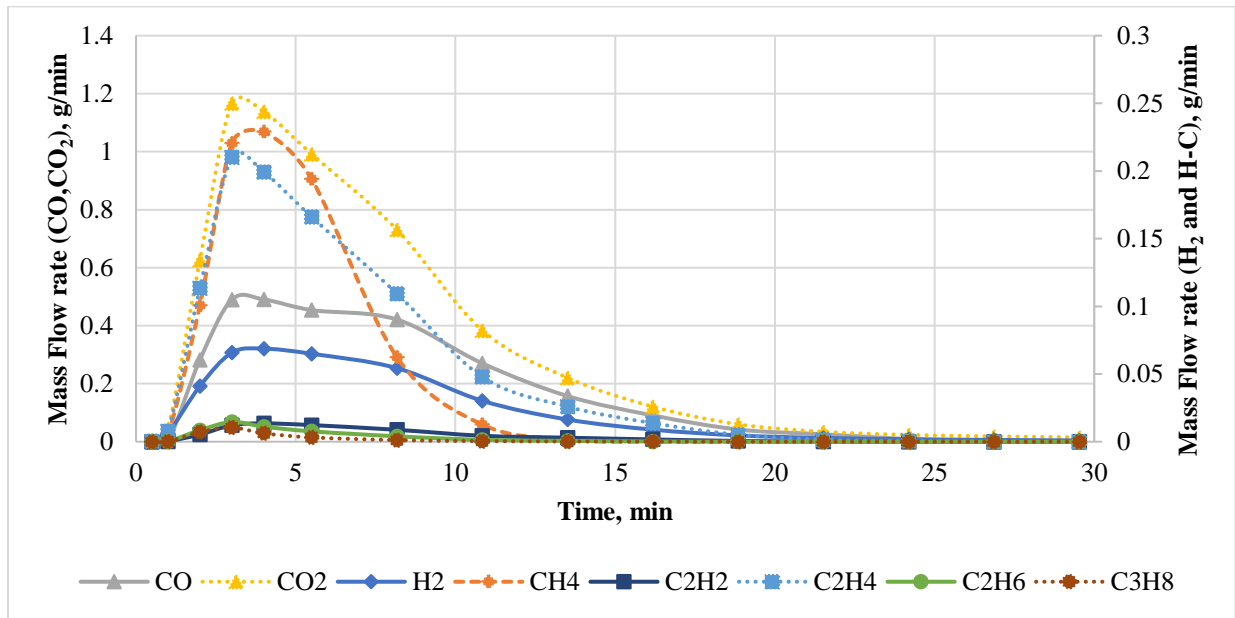
Figure 5-23: Evolved Gas Analysis of Chicken manure at 900 ºC

For the cow manure in Figure 5-24, the peaks started to occur later after 5 minutes, and this is mainly because of the protein and amino acids that need a large amount of energy to be broken.

Another significant results that can be seen is that the amount of the syngas produced during the pyrolysis process is much less compared to the chicken manure. Peak value of the methane produced in the cow manure (0.06 g/min) is one forth this one obtained from the chicken manure (0.23 g/min). Likewise, the methane in the chicken manure, once the methane decays all the other reactions start to produce heavier hydrocarbons and H_2.
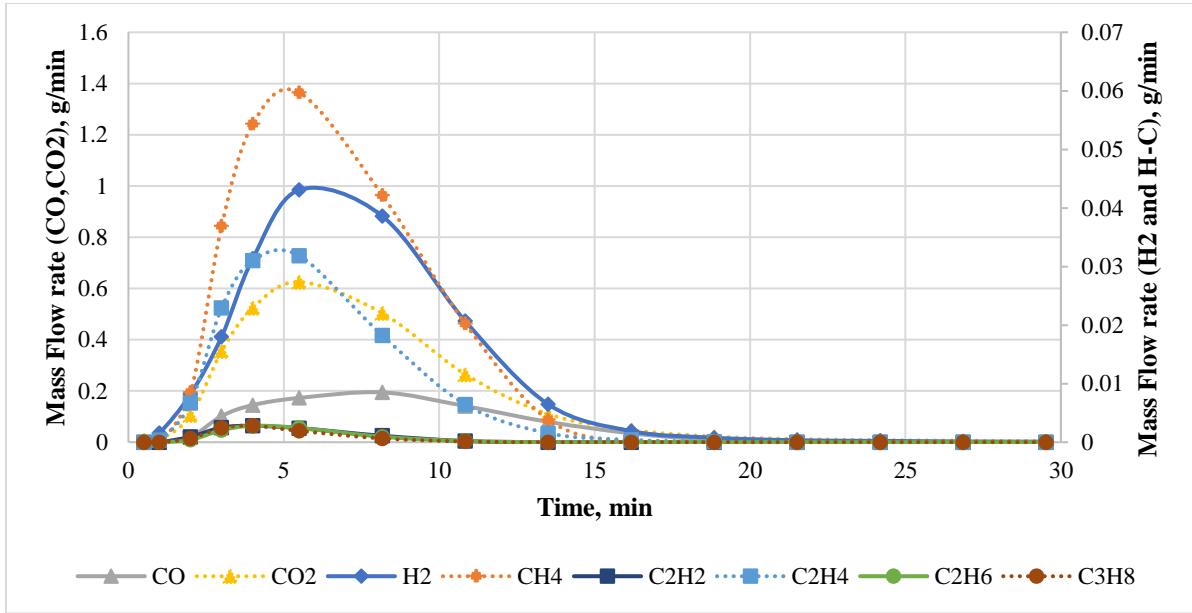
Figure 5-24: Evolved Gas Analysis of Cow Manure at 900 ^{o}C

The following four figures investigating the effect of mixing the cow manure with the chicken manure at different blend ratios. It can be observed in Figure 5-25, where 20% of the sample is cow manure, that the peak value of the hydrocarbons is slightly higher compared to those obtained from the chicken manure standalone (around 9.0 % more) and over four times higher than those from cow manure. The methane peak value in this case is 0.253 g/min while in chicken manure is 0.230 g/min.
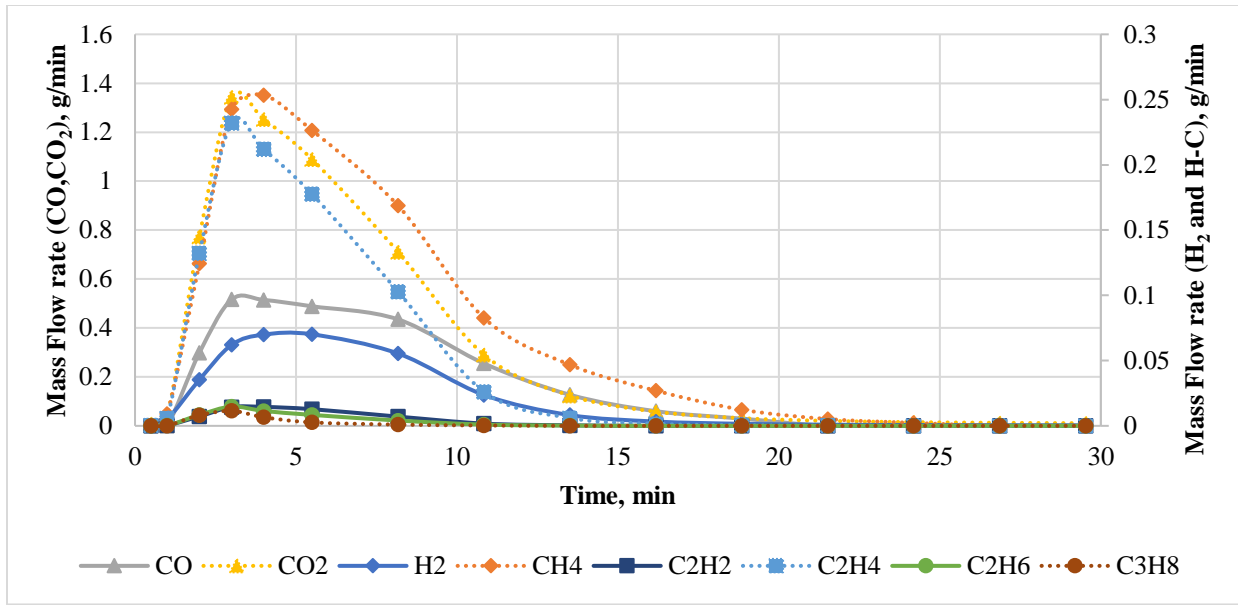
Figure 5-25: Evolved Gas Analysis of 20% COW manure and 80% Chicken at 900 ºC

With 40% Cow manure and 60% chicken manure in Figure 5-26, the peak value for all the hydrocarbons increased to reach 0.262 g/min for the methane as the highest.
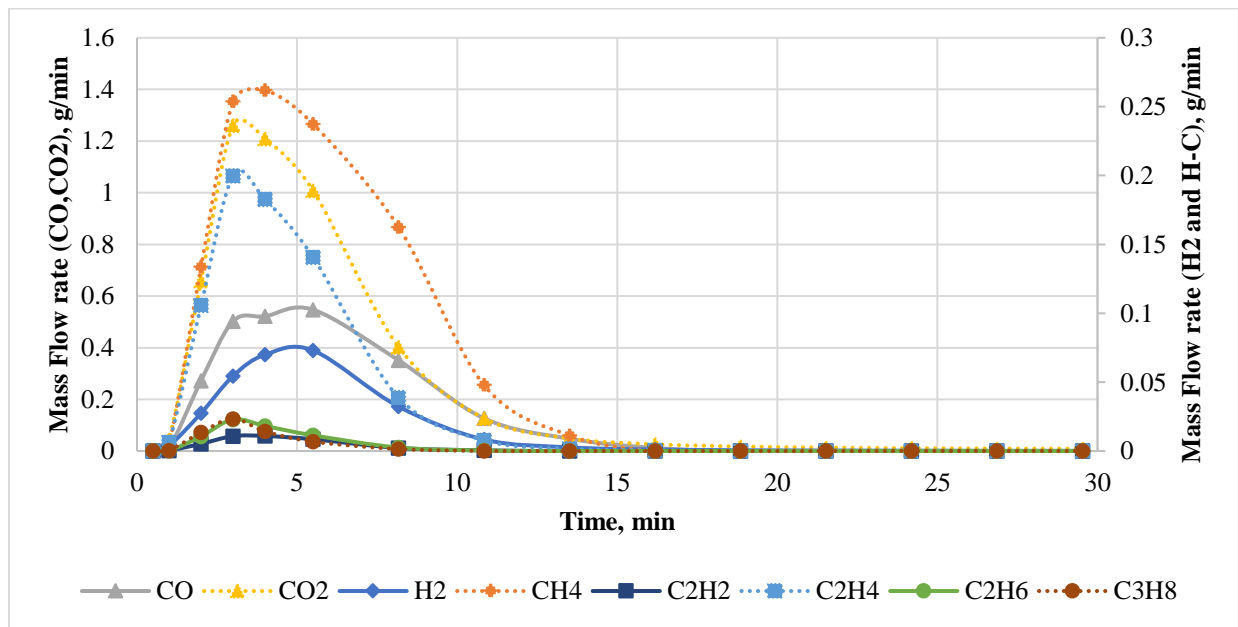
Figure 5-26: Evolved Gas Analysis of 40% COW manure and 60% Chicken Manure at 900 ºC

As expected, increasing the cow manure blend will not always be a privilege for the mixture and it can be observed that the reaction time started to increase while the extracted hydrocarbons

are almost half the value of the previous case. Or even less as shown in Figure 5-27 and Figure 5-28.
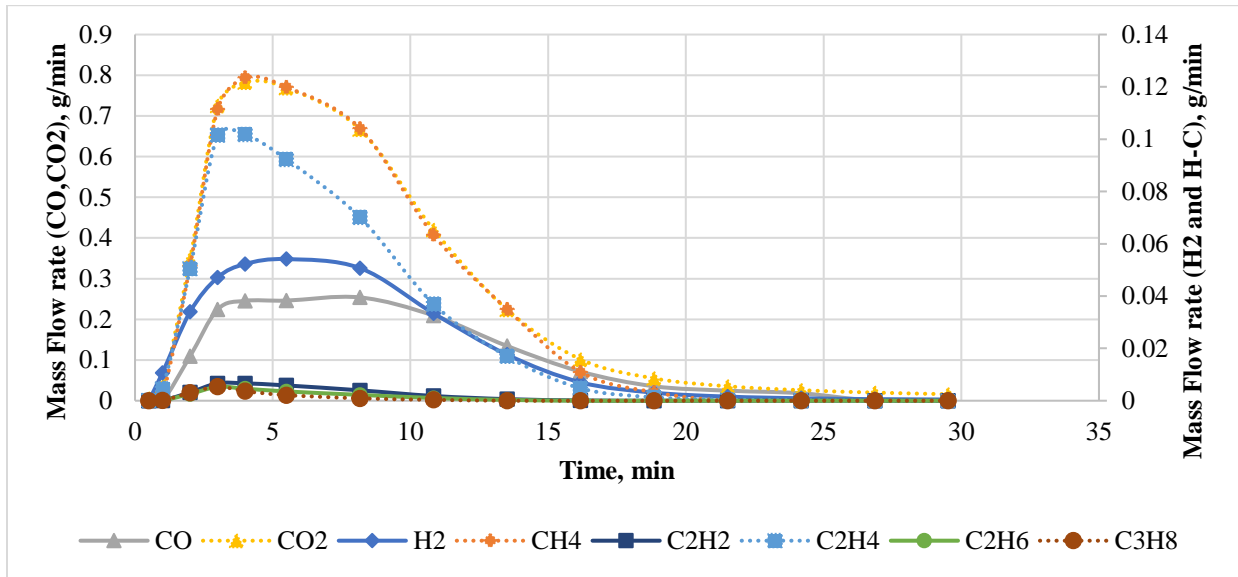
Figure 5-27: Evolved Gas Analysis of 60% Cow Manure and 40% Chicken Manure at 900 °C
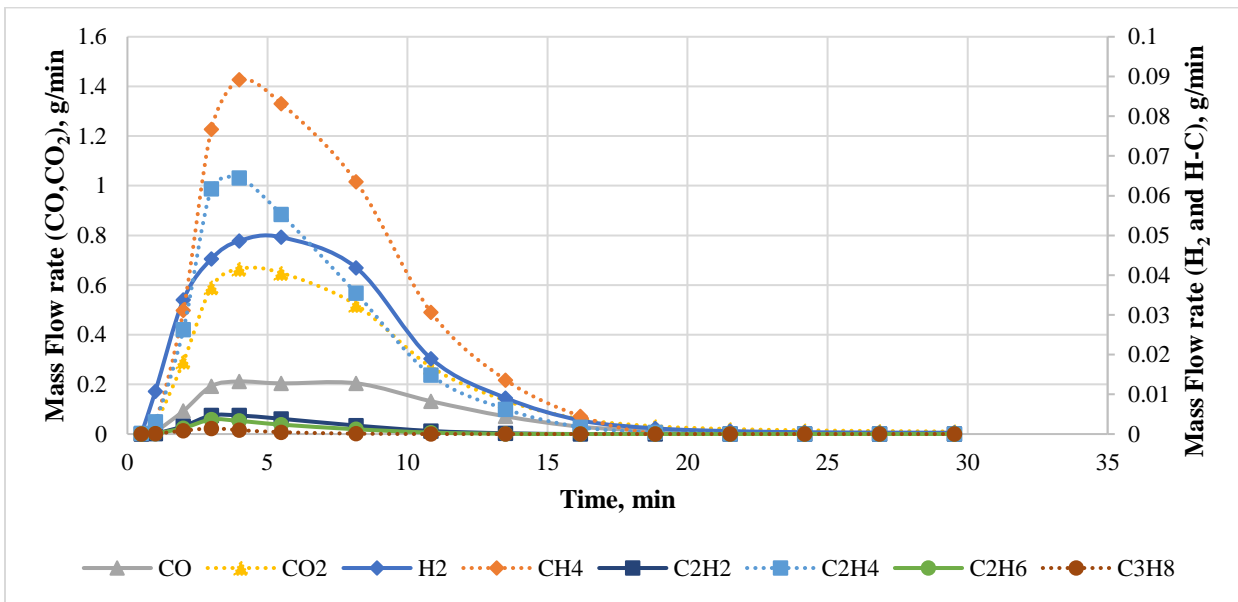
Figure 5-28: Evolved Gas Analysis of 80% Cow Manure and 20% Chicken Manure at 900 C

To make the comparison brilliant clear, the carbon conversion efficiency and the energy conversion efficiency are shown in Figure 5-29. It can be noticed that the 40% Cow manure with 60% chicken manure achieves the highest conversion rate for both carbon and energy followed by

the 20% cow manure. Energy wise, the 40% cow manure achieves an increase of 15.8% higher than the chicken manure stand alone and 195% (almost double) the energy extracted from the pyrolysis of the cow manure by itself.
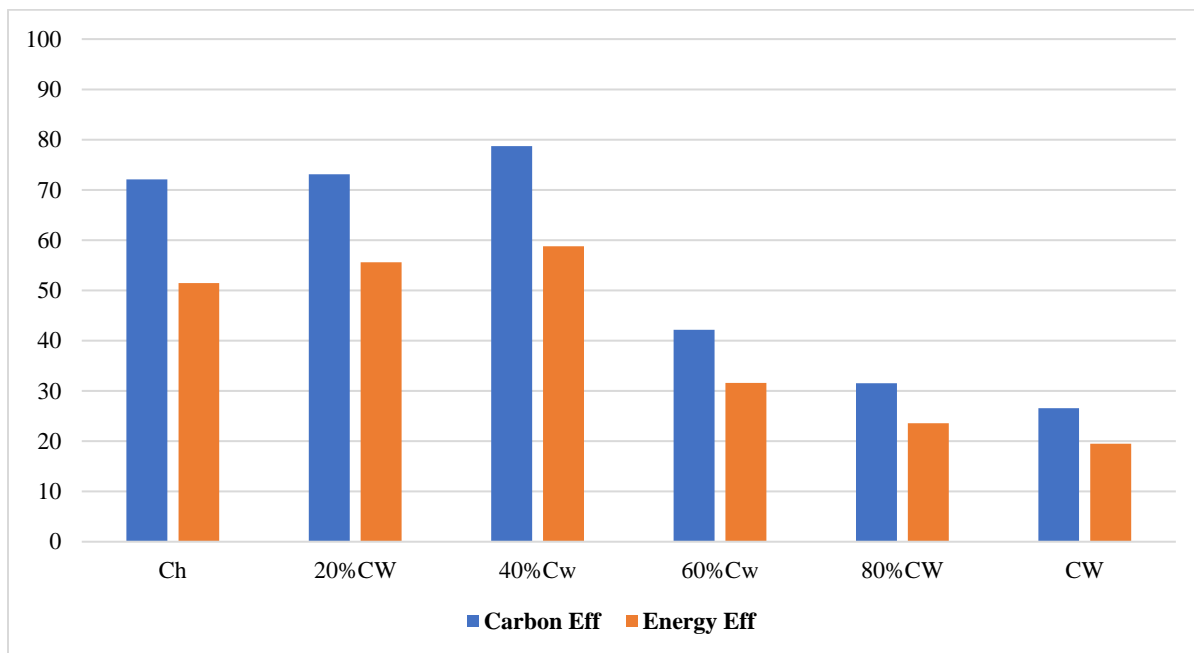
Figure 5-29: Carbon and Energy Efficiency of different blend ratios

5.6 CO-Gasification

5.6.1 CO-Gasification of Cow manure and Sheep Manure

Besides testing the cow manure and sheep manure standalone, the cow manure and sheep manure have been mixed with different blend ratios: 10%, 20%, 30%, 40%, 50%, 60%, 70%, 80% and 90% Sheep manure of the total mixture weight. For figures clarity, only 10%, 20%, 30%, 40%, 60% and 80% have been included. The main reason to include the 10% and 30% sheep manure in the figures, is to compare them with the 20% sheep manure which gives very promising results as will be discussed later. The same three parameters are used to give a better idea of the chemical kinetics for the mixture of thermal degradation. Starting with the extent of reaction, Figure 5-30 shows the extent of reaction for the gasification process of different blend ratios. The gasification

of 100% Sheep manure is faster compared to 100% cow manure: faster weight consumption. The thermal cracking represents the thermal cracking of the samples up to 255 °C. A faster reaction between 250-350 °C which represent the thermal degradation of hemicellulose. With a mild slope compared to the previous region as a preparation for the thermal cracking of cellulose; from 350 to 525 °C. Another stage only for the cow manure which represents the thermal degradation of the lignin and some other components like fats and protein from 550 to 725 °C. Finally, a steady reaction which represents the end of chemical reaction.
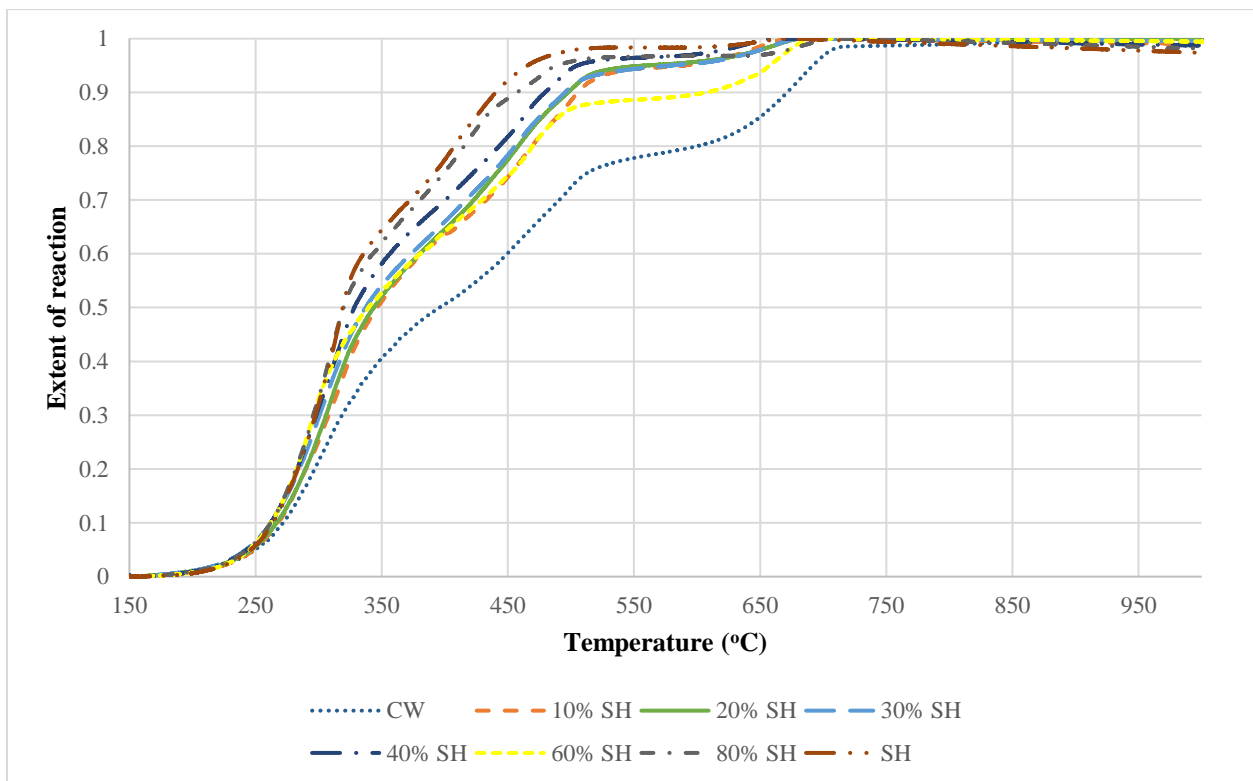
Figure 5-30: Extent of reaction variation with the temperature with different blend ratios

Those stages of thermal degradation can be seen in Figure 5-31, through some significant peaks where the first peak represent the thermal degradation of hemicellulose, second peak is for the cellulose and lastly the thermal degradation of lignin which can be significantly in the cow manure.
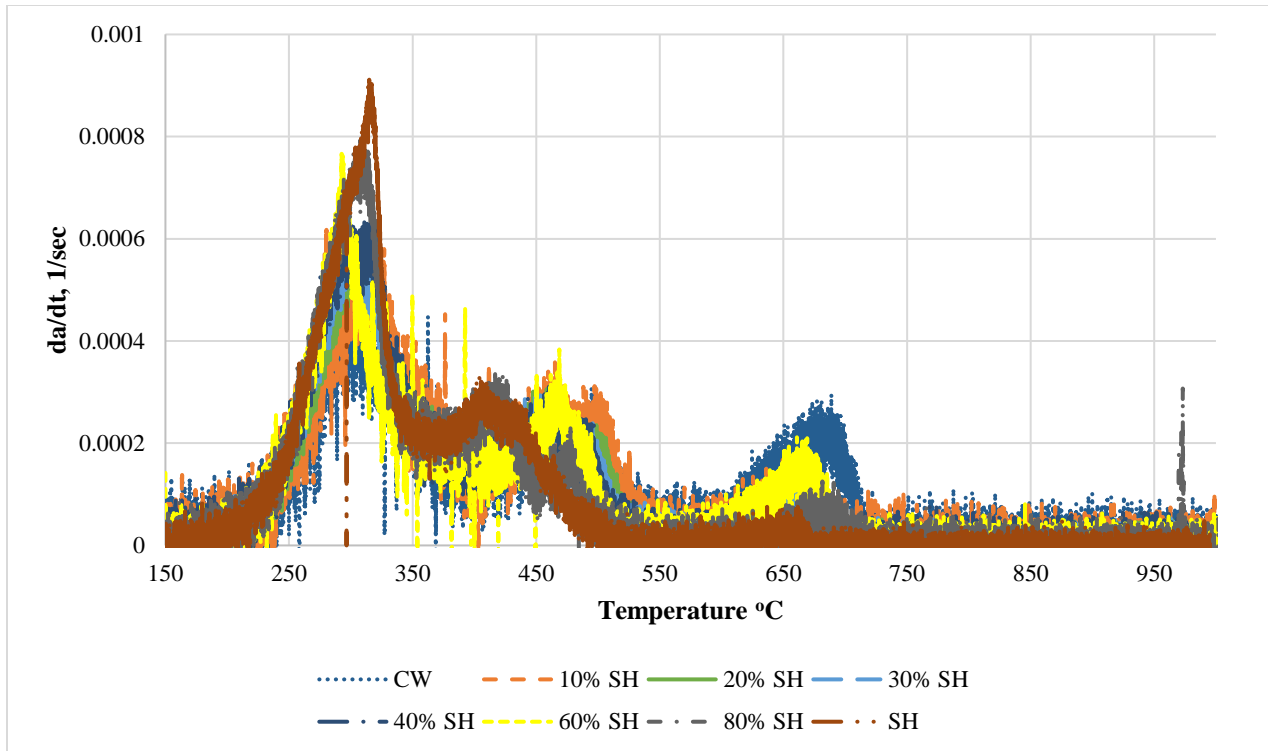
Figure 5-31: The rate of change of the extent of reaction with different blend ratios

The same peaks at the same temperatures are formed in Figure 5-32 which shows the differential thermal analysis. The fact that these peaks are positive (upwards) is due to the oxidation of some of the evolving gases rendering the reaction as exothermic. After 700°C no significant reaction was recorded, and the weight of the sample was stable. Overall, it can be observed that adding the sheep manure to the cow manure, increases the peak value values towards the pure sheep manure values which was expected. It can be noticed from this figure that all the tested samples are exothermic, then the reaction tends to be endothermic after 450 °C for the 100 sheep and 80% sheep and 550 °C for the 20% sheep manure which gives the highest exothermic reaction energy values compared to the other tested samples.

Figure 5-32: The change of the DTA with the temperature with different blend ratios

CHAPTER 6- CONCLUSIONS

6.1   Guide Vanes Optimization

It has been the primary endeavor of this work to develop and test novel passive control techniques which enhance mixing between primary and dilution streams and give better temperature uniformity at the combustor exit with minimum pressure loss. More uniform temperature flow leads to minor damage to turbine blades, reducing its maintenance cost and extending its lifespan. Thus, making the complete gas turbine system more cost-efficient. These techniques are chiefly motivated from the observation that the quality of mixing of two streams is sensitive to the entrance of the dilution jets as well as their penetration into the primary stream. At two different flow rates, two different positions of the internal guide vanes with different orientation were tested. All of these techniques are compared based on the uniformity factor (χ) to show how close the mixture fraction is to the equilibrium factor. Some emerged conclusions are by the variation of the uniformity factor for various techniques tested at different Reynolds Numbers. It was found that the mixing improved at the lower Reynolds Number in general. A plausible reason could be the more residence time available inside the dilution zone due to lower flow rate conditions, which provided sufficient time for the mixing of the primary hot air and the more cooling dilution air, thus, resulting in a better-mixed flow and more uniform temperature profile at the combustor exit. For all cases tested, it was found that the best location for the internal guide vanes is to be attached to the large holes, where a large amount of the secondary stream will be directed and mixed with the primary stream, hence improving the uniformity factor by almost 1% and up for all cases except for the 30º it was improved by 25%. As a result, among the same location, it was observed that the best orientation for the guide vanes is the 30° which enhances the penetration and the swirliness. These two factors are responsible for the quality of the mixing

process. The average uniformity factor for 30° guide vanes χ= 0.24, which was found to be about 14% and up more uniform than other techniques.

This study shows an experimental and numerical comparison between the external and internal guide vanes. For all tested flowrates, the external guide vanes show superiority over the internal guide vanes in terms of thermal uniformity, pressure drop, and thermal stresses.

- Taking the average for uniformity factor, the external guide vanes give a uniformity factor of ($\chi_{\text{avg}} = 0.22$) which is 18.5% more uniform than the staggered holes ($\chi_{\text{avg}} = 0.27$) while the internal guide vanes give 11% ($\chi_{\text{avg}} = 0.24$).

- Another factor was included, which is the pressure drop, where the 30° external guide vanes give less pressure drop, 2% lower, concerning the 30° internal guide vanes.

- In terms of the thermal stresses, the external guide vanes are subjected always to the cold stream which makes them less likely to fail compared to the internal ones as they are absorbing the temperature fluctuation from the hot stream.

A novel study in controlling the angle between the outer combustor surface and the internal chamber to enhance mixing quality in dilution zone, in addition taking into consideration the pressure drop, which is an essential factor that has a significant effect on the extracted power from gas turbines. The following observations were concluded:

- Taking the average uniformity factor, the 45-degree case achieves the lowest uniformity factor of 0.133, which is 37% more uniform than the staggered holes.

- The average uniformity factor of the 30 degrees was 0.134, which can be considered equal to that obtained from the 45 degrees.

- The resultant pressure drop from the 45 degrees is almost the same as the staggered holes as it was only 0.5% higher, while the 30 degrees is practically triple this percentage (1.6% higher).

- It is always preferable to choose the 45 degrees in designs in the industry as it is more accessible in manufacturing compared to all other angles.

6.2   Biomass Energy Enhancement

The thermo-gravimetric and differential thermal analyses were conducted for chicken manure using three different gasifying media (Nitrogen, Air, and Carbon Dioxide) with eight different heating rates (5, 10, 15, 20, 25, 30, 35, and 40°C/min.) from room temperature to 1000°C. The main difference between the Nitrogen Pyrolysis and Carbon Dioxide gasification occurred after the temperature regime (>700 ^{o}C). At this regime, the reaction turned into the endothermic reaction for the CO2 as it is governed by the Boudouard reaction, where the reaction turned into the endothermic reaction for the CO2. Air gasification is exothermic, and ignition was observed between 450-600°C. Therefore, with air gasification, the reaction has the potentials to be self-sustainable with no external heating. The chicken manure thermal degradation implied the presence of the three components: Hemicellulose, Cellulose, and Lignin. The highest reaction rates were observed at temperatures corresponding to known peak characteristics of the three components. Gasification with air had an extra peak for ignition at 600°C. The reaction kinetic parameters for the conversion reaction were calculated for the different media. The Nitrogen Pyrolysis was divided into two regions at 360°C with the order of reaction of five for both regions. Kinetic parameters for air gasification were calculated using a third-order single region reaction. CO_2 had the most complicated mechanism of the three cases and was divided into three regions at 360 and 630°C. The kinetic parameters varied with the heating rate. It is recommended to utilize

values generated by the lowest heating rate because the slow heating rate allows a quasi-equilibrium state and thus decreasing the effects of measurement errors due to delay in response or any transient condition error. For the Cow manure gasification, the CO_2 gasification shows very poor results in terms of energy required to sustain the chemical reaction. For all the heating rates, all the reactions where endothermic which means that the reaction needs energy to be completed.

Four different case studies were examined where the cow manure was added to chicken manure. The 40% Cow manure of the total sample gives a positive result where the reaction is steady exothermic reaction all over the Pyrolysis process. Those results have been reflected on the energy and carbon conversion efficiency to achieve 79% for carbon efficiency and 59% for energy conversion. Finally, CO-gasification, air is used as a gasifying agent, of the cow manure with the sheep manure has been investigated to show that the blend mixture of 20% sheep manure and 80% cow manure give the highest exothermic reaction among all other cases.

REFERENCES

[1]   Agblevor FA, Beis S, Kim SS, Tarrant R, Mante NO. Biocrude oils from the fast Pyrolysis of poultry litter and hardwood. Waste Manage 2010;30:298–307.doi: http://dx.doi.org/10.1016/j.wasman.2009.09.042.

[2]   Al Arni, Saleh. "Comparison of slow and fast Pyrolysis for converting biomass into fuel." Renewable Energy 124 (2018): 197-201.

[3]   Arabloo M, Bahadori A, Ghiasi MM, Lee M, Abbas A, Zendehboudi S. A novel modeling approach to optimize oxygen–steam ratios in coal gasification process. Fuel 2015;153:1–5. Doi: http://dx.doi.org/10.1016/j.fuel.2015.02.083.

[4]   Bahng M-K, Mukarakate C, Robichaud DJ, Nimlos MR. Current technologies for analysis of biomass thermochemical processing: a review. Anal Chim Acta 2009;651:117–38. Doi: http://dx.doi.org/10.1016/j.aca.2009.08.016.

[5]   Basol, A. M., Jenny, P., Ibrahim, M., Kalfas, A. I., and Abhari, R. S., 2011, "Hot Streak Migration in a Turbine Stage: Integrated Design to Improve Aerothermal Performance," ASME J. Eng. Gas Turbines Power, 133(6), p. 061901.

[6]   Broer KM, Woolcock PJ, Johnston PA, Brown RC. Steam/oxygen gasification system for the production of clean Syngas from switchgrass. Fuel 2015;140:282–92. Doi: http://dx.doi.org/10.1016/j.fuel.2014.09.078.

[7]   Bulushev DA, Ross JRH. Catalysis for conversion of biomass to fuels via Pyrolysis and gasification: a review. Catal Today 2011;171:1–13. Doi: http://dx.doi.org/10.1016/j.cattod.2011.02.005.

[8]   Burra, K. G., and A. K. Gupta. "Kinetics of synergistic effects in co-pyrolysis of biomass with plastic wastes." Applied Energy 220 (2018): 408-418.

[9]   Busby, J. J., Sondak, D. D., Staubach, B. B., and Davis, R. R., 1999, "Deterministic Stress Modeling of Hot Gas Segregation in a Turbine." ASME J. Turbomach., 122(1), pp. 62–67.

[10]   Butler, T. L., Sharma, O. P., Joslyn, H. D., and Dring, R. P., 1989, "Redistribution of Inlet Temperature Distortion in an Axial Flow Turbine Stage," AIAA J. Propul. Power, 5(1), pp. 64–71.

[11]   Chen, Hongzhang, and Lan Wang. Technologies for biochemical conversion of biomass. Academic Press, 2016.

[12]   Chhiti Y, Kemiha M. Thermal conversion of biomass, Pyrolysis and gasification: a review. Int J Eng Silences 2013;2:75–85.

[13]   Collot, A-G., Y. Zhuo, D. R. Dugwell, and R. Kandiyoti. "Co-Pyrolysis and co-gasification of coal and biomass in bench-scale fixed-bed and fluidised bed reactors." Fuel 78, no. 6 (1999): 667-679.

[14]   Corde, J. C., "SNECMA M88 Engine Development Status," ASME J. Eng. Gas Turbines Power, 113(1), pp. 20–25.

[15]   Costa, P., Pinto, F., Miranda, M., André, R., & Rodrigues, M. (2014). Study of the experimental conditions of the co-pyrolysis of rice husk and plastic wastes

[16]   Crocker, D. S., and Smith, C. E., 1995, "Numerical Investigation of Enhanced Dilution Zone Mixing in a Reverse Flow Gas Turbine Combustor," ASME J. Eng. Gas Turbines Power, 117(2), pp. 272–281.

[17]   Dai, W., Zhang, Y., Lin, Y., Yang, Q., and Zhang, C., 2014, "Influence of the Arrangement of Dilution Holes for Dilution Mixing in a Three-Injector Reverse Flow Combustor," ASME Turbo Expo 2014: Turbine Technical Conference and Exposition.

[18]   Dayananda, B. S., S. H. Manjunath, K. B. Girish, and L. K. Sreepathi. "An experimental approach on Gasification of the chicken litter with Rice husk." International Journal of Innovative Research in Science, Engineering and Technology 2, no. 7 (2013), pp. 2837-2842

[19]   Dejong W, Dinola G, Venneker B, Spliethoff H, Wojtowicz M. TG-FTIR Pyrolysis of coal and secondary biomass fuels: determination of Pyrolysis kinetic parameters for main species and NOx precursors. Fuel 2007;86:2367–76. Doi: http://dx.doi.org/10.1016/j.fuel.2007.01.032.

[20]   Dorney, D. J., Davis, R. L., Edwards, D. E., and Madavan, N. K., 1992, "Unsteady Analysis of Hot Streak Migration in a Turbine Stage," J. Propul. Power, 8(2), pp. 520–529.

[21]   Dry, Mark E. "Practical and theoretical aspects of the catalytic Fischer-Tropsch process." Applied Catalysis A: General 138, no. 2 (1996): 319-344.

[22]   Elgammal, T., and Amano, R. S., 2018, "Effectiveness of Central Swirlers in the Thermal Uniformity of Jet-in-Crossflow Mixing," ASME J. Energy Resour. Technol., 140(10), p. 101202.

[23]   Elgammal, T., Ibrahim, M. S., Amano, R. S., Rowland, D., Puls, K. S., and Alabbas, M., 2016, "Comparative Study of Using Streamlined Bodies as a Passive Enhancer in Combustor Dilution System," 54th AIAA Aerospace Sciences Meeting, AIAASciTech, San Diego, CA, Jan. 3–8.

[24]   Fan, Yingjie, Yaowu Li, Zhiqiang Wu, Zongyu Sun, and Bolun Yang. "Kinetic analysis on gaseous products during co-Pyrolysis of low-rank coal with lignocellulosic biomass model compound: Effect of Lignin." Energy Procedia 152 (2018): 916-921.

[25]   Font-Palma C. Characterization, kinetics, and modelling of gasification of poultry manure and litter: an overview. Energy Convers Manage 2012;53:92–8. Doi: http://dx.doi.org/10.1016/j.enconman.2011.08.017.

[26]   Gaur, Siddhartha, and Thomas B. Reed. An atlas of thermal data for biomass and other fuels. No. NREL/TP-433-7965. National Renewable Energy Lab., Golden, CO (United States), 1995.

[27]   Gebreegziabher, Tesfaldet, Adetoyese Olajire Oyedun, and Chi Wai Hui. "Optimum biomass drying for combustion–A modeling approach." Energy 53 (2013): 67-73.

[28]   Goyal, H. B., Diptendu Seal, and R. C. Saxena. "Bio-fuels from thermochemical conversion of renewable resources: a review." Renewable and sustainable energy reviews 12, no. 2 (2008): 504-517.

[29]   Guedes, Raquel Escrivani, Aderval S. Luna, and Alexandre Rodrigues Torres. "Operating parameters for bio-oil production in biomass Pyrolysis: A review." Journal of analytical and applied Pyrolysis 129 (2018): 134-149.

[30]   GUO, Xiu-juan, Shu-rong WANG, Kai-ge WANG, L. I. U. Qian, and Zhong-yang LUO. "Influence of extractives on mechanism of biomass Pyrolysis." Journal of fuel Chemistry and Technology 38, no. 1 (2010): pp.42-46.

[31]   Gupta, A., Ibrahim, M. S., and Amano, R. S., 2016, "Effect of Jet to Mainstream Momentum Flux Ratio on Mixing Process," Heat Mass Transfer, 52(3), pp. 621– 634.

[32]   Gupta, A., Ibrahim, M.S. and Amano, R.S., "Experimental study of novel passive control methods to improve combustor exit temperature uniformity", *Heat and Mass Transfer*, Vol. 51, No. 1, 2015, pp.23-32.

[33]   Han, Jaechan, Yeongryeol Choi, and Junghwan Kim. "Development of the Process Model and Optimal Drying Conditions of Biomass Power Plants." ACS omega 5, no. 6 (2020): 2811-2818.

[34]   Hatch, M. S., Sowa, W. A., & Samuelsen, G. S. (1995). Geometry and Flow Influences on Jet Mixing in a Cylindrical Duct. *Journal of Propulsion and Power*, 393-402.

[35]   He, Qing, Qinghua Guo, Lu Ding, Juntao Wei, and Guangsuo Yu. "Rapid Co-Pyrolysis of lignite and biomass blends: Analysis of synergy and gasification reactivity of residue char." Journal of Analytical and Applied Pyrolysis 143 (2019): 104688.

[36]   Heidari, Ava, Eshagh Khaki, Habibollah Younesi, and Hangyong Ray Lu. "Evaluation of fast and slow Pyrolysis methods for bio-oil and activated carbon production from eucalyptus wastes using a life cycle assessment approach." Journal of Cleaner Production 241 (2019): 118394.

[37]   Higman C, van der Burgt M, Higman C, van der Burgt M. Chapter 1 – introduction. Gasification 2008:1–9. Doi: http://dx.doi.org/10.1016/B978-07506-8528-3.00001-.

[38]   Hoke, J.B., Mountz, D.B., Olsen, H. and Sonntag, R.M., United Technologies Corporation, Low emissions can combustor with dilution hole arrangement for a turbine engine, *U.S. Patent* 6,101,814, 2000.

[39]   Holdeman, J. D., and Walker, R., 1977, "Mixing of a Row of Jets with a Confined Crossflow," AIAA J., 15(2), pp. 243–249.

[40]   Holdeman, J. D., Srinivasan, R., and Berenfeld, A., 1984, "Experiments in Dilution Jet Mixing," AIAA Journal, 22(10), pp. 1436–1443.

[41]   Holdeman, J. D., Walker, R. E., & Kors, D. L. (1973). Mixing of Multiple Dilution Jets with a Hot Primary Airstream for Gas Turbine Combustors. *AIAA and Society of Engineers Ninth Propulsion Conference.* Las Vegas

[42]   Holdeman, J.D., "Mixing of multiple jets with a confined subsonic crossflow", *Progress in Energy and Combustion Science*, Vol. 19, No. 1, 1993, pp.31-70.

[43]   Hossain, M. S., Islam, M. R., Rahman, M. S., Kader, M. A., & Haniu, H. (2017). Biofuel from Co-pyrolysis of Solid Tire Waste and Rice Husk. In Energy Procedia (Vol. 110, pp. 453–458). Elsevier Ltd. https://doi.org/10.1016/j.egypro.2017.03.168

[44]   Hussein, Mohamed Hussein, "Experimental Investigation of Chicken Manure Pyrolysis and Gasification" (2016). Ph.D. Thesis, University of Wisconsin-Milwaukee.

[45]   Jenny, P., Lenherr, C., Abhari, R. S., and Kalfas, A., 2012, "Effect of Hot Streak Migration on Unsteady Blade Row Interaction in an Axial Turbine," ASME J. Turbomach., 134(5), p. 051020.

[46]   Joseph P, Tretsiakova-McNally S, McKenna S. Characterization of cellulosic wastes and gasification products from chicken farms. Waste Manage 2012;32:701–9. Doi: http://dx.doi.org/10.1016/j.wasman.2011.09.024.

[47]   Kalinci Y, Hepbasli A, Dincer I. Biomass-based hydrogen production: a review and analysis. Int J Hydrogen Energy 2009;34:8799–817. Doi: http://dx.doi.org/10.1016/j.ijhydene.2009.08.078.

[48]   Kamin´ska-Pietrzak N, Smolin´ski A. Selected environmental aspects of gasification and co-gasification of various types of waste. J Sustain Min 2013;12:6–13. Doi: http://dx.doi.org/10.7424/jsm130402.

[49]   Kamruzzaman, M., and AKM Sadrul Islam. "Physical and thermochemical properties of rice husk in Bangladesh." International Journal of BioResearch 6 (2011): pp.45-49.

[50]   Karatas H, Olgun H, Akgun F. Experimental results of gasification of waste tire with air & CO2, air & steam, and steam in a bubbling fluidized bed gasifier. Fuel Process Technol 2012;102:166–74. Doi: http://dx.doi.org/10.1016/j.fuproc.2012.04.013.

[51]   Kim S-S, Agblevor FA, Lim J. Fast Pyrolysis of chicken litter and turkey litter in a fluidized bed reactor. J Ind Eng Chem 2009;15:247–52. Doi: http://dx.doi.org/10.1016/j.jiec.2008.10.004.

[52]   Kim S-S, Agblevor FA. Pyrolysis characteristics and kinetics of chicken litter. Waste Manage 2007;27:135–40. Doi: http://dx.doi.org/10.1016/j. wasman.2006.01.012.

[53]   Kirubakaran V, Sivaramakrishnan V, Premalatha M, Subramanian P. Kinetics of auto-gasification of poultry litter. Int J Green Energy 2007;4:519–34. Doi: http://dx.doi.org/10.1080/15435070701583102.

[54]   Kumar A, Jones DD, Hanna MA. Thermochemical biomass gasification: a review of the status of the technology. Energies 2009;2:556–81. Doi: http://dx.doi.org/10.3390/en20300556

[55]   Lenertz, J. and Lawrence, K., AlliedSignal Inc., Combustor dilution bypass method, *U.S. Patent* 6,178,737, 2001.

[56]   Liou, T. -M., Hsiao, K. -L., & Tsai, M. -K. (1991). Experimental and Theoretical Studies on Turbulent Mixing of Two Confined Jets. *International Journal of Heat and Fluid Flow* , 210-217

[57]   Lv, Yuexia, Jinpeng Bi, and Jinyue Yan, "State-of-the-art in low carbon community," International Journal of Energy for a Clean Environment 19, no. 3-4, (2018).

[58]   M. Balat (2008) Mechanisms of Thermochemical Biomass Conversion Processes. Part 1: Reactions of Pyrolysis, Energy Sources, Part A: Recovery, Utilization, and Environmental Effects, 30:7, 620-635, DOI:

[59]   Mahinpey N, Gomez A. Review of gasification fundamentals and new findings: reactors, feedstock, and kinetic studies. Chem Eng Sci 2016;148:14–31. Doi: http://dx.doi.org/10.1016/j.ces.2016.03.037.

[60]   Mallick, Debarshi, Maneesh Kumar Poddar, Pinakeswar Mahanta, and Vijayanand S. Moholkar. "Discernment of synergism in Pyrolysis of biomass blends using thermogravimetric analysis." Bioresource technology 261 (2018): 294-305.

[61]   McKendry P. Energy production from biomass (part 1): overview of biomass. Bioresour Technol 2002;83:37–46. Doi: http://dx.doi.org/10.1016/S0960-8524 (01)001183.

[62]   Mohan D, Pittman CU, Steele PH. Pyrolysis of wood/biomass for bio-oil: a critical review. Energy Fuel 2006;20:848–89. Doi: http://dx.doi.org/10.1021/ef0502397.

[63]   Molino, Antonio, Simeone Chianese, and Dino Musmarra. "Biomass gasification technology: The state-of-the-art overview." Journal of Energy Chemistry 25, no. 1 (2016): 10-25.

[64]   N. Ruiz-Gómez, V. Quispe, J. Ábrego, M. Atienza-Martínez, M.B. Murillo, G. Gea,Co-pyrolysis of sewage sludge and manure, Waste Manage 59(2017) 211,https://doi.org/10.1016/j.wasman.2016.11.013

[65]   Neves, Daniel, Henrik Thunman, Arlindo Matos, Luís Tarelho, and Alberto Gómez-Barea. "Characterization and prediction of biomass Pyrolysis products." Progress in Energy and Combustion Science 37, no. 5 (2011): 611-630.

[66]   Ng, Wei Cheng, Siming You, Ran Ling, Karina Yew-Hoong Gin, Yanjun Dai, and Chi-Hwa Wang. "Co-gasification of woody biomass and chicken manure: Syngas production, biochar reutilization, and cost-benefit analysis." Energy 139 (2017): 732-742.

[67]   Norgren, C. T., & Humenik, F. M. (1968). *Dilution-Jet Mixing Study for Gas Turbine Combustors.* National Aeronautics and Space Administration. Springfield: Clearinghouse for Fedral Scientific and Technical Information.

[68]   Ong, Hwai Chyuan, Wei-Hsin Chen, Abid Farooq, Yong Yang Gan, Keat Teong Lee, and Veeramuthu Ashokkumar. "Catalytic thermochemical conversion of biomass for biofuel production: A comprehensive review." Renewable and Sustainable Energy Reviews 113 (2019): 109266.

[69]   Outlook, A.E., 2020. Energy information administration. Department of Energy, Washington, DC 20585, pp.1-161.

[70]   Pandey, Ashok, ed. Biofuels: alternative feedstocks and conversion processes. Academic Press, 2011.

[71]   Pandey, Ashok, Thallada Bhaskar, Michael Stöcker, and Rajeev Sukumaran, eds. Recent advances in thermochemical conversion of biomass. Elsevier, 2015.

[72]   Pandey, Ashok. Handbook of plant-based biofuels. CRC press, 2008.

[73]   Parthasarathy P, Narayanan KS. Hydrogen production from steam gasification of biomass: influence of process parameters on hydrogen yield – a review. Renew Energy 2014;66:570–9. Doi: http://dx.doi.org/10.1016/j. renene.2013.12.025.

[74]   Pereira EG, da Silva JN, de Oliveira JL, Machado CS. Sustainable energy: a review of gasification technologies. Renew Sustain Energy Rev 2012;16:4753–62. Doi: http://dx.doi.org/10.1016/j.rser.2012.04.023.

[75]   Phyllis2, database for biomass and waste, 2015 [Online]. Available at: https://www.ecn.nl/phyllis2/Biomass/View/3501

[76]   Pinto F, André R, Miranda M, Neves D, Varela F, Santos J. Effect of gasification agent on co-gasification of rice production wastes mixtures. Fuel 2016;180:407–16. Doi: http://dx.doi.org/10.1016/j.fuel.2016.04.048.

[77]   Povey, T., and Qureshi, I., 2008, "A Hot-Streak (Combustor) Simulator Suited to Aerodynamic Performance Measurements," Proc. Inst. Mech. Eng., Part G, 222(6), pp. 705–720.

[78]   Povey, T., and Qureshi, I., 2009, "Developments in Hot-Streak Simulators for Turbine Testing," ASME J. Turbomach., 131(3), p. 031009.

[79]   Povey, T., Chana, K. S., Jones, T. V., and Hurrion, J., 2007, "The Effect of Hot Streaks on HP Vane Surface and End Wall Heat Transfer: An Experimental and Numerical Study," ASME J. Turbomach., 129(1), pp. 32–43.

[80]   Powel, S. F., 1991, "On the Leading Edge: Combining Maturity and Advanced Technology on the F404 Turbofan Engine," ASME J. Eng. Gas Turbines Power, 113(1), pp. 1–10.

[81]   Prière, C., Gicquel, L.Y., Gajan, P., Strzelecki, A., Poinsot, T. and Bérat, C., "Experimental and numerical studies of dilution systems for low-emission combustors", *AIAA journal*, Vol. 43, No. 8, 2005, pp.1753-1766.

[82]   Priyadarsan S, Annamalai K, Sweeten JM, Holtzapple MT, Mukhtar S. Co-gasification of blended coal with feedlot and chicken litter biomass. Proc Combust Inst 2005;30:2973–80.doi: http://dx.doi.org/10.1016/j.proci.2004.08.137.

[83]   Puig-Arnavat M, Bruno JC, Coronas A. Review, and analysis of biomass gasification models. Renew Sustain Energy Rev 2010;14:2841–51. Doi: http://dx.doi.org/10.1016/j.rser.2010.07.030.

[84]   Qureshi, I., Beretta, A., and Povey, T., 2011, "Effect of Simulated Combustor Temperature Nonuniformity on HP Vane and End Wall Heat Transfer: An Experimental and Computational Investigation," ASME J. Eng. Gas Turbine Power, 133(3), p. 031901.

[85]   Qureshi, I., Smith, A. D., Chana, K. S., and Povey, T., 2012, "Effect of Temperature Nonuniformity on Heat Transfer in an Unshrouded Transonic HP Turbine: An Experimental and Computational Investigation," ASME J. Turbomach., 134(1), p. 011005.

[86]   Rai, M. M., and Dring, R. P., 1990, "Navier–Stokes Analyses of the Redistribution of Inlet Temperature Distortions in a Turbine," J. Propul. Power, 6(3), pp. 225–226

[87]   Reed, Thomas B. Encyclopedia of biomass thermal conversion: the principles and technology of Pyrolysis, gasification & combustion. Biomass energy foundation Press, 2002.

[88]   Roback, R. J., and Dring, R. P., 1993, "Hot Streaks and Phantom Cooling in a Turbine Rotor Passage: Part 1—Separate Effects." ASME J. Turbomach., 115(4), pp. 657–666.

[89]   Rosendahl, Lasse, ed. Biomass combustion science, technology, and engineering. Elsevier, 2013.

[90]   Ryu, Hae Won, Do Heui Kim, Jungho Jae, Su Shiung Lam, Eun Duck Park, and Young-Kwon Park. "Recent advances in catalytic co-Pyrolysis of biomass and plastic waste for the production of petroleum-like hydrocarbons." Bioresource Technology (2020): 123473.

[91]   Saxena RC, Seal D, Kumar S, Goyal HB. Thermo-chemical routes for hydrogen rich gas from biomass: a review. Renew Sustain Energy Rev 2008;12:1909–27. Doi: http://dx.doi.org/10.1016/j.rser.2007.03.005.

[92]   Saxer, A. P., and Felici, H. M., 1996, "Numerical Analysis of Three-Dimensional Unsteady Hot Streak Migration and Shock Interaction in a Turbine Stage," ASME J. Turbomach., 118(2), pp. 268–277.

[93]   Seçer, Açelya, Nilgün Küçet, Ender Fakı, and Arif Hasanoğlu. "Comparison of co–gasification efficiencies of coal, lignocellulosic biomass and biomass hydrolysate for high yield hydrogen production." international journal of hydrogen energy 43, no. 46 (2018): 21269-21278.

[94]   Sharma S, Sheth PN. Air–steam biomass gasification: experiments, modeling, and simulation. Energy Convers Manage 2016;110:307–18. Doi: http://dx.doi.org/10.1016/j.enconman.2015.12.030.

[95]   SMITH, C., "Mixing characteristics of dilution jets in small gas turbine combustors", *In 26th Joint Propulsion Conference*, July 1990, p. 2728.

[96]   Stevens, S. J., & Carrotte, J. F. (1988). Experimental Studies of Combustor Dilution Zone Aerodynamics. *AIAA/ASME/SAE/ASEE 24th Joint Propulsion Conference.* Boston

[97]   Stevens, S. J., and Carrotte, J. F., 1990, "Experimental Studies of Combustor Dilution Zone Aerodynamics. II—Jet Development," J. Propul. Power, 6(4), pp. 504–511.

[98]   Sutton D, Kelleher B, Ross JRH. Review of literature on catalysts for biomass gasification. Fuel Process Technol 2001;73:155–73. Doi: http://dx.doi.org/10.1016/S0378-3820(01)00208-9.

[99]   Takahashi, R., and Ni, R. H., 1991, "Unsteady Hot Streak Simulation Through 1-1 2 Stage Turbine," AIAA Paper No. 91-3382.

[100]   Tańczuk, Mariusz, Robert Junga, Alicja Kolasa-Więcek, and Patrycja Niemiec. "Assessment of the Energy Potential of Chicken Manure in Poland." Energies 12, no. 7 (2019): pp.1244-1262

[101]   Tanksale A, Beltramini JN, Lu GM. A review of catalytic hydrogen production processes from biomass. Renew Sustain Energy Rev 2010;14:166–82. Doi: http://dx.doi.org/10.1016/j.rser.2009.08.010.

[102] Tanoue, Ken-Iciro, Tatsuya Hinauchi, Thaung Oo, Tatsuo Nishimura, Miki Taniguchi, and Ken-Ichi Sasauchi. "Modeling of heterogeneous chemical reactions caused in Pyrolysis of biomass particles." Advanced Powder Technology 18, no. 6 (2007): 825-840.

[103] Uddin et al. Effects of Pyrolysis parameters on hydrogen formation from biomass: a review.

[104] Verma, M., S. Godbout, S. K. Brar, O. Solomatnikova, S. P. Lemay, and J. P. Larouche. "Biofuels production from biomass by thermochemical conversion technologies." International Journal of Chemical Engineering 2012 (2012).

[105] Vieira, Fábio Roberto, Carlos M. Romero Luna, Gretta LAF Arce, and Ivonete Ávila. "Optimization of slow Pyrolysis process parameters using a fixed bed reactor for biochar yield from rice husk." Biomass and Bioenergy 132 (2020): 105412.

[106] Wang L, Weller CL, Jones DD, Hanna MA. Contemporary issues in thermal gasification of biomass and its application to electricity and fuel production. Biomass Bioenergy 2008;32:573–81. Doi: http://dx.doi.org/10.1016/j.biombioe.2007.12.007.

[107] White, J. E., Catallo, W. J., & Legendre, B. J. (2011). "Biomass pyrolysis kinetics: A comparative critical review with relevant". Journal of Analytical and Applied Pyrolysis

[108] Wittig, S. L., Elbahar, O. M., & Noll, B. E. (1984). Temperature Profile Development in Turbulent Mixing of Coolant Jets with a Confined Hot Crossflow. *Journal of Engineering for Gas Turbines and Power , 106* (1), 193-197

[109] Woolcock PJ, Brown RC. A review of cleaning technologies for biomass-derived Syngas. Biomass Bioenergy 2013;52:54–84. Doi: http://dx.doi.org/10.1016/j.biombioe.2013.02.036.

[110] Xiao X, Le DD, Li L, Meng X, Cao J, Morishita K, et al. Catalytic steam gasification of biomass in fluidized bed at low temperature: conversion from livestock manure compost to hydrogen-rich Syngas. Biomass Bioenergy 2010;34:1505–12. Doi: http://dx.doi.org/10.1016/j.biombioe.2010.05.001.

[111] Yanagida T, Minowa T, Nakamura A, Matsumura Y, Noda Y. Behavior of inorganic elements in poultry manure during supercritical water gasification. Nihon Enerugi Gakkaishi/J. Jpn Inst Energy 2008. Doi: http://dx.doi.org/10.3775/jie.87.731.

[112] Yanagida T, Minowa T, Shimizu Y, Matsumura Y, Noda Y. Recovery of activated carbon catalyst, calcium, Nitrogen, and phosphate from effluent following supercritical water gasification of poultry manure. Bioresour Technol 2009;100:4884–6. Doi: http://dx.doi.org/10.1016/j.biortech.2009.05.042.

[113] Yang, H. (2007). Characteristics of hemicellulose, cellulose, and lignin pyrolysis. Fuel, 1781-1788

[114] Yang, Haiping, Rong Yan, Hanping Chen, Dong Ho Lee, and Chuguang Zheng. "Characteristics of Hemicellulose, Cellulose and Lignin Pyrolysis." Fuel 86, no. 12-13 (2007): 1781-1788.

[115] Yuan, Haoran, Tao Lu, Dandan Zhao, Yazhuo Wang, and Noriyuki Kobayashi. "Influence of Oxygen Concentration and Equivalence Ratio on MSW Oxygen-Enriched Gasification Syngas Compositions." In Progress in Clean Energy, Volume 2, pp. 165-176. Springer, Cham, 2015.

[116] Yuan, Tong, Wenjing He, Guojun Yin, and Shiai Xu. "Comparison of bio-chars formation derived from fast and slow Pyrolysis of walnut shell." Fuel 261 (2020): 116450.

CURRICULUM VITAE

Osama M. Selim

PROFESSIONAL HIGHLIGHTS

- Intern CFD methodology Engineer at Rockwell Automation
- More than 6 academic awards from university of Wisconsin Milwaukee
- Fifteen scientific research publications, including books, journal, and conference papers.
- More than 40 energy audits to serve over 25 different manufacturing companies.
- Certificate from the Department of Energy for completing 21 energy auditing visits to manufacturing companies.
- Member of Cairo University Racing Team, responsible for designing the intake and lubrication system. In 2012, we achieved the third place in the designing phase among 120 team over the world at the competition held in Silverstone Circuit, UK
- Three years of experience as a Sales Engineer in the petroleum sector representing many companies in different fields; Gas compression applications, Oily wastewater treatment, Direct and Indirect heaters. Achievements:
  - ✓ $300,000, Flow metering system to Pesco Energy Services and Contracting, UAE
  - ✓ $70,000, Wastewater treatment study to Gulf of Suez Petroleum Company, Egypt

WORK EXPERIENCE

ACCESS INC, NEENAH, WISCONSIN
Application Engineer, Jan 2022 – Present
- Work with the Sales team and the technical project management team to identify customer technical specifications during the proposal phase of a bid cycle.
- Manage vendor/supplier relationships to deliver customer value
- Support bankability analysis of potential vendor partners with an emphasis on technical capability
- Create quotations and technical proposals for customers

ROCKWELL AUTOMATION, MILWAUKEE, WISCONSIN
Internship CFD Methodology Engineer, Oct 2020 – Jan 2022
- Design, integrate and simulate 3-D CAD models circuit breakers for different applications
- Experimental investigation in temperature and pressure measurements during short circuits and overloads

INDUSTRIAL ASSESSMENT CENTER, UW-MILWAUKEE, WISCONSIN
Lead Student, Oct 2017 – Present
- Inspect and analyze building structures, heating systems, ventilation, air conditioning, water, and industrial processes to ensure energy use is optimal
- Plan and schedule projects and audit methodology and procedures
- Present audit findings to clients
- Prepare cost estimates for potential retrofits

UNIVERSITY OF WISCONSIN MILWAUKEE, WISCONSIN
Teaching Assistant, Aug 2019– Present
- Preparing and conducting tutorials to undergraduate student on Fluid Mechanics Lab

UNIVERSITY OF WISCONSIN MILWAUKEE, WISCONSIN
Research Assistant, Aug 2017 – Present
- Experimental investigation for waste management of biomass species.
- Conduct research that tests and analyzes the feasibility, design, operation and performance of Gas Turbines
- Develop and test models of alternate designs and processing methods to assess feasibility of reducing the maintenance cost of Gas Turbines' Blades

CHAPTER 7- AMERICAN UNIVERSITY IN CAIRO, CAIRO, EGYPT
Part time Lecturer Assistant, Sep 2015- Aug 2017
- Prepared and conducted lectures to undergraduate students on topics such as Engineering Economy, Hydraulic, Heat and Mass Transfer, Refrigeration, Conventional Power Plants

CAIRO UNIVERITY FACULTY OF ENGINEERING CREDIT HOURS SYSTEM, GIZA, EGYPT
Part time Lecturer Assistant, Sep 2015 – Aug 2017
- Prepared and conducted lectures to undergraduate students on topics such as, Fundamentals of Management, Technical Writing, Economics and Marketing

CAIRO UNIVERITY FACULTY OF ENGINEERING, GIZA, EGYPT
Full time Lecturer and Research Assistant, Sep 2015 – Aug 2017
- Supervised undergraduate students working on the research project; Formula student (maintaining records on assignment completion, acting as mediator between the undergraduate students and the faculty researchers
- Wrote and contributed to heat transfer research group publications.
- Conducted tutorials for undergraduate students on topics such as Heat and Mass Transfer, Internal Combustion Engines, Engineering Numerical Methods, Conventional Power Plant, Engineering Economy

SUPERIOR PETROLEUM, CAIRO, EGYPT
CHAPTER 8- Part time Sales Engineer, Dec 2014 – Aug 2017
- Collaborated with sales teams to understand customer requirements to promote the sale of company products and to provide sales support
- Prepared and delivered technical presentations that explain products and services to customers and prospective customers
- Provided technical and non-technical support and services to clients regarding the use, operation and maintenance of equipment

I N T E R N S H I P S
Egyptian Natural Gas Holding Company, Cairo, Egypt
Gas and Oil Engineer, June 2011- Sep. 2011
Gebel El Zeit Petroleum Company, Cairo, Egypt
Mechanical Engineer, June 2010, Sep. 2010
Moog Group for Engineering and Industrial, Cairo, Egypt
Manufacturing Engineer, June 2009, Sep. 2009

E D U C A T I O N
University of Wisconsin Milwaukee, Milwaukee, Wisconsin
PhD-Mechanical Engineering Candidate, expected graduation May 2022
- Current GPA: 4.0
- Area of Research: Thermal Uniformity in Gas Turbines, Energy recovery from Biomass species.

Cairo University Faculty of Engineering, Giza, Egypt
Master of Science-Mechanical Engineering, Mar 2015
- GPA: 3.6
- Area of Research: Residential Fire, Smoke Management and Life Safety

Cairo University Faculty of Engineering, Giza, Egypt
Bachelor of Science-Mechanical Engineering, May 2012
- GPA: 4.0 (Distinction with Honor Degree)
- Graduation Project: Air Conditioning System Design and Building Management

PUBLICATIONS

1. Selim O.M., Espindola J., Amano R.S. (2022) Review of Biomass Energy Resources with Livestock Manure. In: Gupta A.K., De A., Aggarwal S.K., Kushari A., Runchal A.K. (eds) Advances in Energy and Combustion. Green Energy and Technology. Springer, Singapore. https://doi.org/10.1007/978-981-16-2648-7_6

2. Nourin, F. N., Espindola, J., Selim, O. M., and Amano, R. S. (July 20, 2021). "Energy, Exergy, and Emission Analysis on Industrial Air Compressors." ASME. *J. Energy Resour. Technol.* April 2022; 144(4): 042104. https://doi.org/10.1115/1.4051682

3. Hasan, A., Selim, O. M., Abousabae, M., Amano, R. S., and Otieno, W. (April 19, 2021). "Economic, Exergy, and Environmental Analyses of the Energy Assessments for U.S. Industries." ASME. *J. Energy Resour. Technol.* November 2021; 143(11): 112107. https://doi.org/10.1115/1.4050580

4. Qandil, M. D., Abbas, A. I., Salem, A. R., Abdelhadi, A. I., Hasan, A., Nourin, F. N., Abousabae, M., Selim, O. M., Espindola, J., and Amano, R. S. (March 4, 2021). "Net Zero Energy Model for Wastewater Treatment Plants." ASME. *J. Energy Resour. Technol.* December 2021; 143(12): 122101. https://doi.org/10.1115/1.4050082

5. Elgammal, T., Selim, O. M., and Amano, R. S. (January 18, 2021). "Enhancements of the Thermal Uniformity Inside a Gas Turbine Dilution Section Using Dimensional Optmization." ASME. *J. Energy Resour. Technol.* October 2021; 143(10): 102102. https://doi.org/10.1115/1.4049284

6. Selim, O. M., Abousabae, M., Hasan, A., and Amano, R. S. (November 19, 2020). "Analysis of Energy Savings and CO_2 Emission Reduction Contribution for Industrial Facilities in USA." ASME. *J. Energy Resour. Technol.* August 2021; 143(8): 082303. https://doi.org/10.1115/1.4048983

7. Espindola, J., Selim, O. M., and Amano, R. S. (August 3, 2020). "Co-Pyrolysis of Rice Husk and Chicken Manure." ASME. *J. Energy Resour. Technol.* February 2021; 143(2): 022101. https://doi.org/10.1115/1.4047678

8. Alkhafaji, A. A., Selim, O. M., Amano, R. S., Strickler, J. R., Hinow, P., Jiang, H., Sikkel, P. C., and Kohls, N. (February 3, 2021). "Mass Transfer Performance of a Marine Zooplankton Olfactometer." ASME. *J. Energy Resour. Technol.* November 2021; 143(11): 112102. https://doi.org/10.1115/1.4049602

9. Selim, O. M., and Amano, R. S. (July 29, 2020). "Co-Pyrolysis of Chicken and Cow Manure." ASME. *J. Energy Resour. Technol.* January 2021; 143(1): 011301. https://doi.org/10.1115/1.4047597

10. Selim, O. M., Hussein, M. S., and Amano, R. S. (May 26, 2020). "Effect of Heating Rate on Chemical Kinetics of Chicken Manure With Different Gas Agents." ASME. *J. Energy Resour. Technol.* October 2020; 142(10): 102104. https://doi.org/10.1115/1.4047018

11. Selim, O. M., Elgammal, T., and Amano, R. S. (February 24, 2020). "Experimental and Numerical Study on the Use of Guide Vanes in the Dilution Zone." ASME. *J. Energy Resour. Technol.* August 2020; 142(8): 083001. https://doi.org/10.1115/1.4046079

12. Elgammal, T., Selim, O. M. & Amano, R. S. "Numerical Simulation of a Cavitation Treatment in Kaplan Hydro-turbine". AIAA Propulsion and Energy 2019 Forum. https://doi.org/10.2514/6.2019-4408

13. Amano, R. S., & Selim, O. M., "Control Methods to Improve Combustor Exit Temperature Uniformity". AIAA Scitech 2019 Forum, 1773. https://doi.org/10.2514/6.2019-1773

14. Selim, O. M., W. AbdelMaksoud, E. ElBialy, and E. Khalil, "Smoke Behavior and Management in Large-Domed Mosques", Current Environmental Engineering 3 (1), 32-37; DOI : 10.2174/2212717803666160304000609

15. Selim, O. M., W. AbdelMaksoud, E. ElBialy, and E. Khalil, "Smoke Behavior and Management in Domed Mosques", SciTech Forum 2016, San Diego, USA, January 2016, 0995. https://doi.org/10.2514/6.2016-0995

AWARDS AND CERTIFICATES

- Graduate Student Excellence Fellowship Award 2021.
- Mechanical Engineering Department's Chancellor Awards 2021
- UWM Distinguished Graduate Student Fellowship (DGSF) award 2020.
- Mechanical Engineering Department's Award for Poster Competition UWM 2020
- Mechanical Engineering Department's Chancellor Awards 2020
- Certificate from the Department of Energy for completing 21 energy auditing visits to manufacturing companies.
- University of Wisconsin-Milwaukee Chancellors' Graduate Student Award (Fall 2017)
- Certificate of excellence from Schlumberger for the academic year 2010-2011
- Certificate of participation by the institution of mechanical engineers on July 2012 (Silverstone Circuit, UK)
- Certificate of experience from Life Makers Society to participate in the literacy 120 thousand Egyptian.

FFILIATIONS

- American Institute of Aeronautics (AIAA) as a Student Member, since Oct 2017
- Egyptian Engineers Syndicate as a Mechanical Engineer, since 2012
- Cairo University Racing Team, Formula Student United Kingdom Competition, Giza, Egypt. 2011-2012

SYSTEM SKILLS

- Star-CCM+
- Fire Dynamic Simulator (FDS)
- Solidworks
- Hourly Analysis Program (HAP)
- Microsoft Office